

EEG Analysis for Authentication and Affect-Guided Soundscape Exploration

ISURU JAYARATHNE

A DISSERTATION

SUBMITTED IN FULFILLMENT OF THE REQUIREMENTS

FOR THE DEGREE OF DOCTOR OF PHILOSOPHY

IN COMPUTER SCIENCE AND ENGINEERING

Graduate Department of Computer and Information Systems

The University of Aizu

2021



© Copyright by Isuru Jayarathne
All Rights Reserved.

The thesis titled

EEG Analysis for Authentication and Affect-Guided Soundscape Exploration

by

Isuru Jayarathne

is reviewed and approved by:

Chief referee
Professor
Michael Cohen

Michael Cohen



Professor
Qiangfu Zhao

ZHAO, Qiangfu

Feb. 16, 2021

Professor
Wenxi Chen

Wenxi Chen



Associate Professor
Yuichi Yaguchi

Yuichi Yaguchi



The University of Aizu

2021

TO MY PARENTS

Contents

LIST OF FIGURES	iv
LIST OF ABBREVIATIONS	vi
ABSTRACT	1
1 INTRODUCTION	3
1.1 Background and Motivation	3
1.1.1 EEG-based biometric authentication	4
1.1.2 Affect-guided soundscape exploration	5
1.2 Main contributions	6
1.3 Dissertation outline	7
2 BACKGROUND	9
2.1 Electroencephalography	9
2.1.1 Reliability of EEG	13
2.2 Machine learning	13
2.3 EEG-based biometric authentication	14
2.3.1 User Identification vs. authentication	14
2.3.2 EEG as a biometric	15
2.4 EEG affect analysis	16
2.4.1 Music therapy	16
2.4.2 Adaptive music systems	16
2.4.3 Neurofeedback therapy	17
2.4.4 Reinforcement Learning (RL) agent	17
3 EEG-BASED BIOMETRIC AUTHENTICATION	19
3.1 Introduction	19
3.2 Tasks	21
3.3 Computational EEG analysis	22
3.4 Usability concerns	23
3.5 Limitations	25
4 FEATURE EXTRACTION WITH IHAR	27
4.1 Introduction	27
4.2 Experimental framework	28
4.2.1 Pre-processing and Visualization	28

4.3	Data Augmentation	31
4.4	Inter-Hemispheric Amplitude Ratio (IHAR) vs. other features (LC, WL, SSC, AR)	33
4.5	Classification	37
4.5.1	Linear Discriminant Analysis (LDA)	37
4.5.2	Quadratic Discriminant Analysis (QDA)	38
4.5.3	Support Vector Machine (SVM)	38
4.5.4	k-Nearest Neighbor (kNN)	39
4.6	Results	40
4.7	Conclusion	51
5	AUTOENCODER-BASED ONE-CLASS CLASSIFICATION ALGORITHM	53
5.1	Introduction	53
5.2	Methodology	55
5.2.1	Pilot experiment with MNIST dataset	56
	Results of pilot experiment	57
5.2.2	Experiment with EEG data	60
	Results of experiment with EEG data	63
5.3	Conclusion	65
6	AFFECT-GUIDED SOUNDSCAPE EXPLORATION	67
6.1	Introduction	67
6.2	Methodology	68
6.2.1	Music generator	69
6.2.2	Affect analysis environment	70
6.2.3	RL agent	73
6.2.4	Simulator for Performance Test	75
6.2.5	Experiment with human subjects	76
6.3	Results and discussion	77
6.3.1	Conclusion	80
7	CONCLUSIONS	83
7.1	EEG-based authentication system	84
7.2	Affect-guided soundscape analysis	84
	ACKNOWLEDGMENTS	87
	REFERENCES	98

List of Figures

1.1	Dissertation structure and suggested reading order	8
2.1	Standard 10-10 electrode placement system (AF: Anterior Frontal, F: Frontal, FC: Fronto-Central, T: Temporal, P: Parietal, O: Occipital, C: Central, Z: sagittal axis), where odd numbers denote left hemisphere and even numbers represent right	11
2.2	Types of ML algorithms (LDA: Linear Discriminant Analysis, SVM: Support Vector Machine, kNN: k-Nearest Neighbor, ANN: Artificial Neural Networks, PCA: Principal Component Analysis, RBM: Restricted Boltzmann Machine DQN: Deep Q-Networks, SARSA: State-Action-Reward-State-Action). DL algorithms have dashed outline. Shaded algorithms were used in our experiments.	14
2.3	Typical structure of RL scenario	18
3.1	Common flow of EEG-based authentication system	20
4.1	Experimental setup	29
4.2	Structure of experiment: Each subject underwent 15 trials, and each trial comprised three phases. The stimulation phase necessarily precedes recall phase, and relaxation phase also serves as a refractory period, an implicit interval between trials, to be consistent with similar studies. (Each subject has tested for about 10 min.)	30
4.3	Topographic plots of 12 subjects for relaxation phase. (Maroon color represents high power values, and dark blue represents low.)	31
4.4	Visualization of raw and augmented signals subject to jittering, random down-sampling (removal), and permutation techniques. Orange trace represents the original raw signal, and blue trace represents the augmented signal in each plot.	32
4.5	Distribution of features before and after the augmentation, using color to distinguish respective subjects. Top 3 plots show features of 10 training trials, while bottom 3 plots show corresponding features of augmented trials.	33
4.6	Comparison of selected feature distribution of IHAR and LC. Top 5 show scatter plots of IHAR, while bottom 5 plots show LC of corresponding feature pairs.	34
4.7	Frequency response of the MA filter with various window sizes	35
4.8	Accuracy of three phases with 14 electrodes for various Discriminant Analysis, Support Vector Machine, and k-Nearest Neighbor techniques with OVO method	41

4.9	Accuracy of three phases with 14 electrodes with OVA method	42
4.10	Comparison of accuracy across features (AR: auto-regressive coefficients, SSC: slope sign change, WL: waveform length, LC: laterality coefficient, and IHAR: inter-hemispheric amplitude ratio) extracted during relaxation phase using all 14 electrodes	44
4.11	Accuracies of combination of 2 frontal electrode pairs which yielded higher accuracies	46
4.12	Variation of validation and testing accuracy for FC5-FC6 electrode pair of relaxation phase when increasing number of subjects using IHAR	48
5.1	General structure of autoencoder	54
5.2	Structure of training and verification phases	56
5.3	Sample images of MNIST dataset	56
5.4	Comparison of accuracies	58
5.5	ROC curve of three layers and code layer with 64 nodes	59
5.6	Distributions of correlation coefficients of each digit after training the model for digit 0. Red vertical line represents average of correlation coefficients of trained class, while blue vertical line represents defined threshold.	60
5.7	Visualization of raw and augmented signals subject to jittering, magnitude warping, time warping, random sampling, and permutation techniques. Orange trace represents the original raw signal, and blue trace represents the augmented signal in each plot.	62
6.1	System architecture	69
6.2	Max/MSP interface	70
6.3	Muse wireless EEG headband	71
6.4	Russell's circumplex model of affect. Relaxed state quadrant has been highlighted in red, dashed line	72
6.5	Structure of the neural network used in the RL agent	74
6.6	Heat maps of generated reward values. Darker spots represent higher rewards while lighter spots represent penalties.	76
6.7	Visualization of avatar movements for equal rewards. Size of each circle represents frequency of the avatar's visits to that specific point.	77
6.8	Visualization of avatar movements of case 1	78
6.9	Training results of the simulator for case 1 generated using TensorBoard	79
6.10	Visualization of avatar movements of subject 1	80
6.11	Training results of subject 1 generated using TensorBoard	81

List of Abbreviations

ANN	Artificial Neural Network
ASMR	Autonomous Sensory Meridian Response
AUC	Area Under the Curve (ROC)
CNN	Convolution Neural Network
DFT	Discrete Fourier Transform
DNA	Deoxyribonucleic acid
DQN	Deep Q-Network
ECG/EKG	Electrocardiogram
ECoG	Electrocorticography
EEG	Electroencephalography
EMG	Electromyography
EOG	Electrooculography
ERP	Event-Related Potential
fMRI	Functional Magnetic Resonance Imaging
FPR	False Positive Rate
GSR	Galvanic Skin Response
IHAR	Inter-Hemispheric Amplitude Ration
kNN	k-Nearest Neighbors
LC	Laterality Coefficient
LDA	Linear Discriminant Analysis
MA	Moving Average
MEG	Magnetoencephalography
ML	Machine Learning
OCC	One-Class Classification
OSC	Open Sound Control
PCA	Principal Component Analysis
PET	Positron Emission Tomography
PSD	Power Spectral Density
QDA	Quadratic Discriminant Analysis
RBF	Radial Basis Function
RFID	Radio-Frequency Identification
RL	Reinforcement Learning
RNN	Recurrent Neural Network
ROC	Receiver Operating Curve
SSC	Slope Sign Change
SVDD	Support Vector Data Description
SVM	Support Vector Machine
TPR	True Positive Rate
VEP	Visual Evoked Potential
WL	Waveform Length

EEG Analysis for Authentication and Affect-Guided Soundscape Exploration

ABSTRACT

This work is devoted to analyzing and exploiting EEG signals for security and musical relaxation. Such biometric applications are used in several areas because of the non-invasive capturing nature of EEG and affordable availability of consumer-grade devices. In our first study, EEG signals were used as a biometric trait to authenticate access to restricted systems, which provides more security compared to traditional biometrics. As a second study, EEG signals were used as a measurement of relaxation to reinforce the discovery and exploration of the “sweet spot” in a pantophonic musical landscape.

User authentication systems based on EEG has recently become popular, marking an inflection point in the field. Since most of the surveyed related studies achieved high accuracy, our goal was to increase user-friendliness by reducing the number of electrodes using a simple task to collect data. EEG signals were collected across different trial phases: relaxation, visual stimulation, and mental recall. We introduce a novel derived feature, dubbed Inter-Hemispheric Amplitude Ratio (IHAR), which expresses the ratio of amplitudes of laterally corresponding electrode pairs. The extracted feature set was tested with several machine learning (ML) algorithms, including Linear Discriminant Analysis (LDA), Support Vector Machine (SVM), and k-Nearest Neighbor (kNN). Most of the ML algorithms showed 100% accuracy with 14 electrodes, and according to our results, perfect accuracy can also be achieved using as few as 4 electrodes.

A novel one-class classification method was proposed based on autoencoders to overcome the weaknesses of EEG-based authentication systems. In most systems, classification models need to be retrained and a considerably large dataset must be used. Autoencoders were trained for each system user in the proposed system that does not need to retrain the whole system

when adding a new user. Signal augmentation techniques— jittering, amplitude warping, time warping, random downsampling, and permutation— were used to expand the training dataset. Evaluation results showed 97.1% accuracy with a 0.91 AUC value for 8 frontal electrodes.

A system was developed to address the challenge of musical relaxation by using modern machine learning techniques. In our approach, computer-guided audition for spatial soundscapes was investigated, automatically exploring a polyphonic area while using bio-signals as indicators of satisfaction. We propose a reinforcement learning (RL) method to discover the sound relaxation “sweet spot” in a pantophonic soundscape. An avatar roams within a pantophonic space, surrounded by independent audio channels, while a human subject, listening through the avatar’s ears, is connected to an electroencephalographic (EEG) headset. Instead of changing position manually, a Deep Q Network (DQN) in reinforcement learning is used. The reward for the DQN agent was calculated from a derived formula using computed valence and arousal values from collected EEG signals. The performance of the DQN agent was evaluated using a simulator with virtual rewards before testing with human subjects. Test results of human trials were encouraging, suggesting that DQN has the potential to automate such “sweet spot” exploration.

1

Introduction

1.1 Background and Motivation

The brain is the most interesting and most complex organ in the human body, and explanations for many of the brain functions have yet to be found. It contains billions of interconnected neurons that can pass electrochemical messages to process basic sensory functions, memory, thought information, and other cognitive activities. Among all its functions, the most complicated brain function is cognition, which it is completely subjective. The scientific community is working hard on unlocking the mysteries of brain functions using various technologies. According to scientific findings, brains are morphologically different human to human, excepting monozygotic twins [1]. However, there is much evidence that every human is differ

in terms of brain functionality, including monozygotic twins.

Subjective differences or peculiarity of human consideration is vital to make diverse society which fosters novelty. This unique nature of individual people is sometimes used in real world applications such as authentication systems. Even if a person can completely mimic someone else, there are differences in how brains perceive sensory information. Therefore, it is a better way to find subject-specific features by directly accessing brain data.

This dissertation has discussed the utilization of subject-specific features using brain signal data in two different applications. A short introduction to these two research projects, including main contributions and dissertation outline, is discussed in this chapter.

1.1.1 EEG-based biometric authentication

A security system is a prominent method of providing a form of protection for any kind of asset. Most security systems have a sequential process to achieve better protection. Authentication is a part of such sequential processes, verifying that a user has privilege to access a system. There are several types of methods used, including knowledge, possessions, and biometric attributes. Such knowledge can be described as “something one knows,” such as a user name and password pair. Possessions refers to “something one has,” such as smart cards, RFID tags, certificates, etc. Biometrics can be described as encoding “features one has,” such as fingerprints, palm-prints, retina scans, voice profiles, etc. Compared with other methods, biometric authentication provides better reliability, mobility, and easier use [2].

Biometrics is the science of validating the identity of an individual, based on physical, chemical or behavioral attributes. Generally, biometrics are categorized as physiological or behavioral characteristics [3]. Physiological characteristics are usually derived from structural information of the human body, such as features of the finger, palm veins, iris, retina, DNA, or face. Behavioral characteristics are based on behavioral patterns of a person, including, voice, signature, gait, or keystroke dynamics. A biometric system is essentially a pattern recognition system that extracts salient features from collected biometric data from an individual [4].

Availability of consumer-grade EEG sensing devices, attract attention from the research

community who are working on biometrics. Other than that, EEG has several advantages over traditional biometrics:

- A predefined brain state which authenticates a system is impossible to evoke by insistence or coercion.
- No non-living brain can produce an EEG, which prevents breaching an authentication system by assassinating a user.
- Even though most other biometric traits are visible, EEG biometrics are invisible, making them uncapturable by other parties [5].
- If a brain state is selected for authentication, it can be suppressed by a user in coercion situations [6].

Therefore, this kind of authentication system provides protection not only for the asset, but also for users. Though person identification using EEG is an attraction among researchers, the complexity of such sensing limits using such technologies in real-world applications.

1.1.2 Affect-guided soundscape exploration

According to psychological findings, relaxation techniques for reducing effects of stress can improve physical and mental health. Relaxation techniques are discussed widely and deeply in psychological fields. In this study, relaxation is defined in a narrow sense. Among many relaxation techniques, musical relaxation is one of the simplest. The discipline of music therapy recognizes the power of sound to induce relaxation, a power that has been well-appreciated by cultures around the world for millennia. Selecting suitable sounds for a particular subject is challenging due to idiosyncratic tastes and circumstances [7]. Wolfe et al. performed a comparison in selection of relaxation music by musicians and non-musicians [8].

Adaptive music is widely used in video gaming to enhance the mood of players. As in many other interactive experiences, sound designers cannot predict all possible outcomes [9]. Advancement of AI technologies allows to improvise music in real time according to the situation.

Hutchings et al. has proposed a way use an autonomous agent to improvise music [10]. The challenge for music relaxation can be overcome by using these concepts to some extent. In our approach, a reinforcement learning algorithm was used to analyze EEG signals of a listener to optimize a spatial soundscape for relaxation. To find the "sweet spot" in a pantophonic soundscape, a DQN algorithm was used by feeding the analyzed EEG signal as a cumulative reward and state. The DQN RL agent then outputs a discrete value which can be converted into virtual keystrokes to move the sink (avatar or iconic listener) position in the soundscape. The environment generates a new soundscape audio output according the sink position to make subject more relaxed. This approach is a form of music therapy, but conscious activity does not necessarily happen in this process.

1.2 Main contributions

1. *New EEG dataset was obtained*

EEG dataset was captured using low-cost mobile headset. This dataset contains 3 main tasks which can especially be used for person identification or authentication research. The dataset is available online in the PLOS One data repository¹.

2. *Novel feature extraction method for person identification*

A novel feature, dubbed Inter-Hemispheric Amplitude Ratio, was derived. The feature is based on the behavioral-asymmetry of brain hemispheres. The extracted feature was tested with several machine learning algorithms, confirming its subjective discrimination.

3. *Investigated the best electrode configuration and corresponding stimulation to make the authentication system more user-friendly*

In order to increase user-friendliness of the system, we investigate minimum number of electrodes that can be used to find the uniqueness of subjects. Our finding showed considerable accuracy can be achieved with two electrodes. Also, we showed EEG signals of resting state, which arises from comparatively simple task, can be used for subject

¹<https://journals.plos.org/plosone/article?id=10.1371/journal.pone.0238872#sec016>

identification.

4. *Autoencoder-based novel identification technique was introduced*

Unlike traditional classification methods, an autoencoder-based single-class classification method was proposed. When adding a new class to a pre-trained machine learning model, the whole model must be retrained and accuracy can be affected. The proposed method uses separate single class classifiers based on autoencoders to overcome that problem.

5. *Novel affect-guided method to improvise music using reinforcement learning*

To address the idiosyncratic nature of individuals, an affect-guided ML model was proposed to find the relaxation sweet spot in a pantophonic musical soundscape. An avatar roams through the soundscape according to the individual's EEG data to find the best ambient sound combination to reach the relaxation state.

The presented main contributions were published in a refereed journal and international conferences. The publications that comprise the work carried out within the scope of this dissertation are as follows:

- *Survey of EEG-Based Biometric Authentication* (Chapters 2 and 3). IEEE 8th International Conference on Awareness Science and Technology, Taichung, Taiwan, 2017 [11].
- *Relaxation sweet spot exploration in pantophonic musical soundscape using reinforcement learning* (Chapters 2 and 6). In ACM 24th International Conference on Intelligent User Interfaces, Los Angeles, 2019 [12].
- *Person Identification from EEG Using Various Machine Learning Techniques with Inter-Hemispheric Amplitude Ratio* (Chapters 2 and 4). PLOS One, 2020 [13].

1.3 Dissertation outline

The condensed outline of this dissertation can be seen in Figure 1.1. The content of the following chapters is as follows:

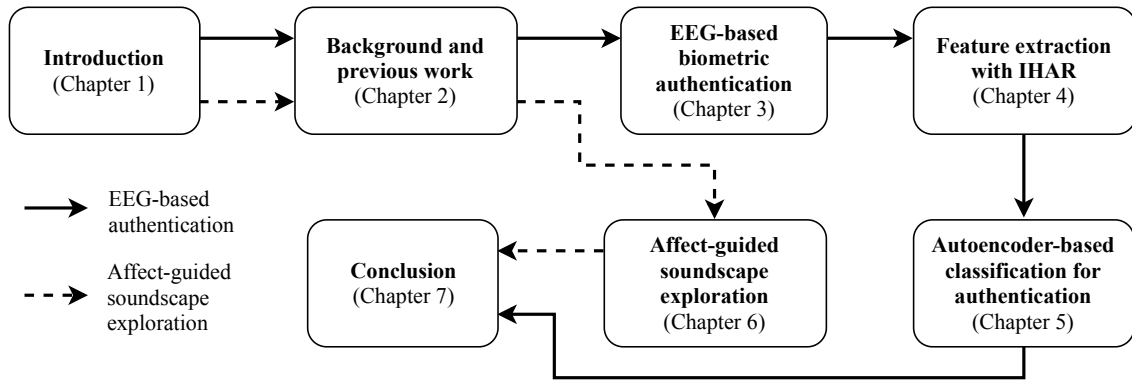


Figure 1.1: Dissertation structure and suggested reading order

- **Chapter 2:** Overview of relevant literature and projects, outline of the EEG-based biometric system and affect-guided soundscape exploration.
- **Chapter 3:** Comprehensive review of EEG-based biometric authentication and design considerations.
- **Chapter 4:** Experimental framework for data acquisition and proposal of novel feature called IHAR. Performance evaluation of proposed feature extraction method with several machine learning techniques.
- **Chapter 5:** Overview of autoencoders and proposal of novel single-class classification method for EEG biometric authentication using autoencoders.
- **Chapter 6:** Design and implementation of the affect-guided soundscape exploration and testing results of the implemented system.
- **Chapter 7:** Summary of main contributions achieved within the scope of this research, discussion of possible impact, and future iterations of the developed methods.

2

Background

2.1 Electroencephalography

Electrical biosignals or bioelectrical signals (a subset of biosignals) refers to the change of electrical voltage and current in living organisms. Usually, these electrical potentials are produced by special tissue, organs, or cell systems such as the nervous system. Common electrical biosignals measurements include Electrocardiogram (ECG/EKG), originating from activity of the heart; Electroencephalogram (EEG), produced in the brain from activity of neurons; Electromyogram (EMG), generated by muscle activity; Electrooculogram (EOG), change of corneo-retinal potential due to eye movements; Magnetoencephalogram (MEG), change of magnetic field in the brain; and Galvanic Skin Response (GSR)/Electrodermal activity (EDA), change of

skin resistance [14][15]. EEG is an electrophysiological monitoring method to record dynamics of electrical activity of a human brain. Unlike other techniques, EEG is not terribly expensive, and is non-invasive, and allows completely passive recording. EEG measures the voltage fluctuations resulting from ionic current within the neurons of the brain, so it may be employed to measure some inner characteristics of the brain. The first EEG was recorded by Hans Berger in 1924 [16]. Since then EEG has been used mainly in medical field to diagnose brain disorders including, but not limited to, epilepsy, sleep disorders, depth of anesthesia, coma, encephalopathies, and brain death [17]. Later it became an inexpensive tool not only for diagnosing brain disease but also understanding usual behaviors of the brain.

Table 2.1: Consumer-grade wireless headsets for EEG data capture

Device name	Channels	Electrode Type	Brain lobe covered
NeuroSky Mindwave	1	Dry	Frontal (FP1)
Bio-Tech AURIS	2	Dry	Temporal (In-the-Ear)
The Aware	4	Dry	Temporal (In-the-Ear)
Muse	4	Dry	Frontal, Temporal (AF7, AF8, TP7, TP8)
EMOTIV Insight	5	Dry	Frontal, Temporal, Parietal (AF3, AF4, T7, T8, Pz)
Vive DSI VR300	7	Dry	Frontal, Parietal, Occipital (FCz, Pz, P3, P4, PO7, PO8, Oz)
EMOTIV Epoc+	14	Wet	Frontal, Temporal, Parietal, Occipital (AF3, AF4, F3, F4, F7, F8, FC5, FC6, T7, T8, P7, P8, O1, O2)
OpenBCI	8–16	Dry	Fully customizable
BioSemi	16	Wet	Frontal, Temporal, Parietal, Occipital
mBrainTrain	24	Wet	Frontal, Temporal, Parietal, Occipital (Customizable)
ENOBIO 32	32	Dry	Customizable with different caps
Cognionics Mobile-72	16–64	Dry	Frontal, Temporal, Parietal, Occipital

Lately, EEG has become popular among researchers because of the recent technological advancement of EEG signal-capturing devices. Compared to other brain experimentation devices, EEG devices are reasonably priced and feature ease of calibration and use. Unlike most

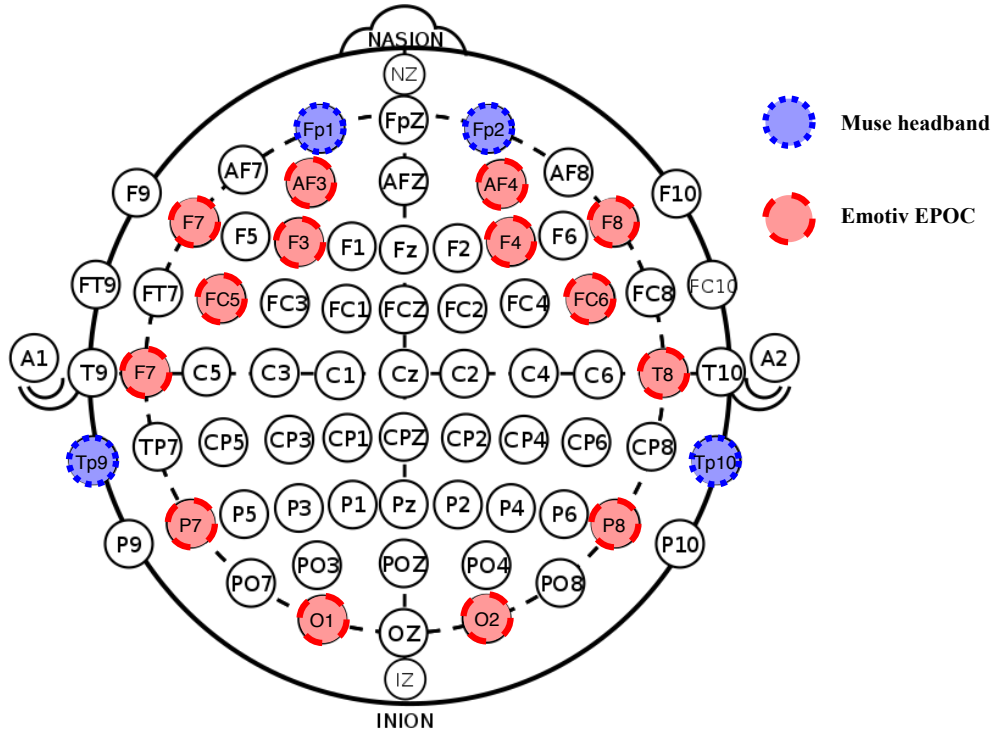


Figure 2.1: Standard 10-10 electrode placement system (AF: Anterior Frontal, F: Frontal, FC: Frontocentral, T: Temporal, P: Parietal, O: Occipital, C: Central, Z: sagittal axis), where odd numbers denote left hemisphere and even numbers represent right

of the brain signal capture techniques mentioned above, specialized medical knowledge is not required to use EEG devices. Table 2.1 lists some consumer-grade wireless EEG acquisition devices [18]. The most important specifications of such devices are the number of electrode channels, electrode type, brain lobes covered, calibration time, portability, and customizability. For best results and for the sake of convenience, a device should be selected based on the particular application as well as affordability.

International standards have been established for electrode placement on the skull of the human brain. Jasper et al. proposed [19] the 10-20 system for the capture of EEG signals. An extension of the 10-20 system, the so-called 10% system or 10-10 system, was proposed by Chatrian et al. [20]. Oostenveld et al. proposed [21] the 10-5 system for high resolution EEG signal acquisition. Many of the listed devices in Table 2.1 are designed according to these international electrode placement standards and conventions. “Bio-Tech AURIS” and “The Aware” follow a new method called “in-the-ear EEG,” which places electrodes inside the ear canal. Each head-

set has its own location on the scalp as reference electrode, including ear lobe, mastoids (on the bone behind the ear), Cz (intersection of sagittal and coronal planes), and FpZ (in Muse headband) [22]. Figure 2.1 shows electrode placement of the Emotiv EPOC+ and the Muse headband as used in our studies.

Table 2.2: Frequency bands and corresponding brain states

Identifier	Frequency band (Hz)	Brain state
Delta, δ	< 4	Primarily associated with deep sleep
Theta, ϑ	$4 - 8$	Appear as consciousness slips towards drowsiness
Alpha, α	$8 - 13$	Usually found over the occipital region. Indicates relaxed awareness without attention
Beta, β	$13 - 30$	Associated with active thinking and concentration.
Gamma, γ	> 30	Represent binding of different populations of neurons.

EEG signals are normally described in terms of rhythmic activity of brain waves according to neuroscience. The amplitudes and frequencies of signals change from one state to another. Five major frequency bands have been identified in clinical practice. In increasing order of frequency, they are called delta (δ), theta (ϑ), alpha (α), beta (β), and gamma (γ). Table 2.2 describes the frequency bands and related brain states [23]. Frequency bands are experimentally chosen according to which brain state is being explored. Most EEG analysis methods fall into five main categories: time domain, frequency domain, time-frequency domain, non-linear methods, and deep learning methods [24].

EEG signals can be contaminated by other electrophysiological signals, such as those captured by an electrocardiogram (ECG/EKG) generated in the heart, electromyogram (EMG) signals generated in muscles, or electrooculogram (EOG) signals generated by eye movements [25]. Since EEG recording devices are highly sensitive, captured EEG signals may be corrupted with 50 or 60 Hz AC power line “hum” interference. However, line noise is normally not a problem because considered frequencies usually lie below 50 Hz.

2.1.1 Reliability of EEG

Clinical-grade systems have been used in hospitals and laboratories with suitable environments to evaluate neurological disorders. Even though EEG is non-invasive, some studies have shown it can achieve similar accuracy to invasive methods such as electrocorticography (ECoG) [26]. Availability of consumer-grade EEG devices make such sensing feasible for real-world applications. Even though EEG has low spatial resolution on the scalp compared to fMRI, it is used in different domains such as emotion classification, prosthetics, epileptic seizure analysis, sleep stage classification, and biometric authentication. Signal quality depends on several parameters of device hardware, such as reference electrodes, electrode type, maximum sampling rate, amplifier type, and communication interface. Maskeliunas et al. [27] did a performance comparison between Neurosky MindWave and EMOTIV Epoc headsets by capturing signals for two different tasks. EMOTIV Epoc showed the best results for both tasks. Also, Wang et al. [28] showed that the EMOTIV Epoc headset can perform as well as the clinical-grade G.Tec system.

2.2 Machine learning

In general, machine learning (ML) is the scientific study that provides ability to automatically learn and improve from experience without being explicitly programmed. ML approaches are widely used in various fields including, but not limited to, image recognition, sentiment analysis, speech recognition, biomedical data analysis, video surveillance, computer security, weather prediction, recommendation systems, self-driving vehicles, and robot control [29]. Figure 2.2 shows the common categorization of various ML techniques. Traditional ML algorithms use an extracted feature set as an input, while Deep learning (DL) methods (a subset of ML) automatically extract features from raw data [30]. Since person identification and authentication is a straightforward classification problem, highlighted classifications were used for EEG-based authentication system. Reinforcement learning (RL) refers to goal-oriented algorithms, which learn and take actions in an specific environment so as to maximize some cumu-

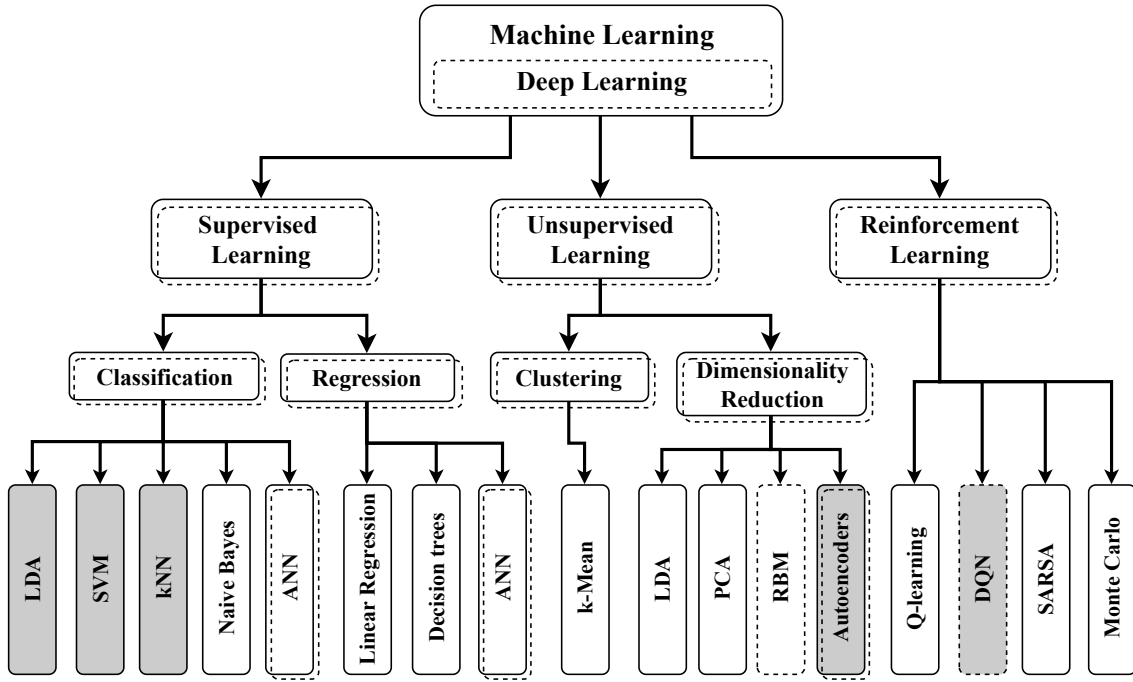


Figure 2.2: Types of ML algorithms (LDA: Linear Discriminant Analysis, SVM: Support Vector Machine, kNN: k-Nearest Neighbor, ANN: Artificial Neural Networks, PCA: Principal Component Analysis, RBM: Restricted Boltzmann Machine DQN: Deep Q-Networks, SARSA: State-Action-Reward-State-Action). DL algorithms have dashed outline. Shaded algorithms were used in our experiments.

lative reward. In our affect-guided soundscape exploration study, we used a Deep Q-Network (DQN) RL algorithm to find the sweet spot in a pantophonic soundscape.

2.3 EEG-based biometric authentication

Biometric authentication is one of the main applications that utilizes subject-specific features to verify identity of a person. EEG can also be used as another biometric trait and the next couple of subsections and Chapter 3 discuss how EEG can be used as a biometric. Further, Chapters 4 and 5 describe proposed identification and authentication system using EEG signals.

2.3.1 User Identification vs. authentication

Ever since information started to be recorded and processed in digital form, in fields such as health care, finance, education, and government, securing information systems has been vital. A so-called “CIA” triad (confidentiality, integrity, availability) model guides policies for

information security [31]. Contemporary information systems use various kinds of security methods. Every security method includes an authentication process. Identification is the process of presenting an identity to a system, and authentication can be described as the validation of such identity. For such validation processes, as mentioned above, some evidence should be provided [32], such as knowledge, possession, or biometric attributes.

2.3.2 EEG as a biometric

Authentication systems currently in use have several vulnerabilities. For example, physical devices such as smart cards, RFID tags, dongles, etc. can be stolen, misplaced, misused, or damaged. On the other hand, conventional authentication methods, which involve knowledge such as username and password, can also be defeated by coercion, besides credentials being vulnerable to being stolen, disfigured, or forgotten. Even though biometrics cannot be stolen, some systems can be easily misled with forgery or fake replicas. Also, some protection procedures can be overridden by spoofing and forcing. Fingerprints and palm-prints can be duplicated, and iris scans can be tricked by high-resolution images. Such weaknesses suggest how conventional security systems become vulnerable, even with simple attack tactics, and such considerations highlight the importance of considering new strategies which can prevent unauthorized parties from entering a system.

With state of art of signal processing and machine learning techniques, researchers are exploring novel styles of authentication using electroencephalography (EEG). EEG is a robust biometric trait, and EEG-based authentication is safer than older techniques. The Chapter 3 reviews four EEG-based authentication studies. Additionally, several other studies are briefly discussed, comparing results and indicating the most sensitive and important design considerations, which have heavy interdependence with accuracy and user-friendliness. This comprehensive survey was performed to report and understand the state-of-the-art in EEG-based biometric authentication.

2.4 EEG affect analysis

The main goal of this research project is to produce most suitable soundscape to relax an individual depending on the personal taste. This system utilizes EEG to find relaxation state of an individual in real time. DQN in RL was used to produce new soundscape according to analysed EEG data. The proposed affect-guided soundscape exploration method can be explained with the following commonly understood concepts.

2.4.1 Music therapy

According to psychological findings, relaxation techniques for reducing the effects of stress can improve physical and mental health. Music therapy is a popular technique which uses musical intervention to improve individual's quality of life. In general, music is the most common entertainment source in contemporary life. Besides taking part in live music venues, concert halls, opera houses, jazz, rocks, and blues clubs, people listen to music with portable devices. Music can use to change mood or reduce the level of stress. However, music therapy is more of a research-based practice which helps to improve mental health [33]. Moreover, concepts such as Autonomous Sensory Meridian Response (ASMR) uses auditory triggers—including whispering, finger scratching or tapping, brushing hair, rubbing hands together—to provide a 'brain tingling' sensation, reported to be accompanied by feelings of relaxation and well-being [34]. Nevertheless, it is challenging to find common music because of idiosyncratic nature of humans and variety of taste. Our approach is a limited style of music therapy, involving no performance but audition.

2.4.2 Adaptive music systems

Adaptive or interactive music is a popular method in video games to provide dynamic immersive experience to users. In video games, music changes depending on parameters which change with events and actions the player performs or experiences during gameplay [35]. DirectSound, which is a component of the Microsoft DirectX platform, allows developers to

make interactive music environments for video games [36]. LucasArts Entertainment Co. has a patent for dynamically composed music for computer entertainment systems, deployed in several video games [37]. These methods enable enhanced game play experience by generating different music depending on the scenario. Also, adaptive music can be used in music therapy to overcome idiosyncrasy problems by changing it accordingly. In our approach, we used a Max/MSP patch to generate different combinations ("mixes") of given multistem soundtrack based on the sink (virtual listener) position in a 2D pantophonic soundscape.

2.4.3 Neurofeedback therapy

Neurofeedback (NFB) uses biosignals (typically EEG) and provides immediate feedback from a computer-based program that evaluates individual's brain activity [38]. This therapeutic process is known as a complementary treatment of many brain dysfunctions, such as autism, attention deficit hyperactivity disorder (ADHD), anxiety, post-traumatic stress disorder (PTSD), seizure conditions, and insomnia. This idea is basically conscious control over the autonomic nervous system (ANS) [39]. This therapy has been used as medical treatment in clinical environments since late 1960s, but now there are mobile applications that facilitate meditation [40], relaxation, or insomnia therapy. The proposed approach is a soft kind of (non-medical, non-clinical) neurofeedback therapy, not with expectation of relaxation, but of soundscape automatic tuning of user self-regulation of brain function.

2.4.4 Reinforcement Learning (RL) agent

The term "Reinforcement Learning" was coined by Minsky in 1961 and independently in control theory by Waltz and Fu in 1965 [41]. As discussed in § 2.2, RL is a trial and error system as an online learning system. This concept got a huge attention due to successful results of the Google AlphaGo project which can play the game Go [42]. In addition to that, Mnih et al. proposed a convolution neural network (CNN) model, trained with a variant of Q-learning [43]. This method was tested with seven Atari 2600 video games and outperformed all previous approaches on six of them. Figure 2.3 shows the main components and connections of an RL

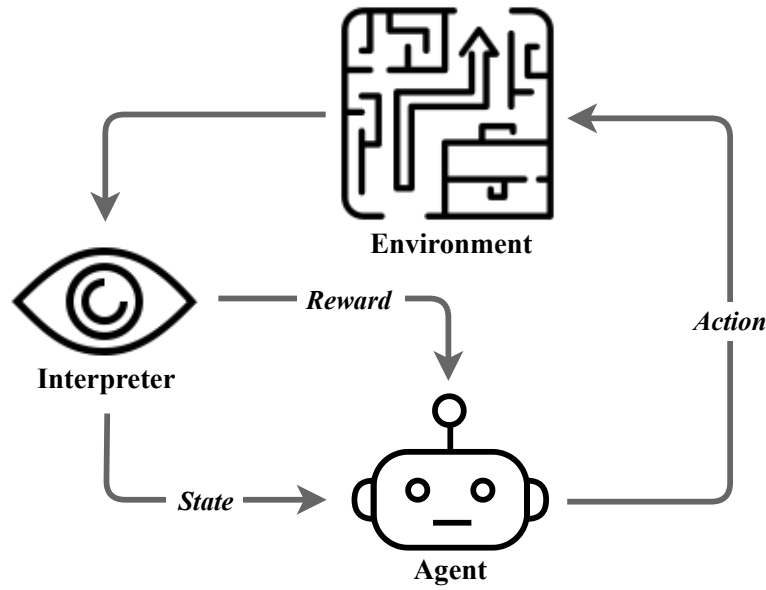


Figure 2.3: Typical structure of RL scenario

scenario. The environment is basically a function that transforms an action taken in the current state into the next state. The interpreter observes the environment and provides a new reward and refreshes the state of the environment. The agent has set of functions that transform the new state and accept reward to trigger a next action.

In our study, an RL agent has been used to control an avatar in a soundscape. The interpreter comprises two components: 1) sound composer (Max/MSP patch), and 2) signal analyzer. The reward and state were derived from EEG signals captured from the subject (human or simulator) and fed to the RL agent. The complete system architecture and methodology are described in Chapter 6.

3

EEG-based biometric authentication

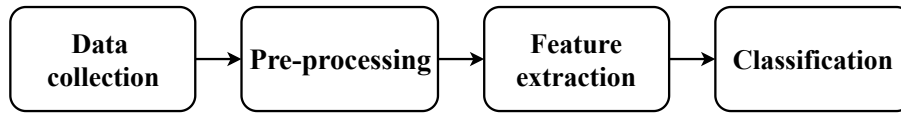
3.1 Introduction

Biometrics—measurable physical characteristics or behavioral traits—is comparatively safer, reliable, and convenient to use in security domain. Most popular behavioral approaches include signature recognition, keystroke dynamics, and gait analysis, and physiological approaches include fingerprints, iris, retina, face, ear, and palm prints [44]. Biometric authentication systems verify the identity of the person by processing biometric data. Any human physiological or behavioural characteristic can be used as a biometric for authentication, if it has properties stated in Table 3.1 [45, 46].

After Hans Berger’s discovery of EEG, neurophysiologist Adrian and Matthews reported

Table 3.1: Properties of biometric systems

Property	Definition	EEG compliance
Universality	The trait or the biometric element should exist in all people.	Every person produces EEGs.
Uniqueness	The characteristic must be distinctive for each person. Probability of two people having same biometric characteristic should be negligible.	Different signal patterns are produced unique to each person (P300, N200).
Permanence	Biometric element should be invariant over time.	Invariance is questionable, but some studies showed stability over time [47, 48].
Collectibility	The trait should be quantitatively measurable and easily collected.	Various consumer-grade EEG capturing devices are available.
Performance	Accuracy, speed, and resource requirements should be satisfied in order for a biometrics-based system to be practical	Various machine learning and deep learning methods have good performance.
Acceptability	The system shouldn't be harmful and should be accepted by users.	Collecting brain waves might not be acceptable by some.
Circumvention	The system should be robust against various attacks and fraudulent methods.	EEG patterns are not visible and universal compared to other biometrics.

**Figure 3.1:** Common flow of EEG-based authentication system

inter-individual variation in the normal EEG. They observed a voltage difference of classical alpha rhythm between EEG recordings of themselves in 1934 [49]. In early age of EEG studies, Davies et al. in 1936 and Gibbs et al. investigated genetic aspects of brain function in health and disease, such as normal and abnormal EEG phenomena in twins and families. Since then various studies have been performed by the scientific community including, but not limited to, genetic variation of monozygotic and dizygotic twins, changes of EEG in childhood and youth, EEG differences between male and female, genetic basis of epilepsy. These studies, especially twin studies indicate that EEG signals contain some genetic attributes as well. The uniqueness or individuality can be highly depends on human's genetics. Therefore, biometric authentication systems always trying to find the phenotypes of individuals.

EEG-based biometric is a relatively new biometric modality. The first study was proposed by Poulos et al. in 1998 [50]. As seen in Table 3.1, this technique also fulfills requirements of biometric systems. Advancement of EEG devices, signal processing methods, and machine learning techniques accelerate the improvement of quality and practicality. As seen in Figure 3.1, most of the proposed approaches followed common pipeline main stages. In the data collection stage, various stimuli or tasks have been used to obtain more specific pattern and overcome the ambiguity. Common digital signal process techniques—such as filtering, blind source separation (PCA: principal component analysis, ICA: independent component analysis)—are applied in the pre-processing stage, especially to remove artefacts and condition a cleaner signal. When using traditional ML techniques feature extraction is import stage, but current DL techniques contains separate phases to extract more compatible features automatically. Extracted features are fed to either linear or non-linear legacy classification algorithm, depending on extracted features. Also, some approaches have used template machine algorithm, which doesn't follow above exact pipeline.

3.2 Tasks

Tasks are important when recording EEG signals for identification or authentication purposes. Besides type of task, duration of each trial, number of trials, and task complexity also affect accuracy of the system. Recording paradigms used in literature can be categorize as follows [16]:

- *REC and REO*: Resting with eyes closed (REC) and resting with eyes open (REO) are the most popular and comparatively simplest task in literature. REC helps to reduce artefacts produced by eye blinking. However, eye blinking also can contain some subjective patterns [51].
- *ERP*: Event-related potentials (ERP) has different types depending on given stimulus. Visual stimulation is widely used in this field compared to auditory stimuli. Therefore, EEG signals that are acquired with visual stimuli are called visual evoked potentials

(VEP) [52–54].

- *Multi-task*: Some studies have used multiple tasks from single subject, such as performing mathematical operations, writing letters, limb movements, and imagined limb movements [55, 56].
- *Indirect*: This method uses EEG signals evoked by some thoughts and interprets it as a password [57, 58].
- *multimodal*: To strengthen the reliability of system some researchers have proposed approaches which use extra biometric trait besides EEG. For instance, gait [59], iris [60], and ECG [61] have been used with EEG.

3.3 Computational EEG analysis

EEG analysis involves, extracting information from raw signals using mathematical signal analysis methods. Once digital EEG signals stored as numeric data, a variety of forms of information characterizing underlying brain activity can be extracted [62]. Traditional EEG evaluation has been performed by visual inspection of EEG curves, knowing certain criteria such as wave forms, especially when diagnosing epileptic seizures or certain brain tumors. Development of computational power of machines allows mathematicians and scientists to introduce numerous digital signals processing algorithms. Traditional analysis methods which have been used in studies can be broken down into four categories [24]. In addition to that, new approaches which use DL techniques can be considered a fifth category. Both pre-processing and feature-extraction methods fall into following categories.

- *Temporal analysis (time domain)*: This can be further divided into two parts, linear predictions and BSS (including PCA and ICA). In authentication studies, signal averaging (especially ERP signals), statistical feature extraction, and autoregressive (AR) model fall into this category.

- *Spectral analysis (frequency domain)*: This refers to examination of information contained in the frequency domain by using statistical and Fourier transform (FT) methods. This also can be further categorized as parametric and non-parametric method. Most commonly, power spectral analysis is used since the power spectrum contains distribution of power frequency.
- *Tempo-spectral analysis (time-frequency domain)*: The most common time-frequency method is wavelet transform (WT) which contain both time and frequency information at the same time [63]. Besides that, Hilbert-Huang transform, which can decompose EEG signals into a set of oscillatory components, is also used [64].
- *Nonlinear methods*: Some studies have used nonlinear methods such as bilinear models [65], fractal dimensions (FD) [66], and entropy based methods [67, 68]. Nonlinear methods can capture nonlinear coupling and phase-locking among harmonics that cannot be captured by frequency domain methods.
- *ANN methods*: DL approaches such as, convolution neural networks (CNN) [69] and recurrent neural networks (RNN) [59] automatically extract features from given EEG raw data to obtain maximum classification accuracy. In this method, large dataset and powerful processor must be used in training phase to achieve better and efficiently.

3.4 Usability concerns

The experimental conclusions reviewed above further emphasize the notion that EEG signals can be used to implement robust authentication systems. However, the best method is still not obvious, since it depends on the required security level and user friendliness. The parameters should be carefully tuned to implement a fairly good EEG-based authentication system, as detailed below.

- *Task simplicity or complexity*

Most of the studies surveyed reported that more robustness and high accuracy can be

achieved with higher task complexities [5, 6, 70], but higher task complexities make a system less usable, because both authentication and system training are highly time-consuming, which compromises an important property of good authentication systems.

- *Number of channels and electrode type*

As mentioned earlier, both consumer- and clinical-grade headsets are used in this kind of research. Some studies especially focus on accuracy changing against the number of channels used [5]. Even though the number of channels has less impact on accuracy, in case security is significantly prioritized, a large number of channels ensures extra protection. Fewer channels can be processed at reduced computational power and provides extra user-friendliness [71]. Chen et al. [6] reported that wet electrodes generally have better signal quality compared to dry ones, but calibration time is higher.

- *Number of subjects and trials*

Using more data points increases accuracy of classification algorithms. Chen et al. [6] confirmed that by performing single- and multi-trial classification. According to the La Rocca et al. [72] classifications, using fewer subjects provides better accuracy than considering more subjects, as similar subjects can be found in a large set. Therefore, systems which show fairly good accuracies with fewer numbers of subjects may not represent a robust solution for larger populations, as there is increased risk of hacking the system. Yeom et al. [73] proposed performing subject-specific stimulation to overcome such problems.

- *Computational cost*

Generally, computational cost depends on several factors, including feature-extraction algorithms, machine learning or pattern recognition algorithms, task complexity, and number of channels. Combination of several extracted features can increase accuracy even if the classification takes a long time to process. Methods can be selected according to requirements of the system.

- *Stability of EEG patterns over time*

Some EEG signal patterns for specific stimuli can change over time. In particular, accuracy of systems trained by preference-based tasks [5] can degrade as user tastes change. Some studies [66] collected data over a long period of time to confirm persistence. In practical situations, training such a system is laborious, since training data must be collected for a considerable time period to ensure permanency.

- *Changeability of EEG-based biometrics*

Conventional biometrics cannot be changed because they are fixed attributes of humans, but username-password system credentials can be changed. However, EEG-based biometrics can be used either way. Suggested tasks of most studies assume changeable brain activities. Even though an EEG signal pattern differs from person to person, the task can be changed to ensure protection of an asset [5]. The proposed system of Yeom et al. [73] mentioned above cannot be changed because it uses subject-specific stimulation.

3.5 Limitations

As discussed in this chapter and Chapter 2, EEG-based biometric system have several advantage over legacy systems. Even though most proposed approaches have achieved highest accuracy, still such a system is not available for practical use. Permanence is one of the important property of biometric system, but there are still no proofs of stability over long time span. Anokhin et al. [74] examined and confirmed the hypothesis that EEG dimension steadily increases with age by analysing resting EEGs of 5 age groups from 7 to 60 years, confirming that there can be issues when EEG biometrics use for long time. In addition, EEG sensors need to contact with the skull, and the preparation time is longer than other modalities even if consumer-grade, portable headsets are available.

This page intentionally left blank.

4

Feature Extraction with IHAR

4.1 Introduction

Association between electroencephalography (EEG) and individually personal information is being explored by the scientific community. Though person identification using EEG is an attraction among researchers, the complexity of such sensing limits using such technologies in real-world applications. In this research, the challenge has been addressed by reducing the complexity of the brain signal acquisition and analysis processes. This was achieved by reducing the number of electrodes, simplifying the critical task without compromising accuracy. Event-related potentials (ERP), a.k.a. time-locked stimulation, was used to collect data from each subject's head. Following a relaxation period, each subject was visually presented a random four-

digit number and then asked to think of it for 10 seconds. Fifteen trials were taken with each subject with relaxation and visual stimulation preceding each mental recall segment. We introduce a novel derived feature, dubbed Inter-Hemispheric Amplitude Ratio (IHAR), which expresses the ratio of amplitudes of laterally corresponding electrode pairs. The extracted feature set was tested with several machine learning (ML) algorithms, including Linear Discriminant Analysis (LDA), Support Vector Machine (SVM), and k-Nearest Neighbor (kNN). Most of the ML algorithms showed 100% accuracy with 14 electrodes, and according to our results, perfect accuracy can also be achieved using fewer electrodes. Surprisingly, the relaxation phase manifested the highest accuracy compared to other phases.

4.2 Experimental framework

Each experimental trial included three main phases — relaxation, visual stimulation, and mental recall — as shown in Fig 4.2. Calm music (“Magic Forest,” by Alexander Blu) was used to relax each subject with closed eyes for 10 s. Then a four-digit random number (white characters on black background) was shown on a screen (17 inches LCD monitor, 1366×768 pixel resolution) for 10 s. Finally, the subject was instructed to imagine the number seen on the screen for 10 s with closed eyes. The four-digit number was used assuming it helps to evoke more distinctive brain signal patterns in visual and mental recall phases. A single trial consisted of these three phases, and trials were recorded continuously with 128 Hz sampling rate. For each subject, 15 trials were conducted, separating trials using time-stamped markers. An inconvenience of the wet electrode system is that the electrodes dry out over time, lowering signal quality. Therefore, the time allocated to each subject was determined by the interval which allowed consistent signal quality.

4.2.1 Pre-processing and Visualization

One way of visualizing collected EEG data is by plotting a topographic distribution. Even though topographs are usually used in geomatics, here the power distribution is plotted as the third dimension (instead of elevation) as a contour map. First, the data was normalized and

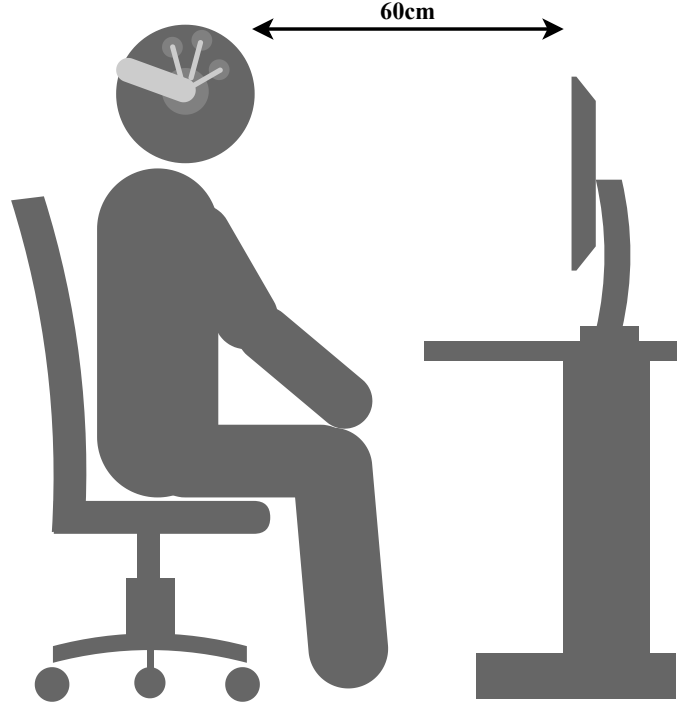


Figure 4.1: Experimental setup

converted to the frequency domain, using Discrete Fourier Transform (DFT) to calculate the power of each channel:

$$\hat{x}[n] = \frac{x[n] - \min(x)}{\max(x) - \min(x)}, \quad (4.1)$$

where $x[n]$ is a sequence of raw samples and $\hat{x}[n]$ is the corresponding vector of normalized samples. The DFT is calculated as

$$\hat{X}[k] = \sum_{n=0}^{N-1} \hat{x}[n] e^{-j(\frac{2\pi}{N})nk}, \quad (4.2)$$

where $\hat{X}[k]$ are the frequency-domain coefficients, N is the window size, and $k = 0, 1, 2, \dots, N-1$.

1. Finally power is calculated as

$$P = \hat{X} \cdot \overline{\hat{X}} = \sum |\hat{X}[k]|^2, \quad (4.3)$$

where $\overline{\hat{X}}$ is the complex conjugate of the sample sequence, and P is power (strictly speaking, energy) of the channel. After calculating the power values, Natural Neighbor Interpolation

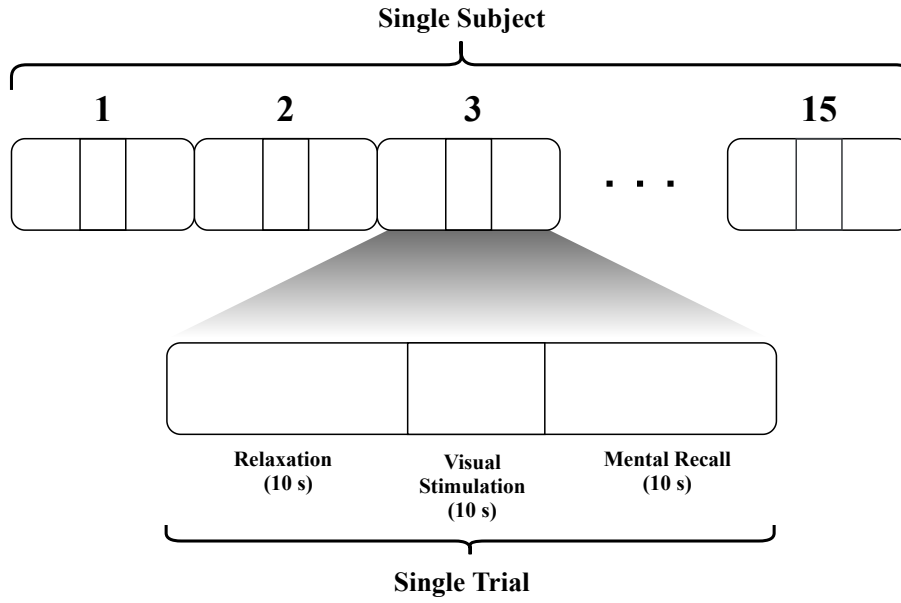


Figure 4.2: Structure of experiment: Each subject underwent 15 trials, and each trial comprised three phases. The stimulation phase necessarily precedes recall phase, and relaxation phase also serves as a refractory period, an implicit interval between trials, to be consistent with similar studies. (Each subject has tested for about 10 min.)

[75] is used to infer power values between the electrodes. Plotting the contours for the calculated values gives presumed topographic fields. Our MATLAB code is shared on GitHub.¹

The three trial phases (relaxation, visual stimulation, and mental recall) were separated from the continuous signals and saved as separate datasets. Each phase was set to fixed duration to maintain consistency, but the actual length differed slightly from phase to phase. Each phase for each trial for each subject had around 1280 samples because each signal was recorded at 128 Hz sampling rate for 10 seconds. The sample length of each phase was truncated to a fixed size (1280) by removing excess samples from the end. When using 14 electrode channels, each phase can be considered a 14×1280 matrix. Each phase set contains 180 trials, because 12 subjects were recruited and 15 trials were conducted for each subject. Fig 4.3 shows the topographic distribution plots of 12 subjects. Clear differences among these power distributions can be seen through this visualization. Every subject seems to have a uniquely personal brain wave patterns, even when performing the same task. Also, maximum and minimum power values differ from

¹<https://github.com/ijmax/EEG-processing/blob/master/topograph.m>

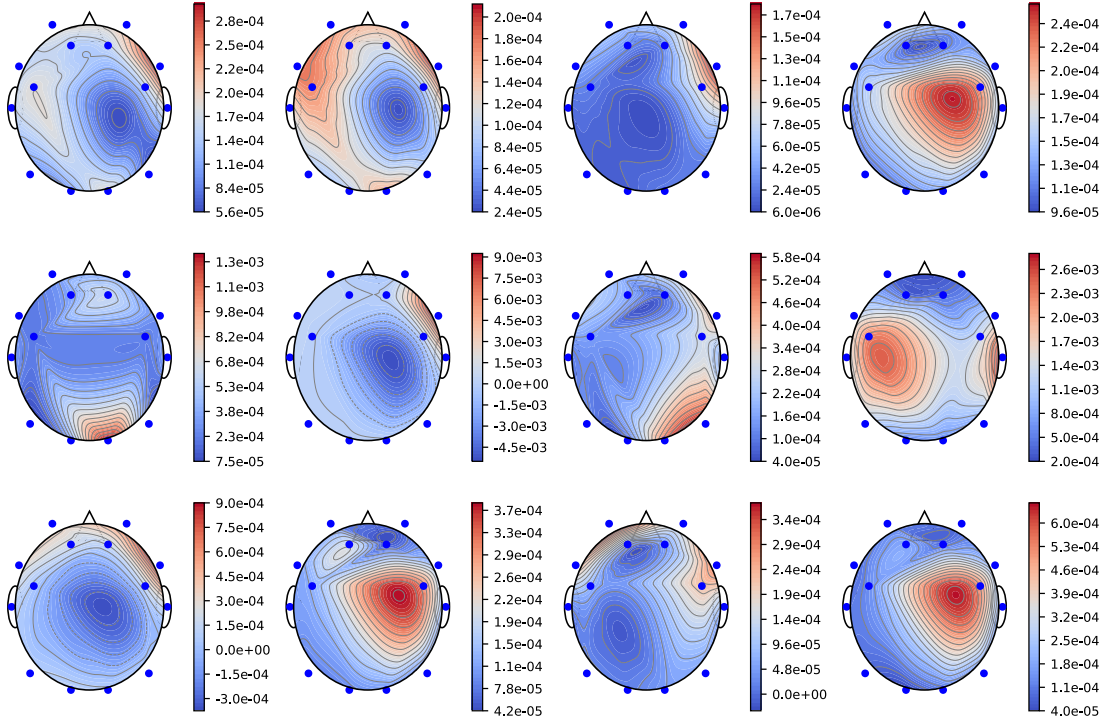


Figure 4.3: Topographic plots of 12 subjects for relaxation phase. (Maroon color represents high power values, and dark blue represents low.)

subject to subject.

4.3 Data Augmentation

Data augmentation is a technique to increase the diversity of training data to improve results and avoid overfitting without collecting new data. Due to lack of trials per subject in our experiment, data augmentation techniques were used to expand the dataset. These techniques are usually domain-specific. Therefore, three signal augmentation techniques which have been used to improve classification performance of wearable sensor data was used [76].

Fig 4.4 shows visualization of raw and augmented signals using following techniques:

- *Jittering*: This is a process of adding random noise to the signal. Normally distributed random noise was generated with standard deviation of 0.05.
- *Random downsampling*: In this process, some samples are randomly removed, interpolation of remaining samples recovering the original length of the signal.

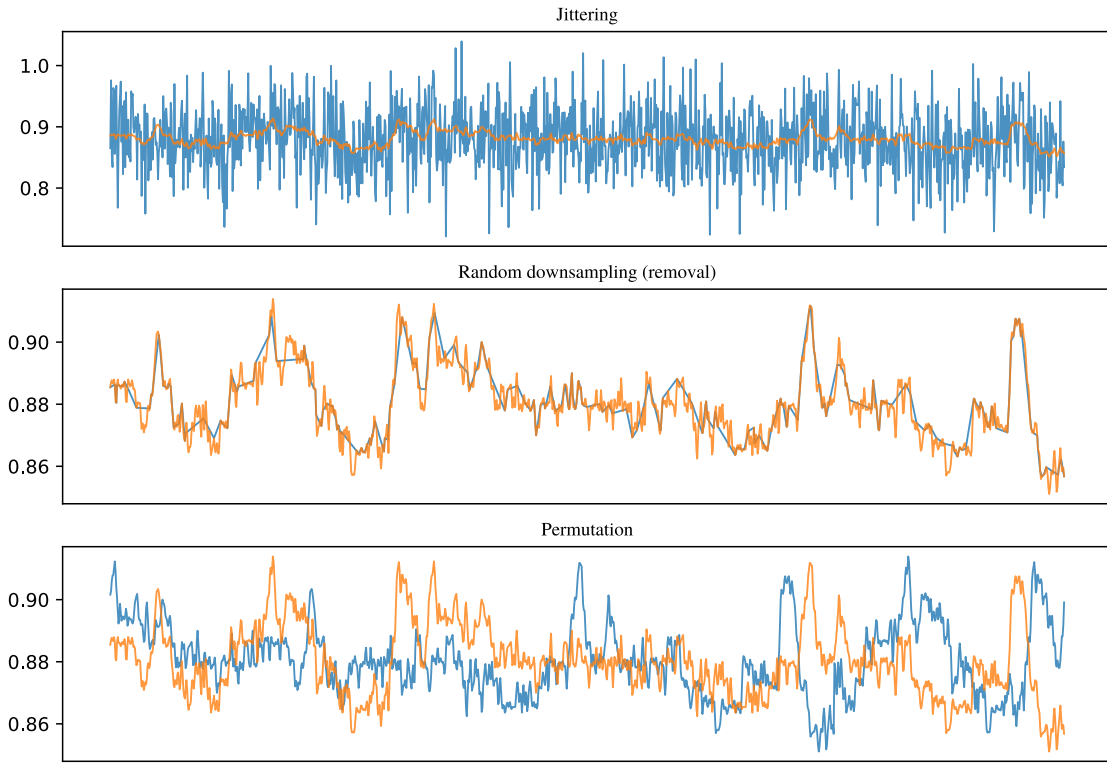


Figure 4.4: Visualization of raw and augmented signals subject to jittering, random downsampling (removal), and permutation techniques. Orange trace represents the original raw signal, and blue trace represents the augmented signal in each plot.

- *Permutation:* In this process, the temporal location of within-window events are randomly shuffled. 4 randomly selected segments with random length (minimum 5 samples) were altered randomly. To allow symmetry testing such as IHAR, time-wise alignment must be preserved, so the same permutation was applied to all 14 electrode channels.

Ten trials were separated after shuffling (to avoid bias from ordering such as learning effects) from each subject as training data and each 10 second trial was used to generate 10 instances from each augmentation technique, resulting 300 new trials. Final training set contained $12 \times 310 = 3720$ trials in total. Remaining 5 trials for each subject were kept as testing set. The same process was performed for all three phases.

Scatter plots of some selected features as seen in Fig 4.5 were used to confirm that distribution of features of augmented signals were not changed significantly. According to the scatter

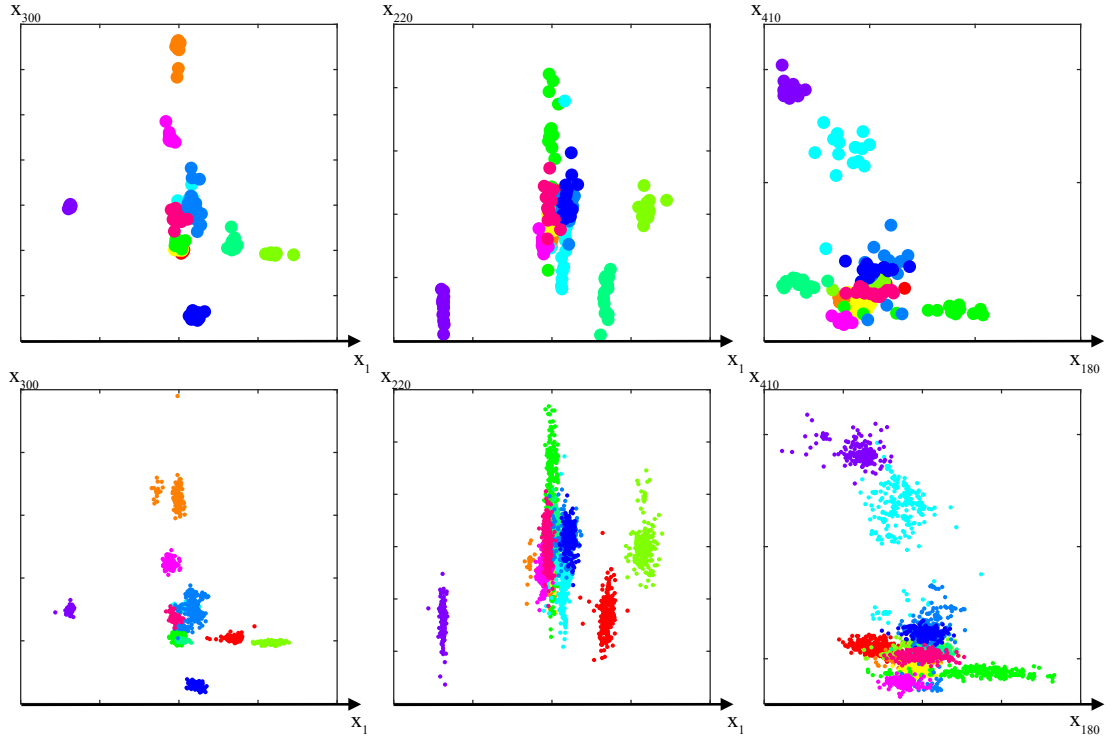


Figure 4.5: Distribution of features before and after the augmentation, using color to distinguish respective subjects. Top 3 plots show features of 10 training trials, while bottom 3 plots show corresponding features of augmented trials.

plots, augmentation has widened the margins of each class while preserving the separable nature of features.

4.4 Inter-Hemispheric Amplitude Ratio (IHAR) vs. other features (LC, WL, SSC, AR)

There is asymmetry between brain hemispheres [77]. In human neuroanatomy, brain asymmetry can be categorized into two classes: (a) neuroanatomical differences such as neuronal densities, size of regions, etc., and (b) functional differences [78]. Such asymmetry can be seen in the power distributions of EEG data. All standard electrode placement systems (10-20, 10-10, 10-5) are bilaterally symmetric across the inion-nasion line, the median or sagittal plane. Also, most experimental results have shown that time-domain data contains discriminative as-

pects such as Autoregressive (AR) features [79], matching peaks [80] [5], and statistical features [81]. IHAR is also calculated in the time domain, and symmetric electrode pairs are needed. The proposed feature extraction method has two stages: (1) smoothing and (2) calculating ratio of corresponding channel pairs. Instead of using frequency-domain low-pass filtering for smoothing, a moving average (MA) filter [82] was used to remove high frequencies and random noise. The MA filter, applied in our analysis only for the IHAR feature, is an efficient way of extracting low-frequency signals compared to frequency-domain low-pass filters. It can also be calculated quickly, so is appropriate for modest embedded systems, such as anticipated practical deployment. Furthermore, power line noise can be easily removed from a captured raw signal [83].

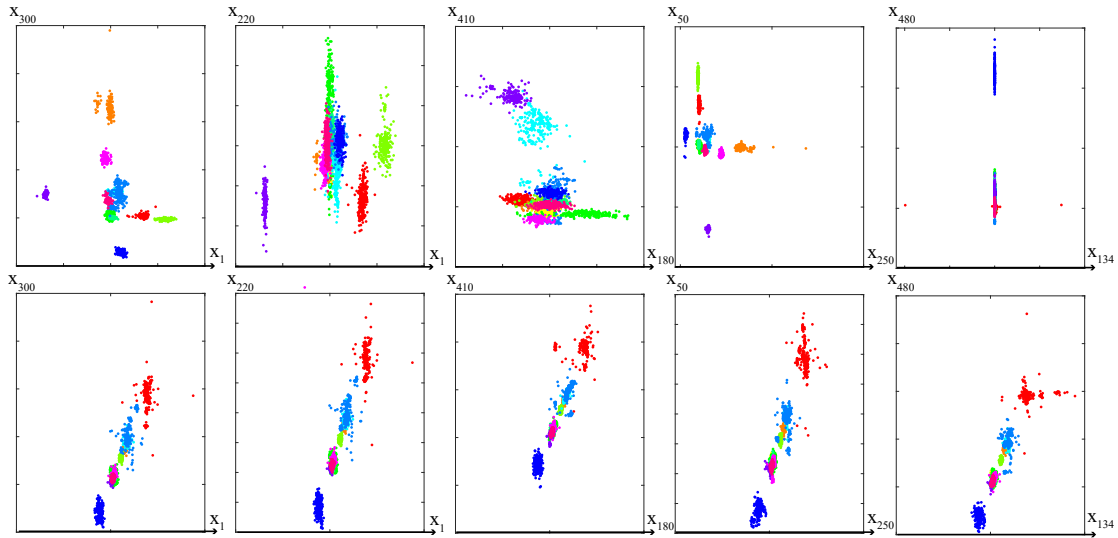


Figure 4.6: Comparison of selected feature distribution of IHAR and LC. Top 5 show scatter plots of IHAR, while bottom 5 plots show LC of corresponding feature pairs.

A similar derived parameter, dubbed “laterality coefficient” (LC), had been introduced [84] to study motor rehabilitation after a stroke. However, LC has not been used to find subjective differences among human subjects. Comparison of feature distribution of LC and IHAR can be seen in Fig 4.6. The same feature pair for both IHAR and LC were plotted, and IHAR showed more discrimination compared to LC as suggested by heterogeneous distributions across varied feature pairs.

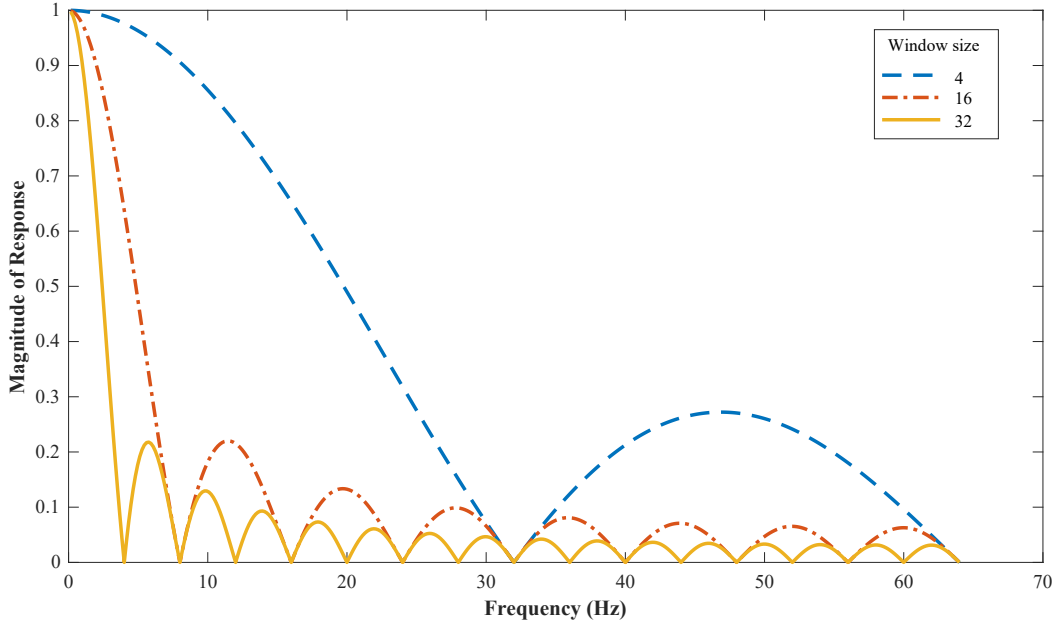


Figure 4.7: Frequency response of the MA filter with various window sizes

Fig 4.7 shows the frequency response for a MA filter with three different window sizes. Three comprehensive analyses were performed, for window sizes 4, 16, and 32. Unlike other low-pass filters, MA filter does not have a sharp cut-off. The frequency response of an MA filter can be expressed as

$$H(\omega) = \frac{1}{L} \left(\frac{1 - e^{-j\omega L}}{1 - e^{-j\omega}} \right), \quad (4.4)$$

where angular frequency $\omega = 2\pi f$, $e^{-j\omega}$ is complex phasor of filter transfer function, and L is window size. As seen in Fig 4.7, when the window size is 4, the cut-off frequency (at which magnitude is attenuated by 3 dB so full-scale gain is $1/\sqrt{2} \approx .7$) is ~ 15 Hz ($f_s = 128$ Hz), so the passband includes Delta (δ), Theta (θ), and Alpha (α) frequency ranges. Only δ band can be extracted when window size 16 or 32 is used. Most cognitive tasks, including relaxation and mental recall, produce low-frequency EEG signals [85]. Therefore, the above-mentioned window sizes were used to extract information in low-frequency signals. Furthermore, this filtering process eliminates power line noise, which “hum” lies between 50–60 Hz. The MA filter can

be expressed as

$$x_A[n] = \frac{1}{L} \sum_{k=0}^{L-1} x[n+k], \quad (4.5)$$

where L is the window size, and $x[\cdot]$ are the time-domain samples. Finally, IHAR is calculated by dividing samples of a left channel by samples of its corresponding right channel:

$$x_{\text{IHAR}}[i, \tilde{n}] = \frac{x[\text{left}[i], \tilde{n}]}{x[\text{right}[i], \tilde{n}]}, \quad (4.6)$$

where $i = 1, 2, \dots, 7$ or total number of channel pairs, $\tilde{n} = 1, 2, \dots$, total samples in the phase sequence. $\text{left}[\cdot]$ & $\text{right}[\cdot]$ are left and right channels lists arranged to align corresponding bilateral pairs, as in

$$\begin{aligned} \text{left} &= \text{AF3, F7, F3, FC5, T7, P7, O1;} \\ \text{right} &= \text{AF4, F8, F4, FC6, T8, P8, O2.} \end{aligned}$$

For simplicity, henceforth the “IHAR” subscript is elided, and x is understood to refer to x_{IHAR} .

To validate performance of the proposed feature, several time-domain features were calculated for comparison:

- *Laterality Coefficient (LC)*: ratio of difference and sum of a bilateral EEG pair, $(L - R)/(L + R)$.
- *Waveform Length (WL)*: cumulative length of a particular segment of a signal.
- *Slope Sign Change (SSC)*: number of times the slope of a signal changes its sign.
- *Auto-regressive coefficients (AR)*: AR modeling is a process of predicting future values based on past values of time series data. Scalar values which model the prediction.

Except for LC, these features have especially been used in EMG analysis studies, including limb movement classification. Geethanjali et al. [86] conducted a performance comparison of some of these features using LDA classifier and obtained 67–100% accuracy range for pair-wise

mental tasks classification. Each feature was extracted using a sliding window similar to MA filter process applied in our calculation of IHAR, so the extraction process was consistent for all features types. To calculate these four comparing features, some functions in “Myoelectric control development toolbox” developed by Chan et al. [87] were used. No smoothing, low-pass filtering, or averaging was applied to these compared features (besides IHAR).

When calculating each of these four features, the kernel window convolves through rows of the trial phase matrix (14×1280). The size of the output matrix after feature calculation depends upon the window size. Then the output matrix is flattened in row-major order to make a feature vector and fed to a classifier.

4.5 Classification

The extracted feature set was tested with several ML techniques to determine which algorithms show high accuracy for person identification. Unlike authentication, person identification is a straightforward classification problem, so traditional ML algorithms can be applied. Not knowing a priori which are best suited for this problem domain, we compared four well-known techniques.

4.5.1 Linear Discriminant Analysis (LDA)

LDA [88, 89] is most commonly used as a dimensionality reduction method, similar to Principal Component Analysis (PCA). Assuming equal covariance for each class, and that conditional classes are multivariate, the LDA discriminant function $\delta_k(x)$ (which separates inferred classes) can be defined as in Eqn. 4.7 and the classification rule shown in Eqn. 4.8:

$$\delta_k(x) = \log \pi_k + x^T \Sigma^{-1} \mu_k - \frac{1}{2} \mu_k^T \Sigma^{-1} \mu_k, \quad (4.7)$$

where π_k denotes the prior probability that an observation belongs to the k th class, Σ is the common covariance matrix (not to be confused with the \sum operator for summation), and μ_k is the mean of class k . The classification rule can be defined as

$$\hat{G}(x) = \arg \max_k (\delta_k(x)). \quad (4.8)$$

4.5.2 Quadratic Discriminant Analysis (QDA)

The main difference of QDA from LDA is that QDA relaxes the assumption that the inputs of every class have the same covariance. Also, class decision boundaries are not linear but quadratic [90]. Eqn. 4.9 shows the QDA discriminant function. The classification rule is the same as that for LDA.

$$\delta_k(x) = \log \pi_k - \frac{1}{2}(x - \mu_k)^T \Sigma_k^{-1} (x - \mu_k) - \frac{1}{2} \log |\Sigma_k|, \quad (4.9)$$

where Σ_k is the covariance matrix of the k th class.

4.5.3 Support Vector Machine (SVM)

SVM, a.k.a. Support Vector Network, is also a classification technique, finding the hyperplane which maximizes the margin between two classes [91]. So-called support vectors define the hyperplane that makes the separation. Linear, polynomial, Radial Basis Function (RBF), and sigmoid are the basic types of SVM kernels [92]. The SVM decision function can be expressed as

$$f(x) = \text{sign} \left(\sum_{i=1}^N \alpha_i y_i K(x_i, x) + b \right), \quad (4.10)$$

where N is the size of training data, K is the kernel function that measures similarity between x_i (support vector) and x (feature values), α_i is Lagrange multiplier, y_i represents the membership class of each datum (± 1), and b is a numeric constant. We used linear, polynomial, and RBF kernels to determine accuracy of the extracted features, respectively described following.

Linear SVM: a linear kernel was used, and its kernel function can be expressed as inner

(“dot”) product of support vector and feature values:

$$K(x_i, x) = x_i^T \cdot x. \quad (4.11)$$

Quadratic and cubic ($d = 2$ and 3) SVM polynomial kernels were used,

$$K(x_i, x) = (x_i^T x + c)^d, \quad (4.12)$$

with $c = 1$ for both cases.

Medium and Coarse Gaussian SVM: An RBF kernel function was used with $\sigma = 16$ and 64 :

$$K(x_i, x) = \exp\left(-\frac{\|x_i - x\|^2}{2\sigma^2}\right), \quad (4.13)$$

where $\|x_i - x\|$ is Euclidean distance, and standard deviation σ determines the width of the Gaussian kernel.

4.5.4 k-Nearest Neighbor (kNN)

kNN is the simplest machine learning algorithm, measuring distance to a given data point. k stands for the number of neighbors which should be taken into account, and accuracy can be varied by adjusting its value. There are several distance measurements, including Euclidean distance (Eqn. 4.14):

$$d(x, x') = \|x - x'\| = \sqrt{\sum_{i=1}^k w_i (x_i - x'_i)^2}, \quad (4.14)$$

where $d(x, x')$ is the distance between points x and x' , and w_i is edge weight.

kNN ($k = 1$) with Euclidean distance with equal weights were used in this analysis.

After extracting the IHAR feature, accuracy was tested in several ways. First we tested three phases with all 14 electrodes (7 electrode pairs). Further, accuracy was checked for three trial

phases while reducing the number of electrodes. An augmented training dataset (3720 trials) was used to train all the above-discussed ML models, and remaining 60 trials (5 trials per each subject) with original signal data was used to test the models.

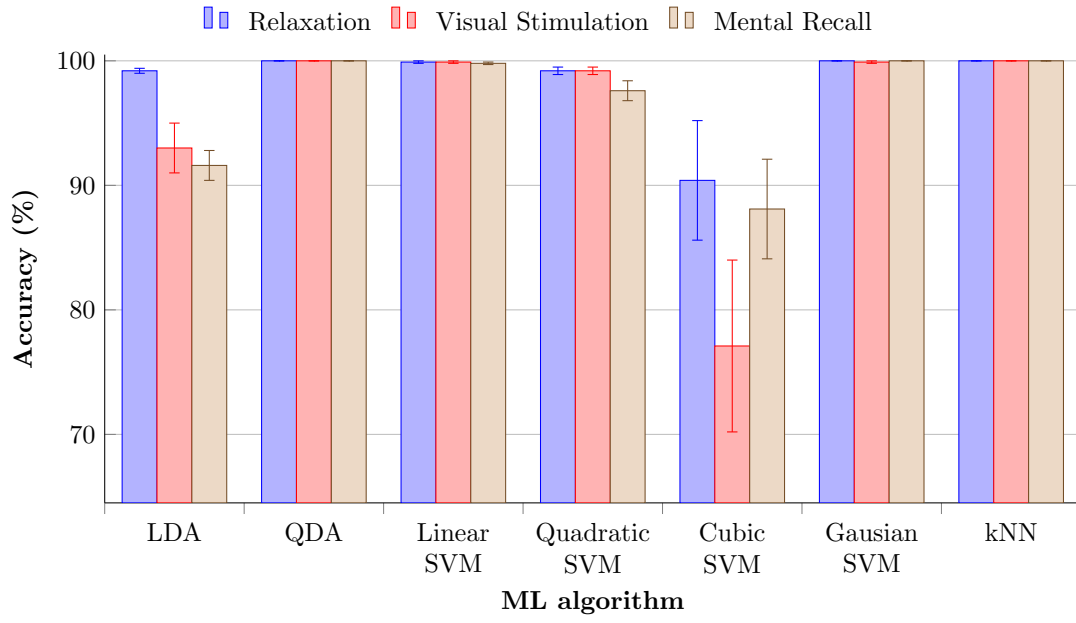
K-fold cross-validation with 10 folds was used to validate the trained model. Accuracy was calculated as the ratio of correctly classified trials to all testing trials.

4.6 Results

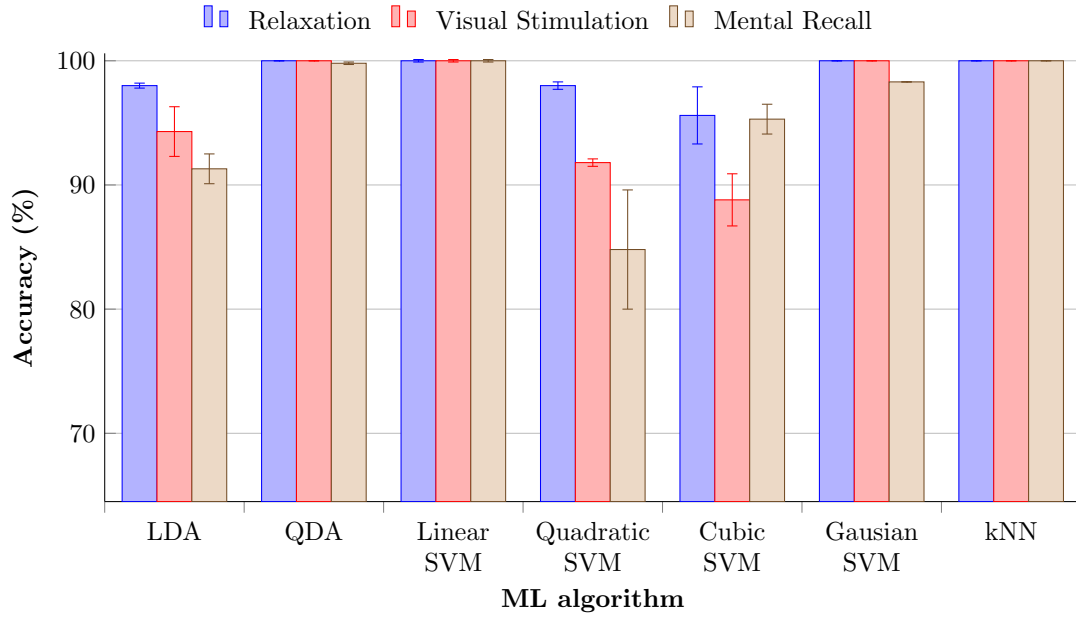
After separating three trial phases from each single EEG signal, each phase was visualized using a custom MATLAB script. Fig 4.3 depicts the distribution of power of the relaxation phase, over crania of 12 subjects, showing some differences after channel-wise normalization (linear scaling with bias to remap to 0–1). Original unipolar (unbalanced) unsigned electrode data remain so after normalization. Clear asymmetry can be observed across all the nasion-inion lines. The EMOTIV Epoc+ headset uses mastoid bones as reference electrodes which helps to maintain a fair alignment of electrodes. Moreover, symmetry of electrodes was roughly checked by measuring distances from the sagittal line before recording. However, phrenology discredited measurement of head shapes, and the helmet, cap, or headset were sometimes not perfectly aligned with the subject’s sagittal plane. Perfectly consistent electrode alignment is practically impossible (without extreme invasive techniques such as Neural Lace [93]).

Data augmentation is used in machine learning when the training dataset is significantly small. Even if large number of trials provide more reliable classification results, such collection reduces the practicality in this domain. Therefore, data augmentation provides extra convenience to users when they record their brain signals for training. In this experiment, augmentation techniques and parameters were selected heuristically. However, drastic changes of parameters could affect classification results.

Validation and testing accuracies of the three phases with 14 electrodes for the above-discussed machine learning techniques are shown in Fig 4.8. The data of each subject was trained against that of every other subject, which creates $N(N - 1)/2 = 66$ classifiers, the so-called One-vs.-One (OVO) multiclass classification method. This method shows slightly better accuracy than



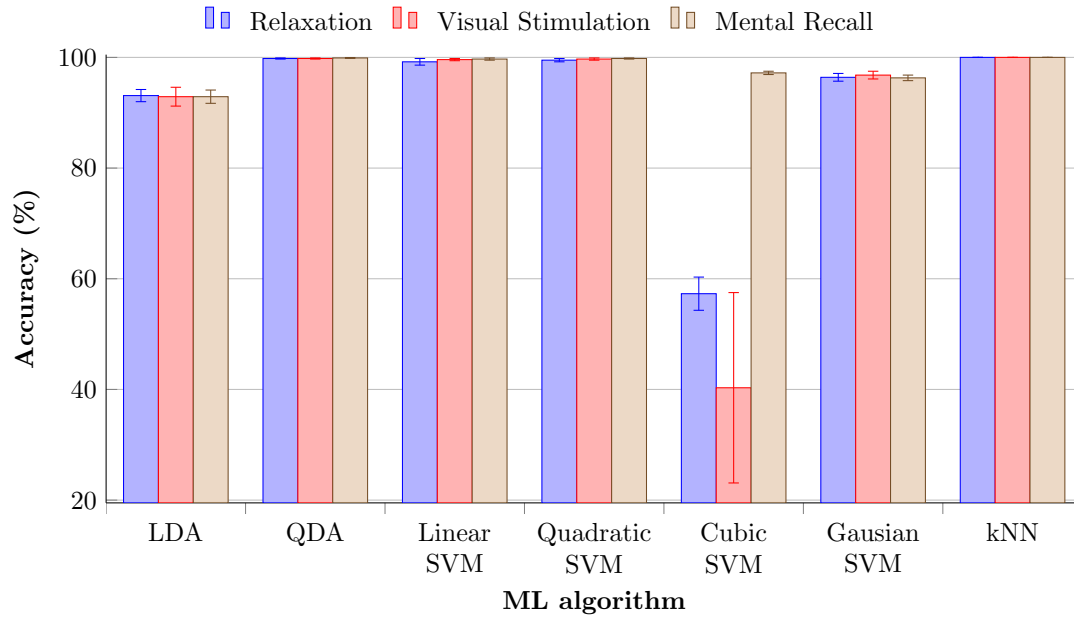
(a) Validation accuracies



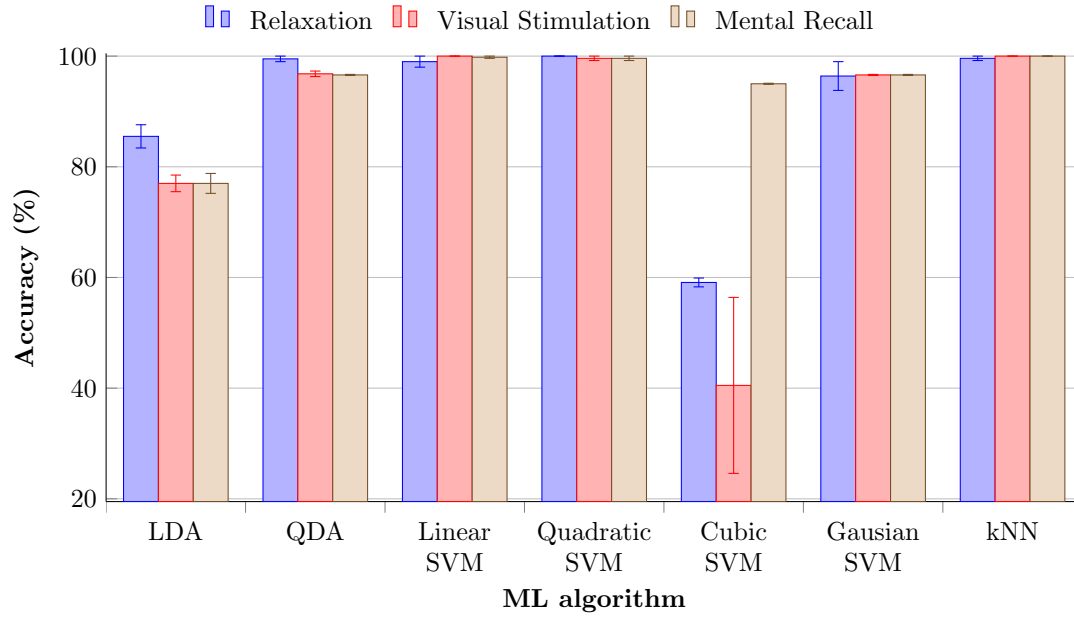
(b) Testing accuracies

Figure 4.8: Accuracy of three phases with 14 electrodes for various Discriminant Analysis, Support Vector Machine, and k-Nearest Neighbor techniques with OVO method

One-vs.-All (OVA). Validation and testing accuracies for the same data set with OVA method can be seen in Fig 4.9. OVO is usually better than OVA because class imbalance occurs us-



(a) Validation accuracies



(b) Testing accuracies

Figure 4.9: Accuracy of three phases with 14 electrodes with OVA method

ing OVA method even if it is faster in training. QDA, linear SVM, Gaussian SVM, and kNN showed the highest validation accuracy for all three phases. The testing results also were close to 100% for the same ML techniques. Furthermore, relaxation phase showed higher validation

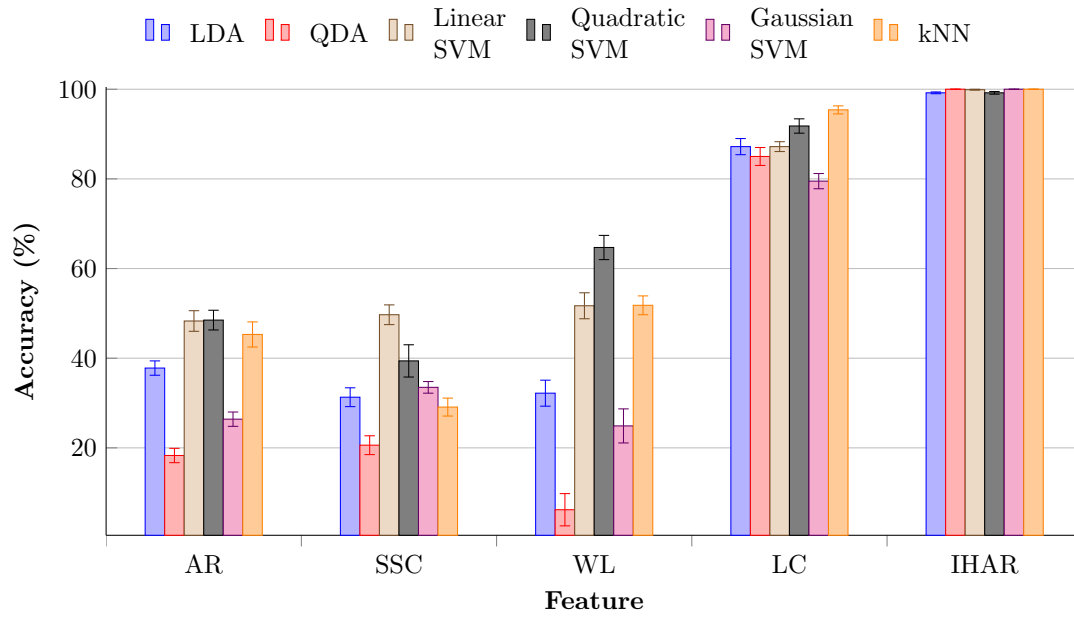
and testing accuracy than other phases. Signal patterns evoked in the relaxation phase seem more stable compared to those from the other phases. Lateral asymmetry or energy difference of alpha activity between two hemispheres during the relaxation explains the high performance of relaxation phase [94]. Quadratic SVM showed better validation accuracy, but testing accuracy was slightly lower. Even though cubic SVM achieved lowest validation accuracy among all techniques, testing accuracy was lightly increased. The relaxation phase generally yielded highest accuracy with OVO method.

Comparison of performances with other time-domain features for same conditions is shown in Fig 4.10. All 14 channels were used to test each feature extraction method. While IHAR achieved highest accuracy, LC was the next best-performing feature, achieving $95.4 \pm 0.9\%$ validation accuracy for kNN classifier, and $83.3 \pm 0.1\%$ maximum testing accuracy for QDA. The conceptual similarity of the LC feature to proposed IHAR explains why it achieved comparable results, especially for validation (but not testing). AR, SSC, and WL showed less than 50% validation accuracies for most of the ML techniques. Even though the AR feature has been used in many EEG-related studies, it did not show considerable results for any classifier.

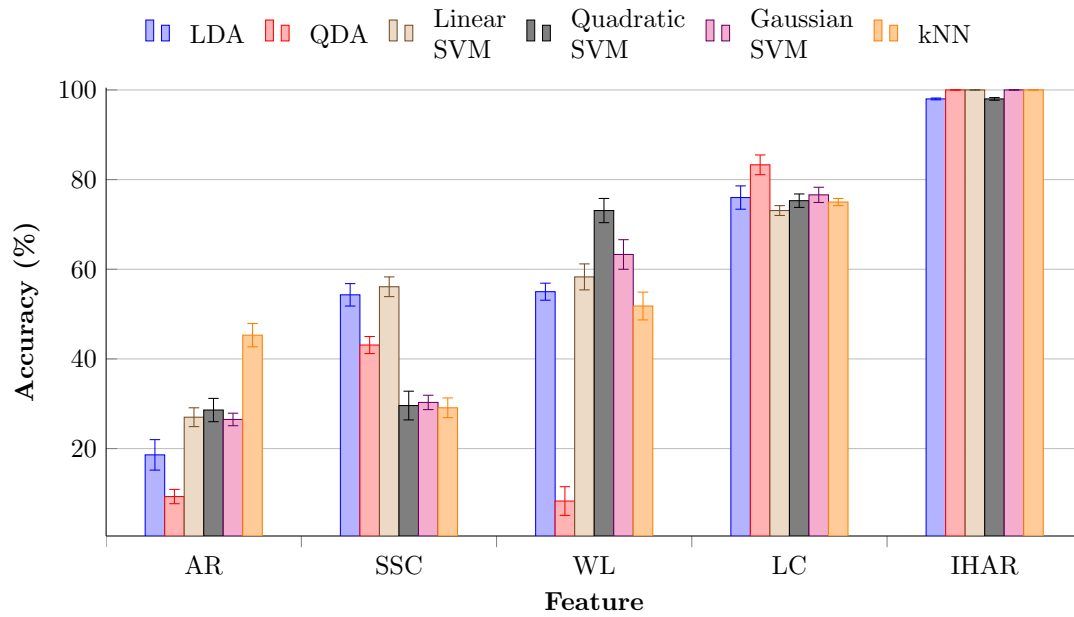
Table 4.1: Accuracy of each electrode pair for three task phases (white: relaxation; light gray: visual task; dark gray: mental recall) for various analysis techniques. Significant accuracies are emboldened.

ML algorithm	AF3-AF4		F7-F8		F3-F4		FC5-FC6		T7-T8		P7-P8		O1-O2	
	VA	TA	VA	TA	VA	TA	VA	TA	VA	TA	VA	TA	VA	TA
LDA	86.7 \pm 1.9	70.5 \pm 2.2	91.8 \pm 1.4	83.5 \pm 1.4	67.6 \pm 1.5	50.1 \pm 2.4	94.3 \pm 1.4	87.4 \pm 1.2	82.0 \pm 1.6	69.1 \pm 2.2	80.2 \pm 1.3	65.0 \pm 1.5	65.2 \pm 2.2	47.1 \pm 2.4
	85.0 \pm 1.4	76.1 \pm 1.3	91.2 \pm 1.3	85.3 \pm 1.8	62.9 \pm 1.8	50.8 \pm 2.5	90.2 \pm 1.5	78.0 \pm 1.7	77.2 \pm 2.3	55.0 \pm 2.2	79.3 \pm 2.2	75.8 \pm 3.2	62.3 \pm 2.4	51.1 \pm 1.7
	86.9 \pm 1.6	73.6 \pm 1.8	92.1 \pm 1.1	74.6 \pm 1.7	67.3 \pm 1.6	60.0 \pm 1.3	93.4 \pm 0.8	89.1 \pm 0.8	78.9 \pm 1.9	59.8 \pm 1.4	79.8 \pm 1.9	77.8 \pm 2.0	68.6 \pm 2.6	59.3 \pm 2.2
QDA	86.0 \pm 1.2	73.3 \pm 1.5	94.9 \pm 1.0	88.3 \pm 2.1	60.2 \pm 2.7	57.1 \pm 2.3	91.8 \pm 0.8	94.7 \pm 1.1	79.0 \pm 1.6	80.6 \pm 2.1	78.8 \pm 1.7	73.3 \pm 2.6	59.8 \pm 1.3	55.3 \pm 3.2
	81.4 \pm 2.1	90.1 \pm 0.5	86.1 \pm 1.7	83.5 \pm 1.2	50.8 \pm 3.1	62.8 \pm 0.8	88.5 \pm 1.7	82.3 \pm 0.8	75.8 \pm 1.5	76.0 \pm 0.8	75.4 \pm 1.7	72.5 \pm 1.1	55.8 \pm 3.1	51.0 \pm 1.4
	85.1 \pm 1.8	84.0 \pm 1.4	94.3 \pm 1.3	81.5 \pm 0.5	55.0 \pm 2.7	55.3 \pm 2.1	94.9 \pm 1.1	92.0 \pm 0.1	76.5 \pm 2.0	68.5 \pm 0.5	78.1 \pm 1.7	76.8 \pm 0.9	63.1 \pm 1.7	59.3 \pm 0.8
Linear SVM	89.1 \pm 1.4	74.6 \pm 1.8	93.1 \pm 1.1	89.1 \pm 2.3	70.2 \pm 2.3	47.8 \pm 2.3	95.1 \pm 1.1	86.3 \pm 2.2	84.0 \pm 1.1	68.8 \pm 2.6	83.1 \pm 2.3	61.3 \pm 2.3	70.6 \pm 2.5	43.5 \pm 2.8
	86.5 \pm 1.2	73.6 \pm 1.5	92.7 \pm 1.2	83.1 \pm 1.6	65.8 \pm 2.1	52.5 \pm 2.5	90.9 \pm 0.5	79.3 \pm 1.6	80.6 \pm 1.1	57.1 \pm 1.7	82.0 \pm 1.8	73.3 \pm 2.6	64.6 \pm 2.1	47.5 \pm 2.7
	88.7 \pm 1.3	75.0 \pm 2.3	93.8 \pm 1.4	82.8 \pm 1.9	69.0 \pm 3.1	61.3 \pm 1.3	94.1 \pm 1.0	90.0 \pm 0.1	80.6 \pm 1.3	61.6 \pm 1.3	81.6 \pm 2.1	76.1 \pm 2.3	70.9 \pm 2.4	57.3 \pm 1.7
Quadratic SVM	93.1 \pm 1.3	80.5 \pm 1.2	95.3 \pm 1.5	85.3 \pm 2.6	79.2 \pm 1.5	57.0 \pm 2.3	96.6 \pm 0.1	83.1 \pm 1.1	89.1 \pm 0.1	77.3 \pm 2.1	89.7 \pm 1.2	74.1 \pm 1.7	81.9 \pm 2.3	60.0 \pm 2.2
	89.1 \pm 1.4	76.1 \pm 1.5	96.0 \pm 1.1	85.8 \pm 0.8	76.3 \pm 1.1	62.5 \pm 1.4	95.3 \pm 0.7	84.5 \pm 1.1	87.4 \pm 1.2	68.3 \pm 1.9	86.8 \pm 1.5	74.8 \pm 2.2	76.8 \pm 2.2	65.8 \pm 3.4
	92.7 \pm 1.1	82.5 \pm 2.5	96.5 \pm 0.6	78.5 \pm 1.2	78.5 \pm 2.5	67.1 \pm 1.1	96.9 \pm 0.8	94.3 \pm 0.8	88.1 \pm 1.6	73.3 \pm 3.0	87.6 \pm 1.9	74.8 \pm 2.7	78.2 \pm 2.8	53.3 \pm 2.4
Gaussian SVM	79.1 \pm 1.6	69.1 \pm 1.2	86.9 \pm 1.9	82.8 \pm 2.6	54.0 \pm 2.9	56.7 \pm 2.7	90.1 \pm 3.5	87.2 \pm 2.2	76.1 \pm 1.6	77.4 \pm 2.8	73.0 \pm 1.4	73.1 \pm 2.6	53.4 \pm 1.6	71.0 \pm 1.4
	78.6 \pm 1.3	77.6 \pm 0.8	84.3 \pm 1.5	83.3 \pm 0.1	46.3 \pm 1.7	49.1 \pm 1.1	81.2 \pm 1.2	82.8 \pm 1.1	66.4 \pm 1.8	53.5 \pm 0.9	68.7 \pm 1.8	68.3 \pm 0.1	49.1 \pm 1.9	45.8 \pm 1.4
	76.9 \pm 0.9	83.1 \pm 0.5	91.6 \pm 1.3	85.0 \pm 0.1	48.4 \pm 2.2	50.3 \pm 1.0	90.5 \pm 1.6	93.3 \pm 0.1	71.2 \pm 0.8	52.3 \pm 1.1	73.1 \pm 1.5	63.3 \pm 1.1	54.1 \pm 1.9	47.6 \pm 1.1
kNN	95.6 \pm 1.2	75.0 \pm 1.2	98.1 \pm 0.5	88.0 \pm 2.1	86.1 \pm 2.1	51.1 \pm 3.6	97.2 \pm 0.9	85.6 \pm 1.3	93.7 \pm 1.1	72.0 \pm 1.9	93.6 \pm 0.4	67.9 \pm 3.1	89.4 \pm 1.2	59.1 \pm 2.7
	93.5 \pm 0.8	82.3 \pm 1.1	97.6 \pm 0.5	88.3 \pm 0.7	83.9 \pm 2.4	58.1 \pm 3.0	96.7 \pm 0.9	83.5 \pm 0.5	92.2 \pm 1.4	75.0 \pm 2.3	93.8 \pm 1.5	72.5 \pm 1.1	85.0 \pm 1.3	49.6 \pm 2.3
	94.1 \pm 0.5	87.8 \pm 1.3	98.1 \pm 0.5	88.1 \pm 0.9	85.8 \pm 1.8	62.8 \pm 1.7	97.2 \pm 0.4	94.6 \pm 0.5	91.4 \pm 0.8	65.5 \pm 1.7	93.4 \pm 1.4	65.5 \pm 1.7	86.6 \pm 1.3	60.5 \pm 2.6

After selecting the best ML algorithms among tested candidates, accuracy was checked for each electrode pair. Results can be seen in Table 4.1. The highest testing accuracy, $94.7 \pm 1.1\%$, was from the FC5-FC6 electrode pair for QDA with relaxation phase. According to the results, FC5-FC6 electrode pair yielded over 90% accuracy for most of the ML algorithms. Other frontal



(a) Validation accuracies



(b) Testing accuracies

Figure 4.10: Comparison of accuracy across features (AR: auto-regressive coefficients, SSC: slope sign change, WL: waveform length, LC: laterality coefficient, and IHAR: inter-hemispheric amplitude ratio) extracted during relaxation phase using all 14 electrodes

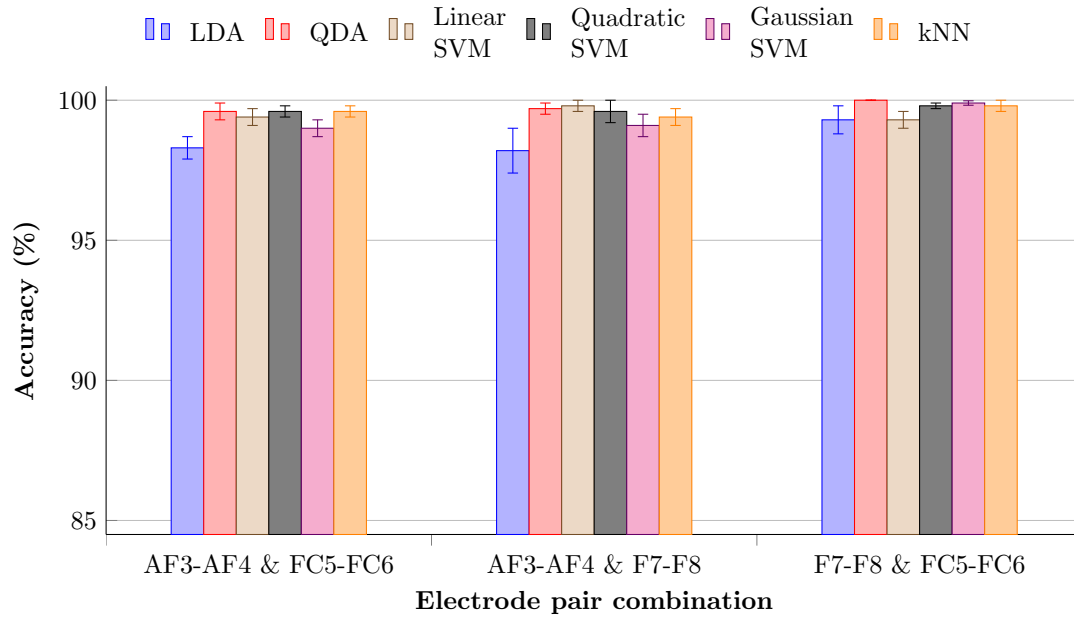
electrode pairs F7-F8 and AF3-AF4 were the next highest. Occipital electrodes (O1-O2) showed the worst accuracy, $43.5 \pm 2.8\%$ for the linear SVM with relaxation task. In addition, O1-O2

showed the worst testing accuracy even for the visual stimulation phase in contrast to most research findings [53, 54]. In most of the studies, so-called oddball stimulus has been used to get the P300 (positive peak at 300 ms after the stimulation) spike from the occipital area. In our study, the image (four-digit number) was shown without making any changes (blinking or switching with another image) as visual stimulation. This explains the poor performance of occipital electrodes for visual stimulation. Several studies have considered frontal asymmetry in cognitive processes of the brain [95, 96]. Our results also showed considerable accuracy for the frontal electrodes for relaxation and mental recall phases.

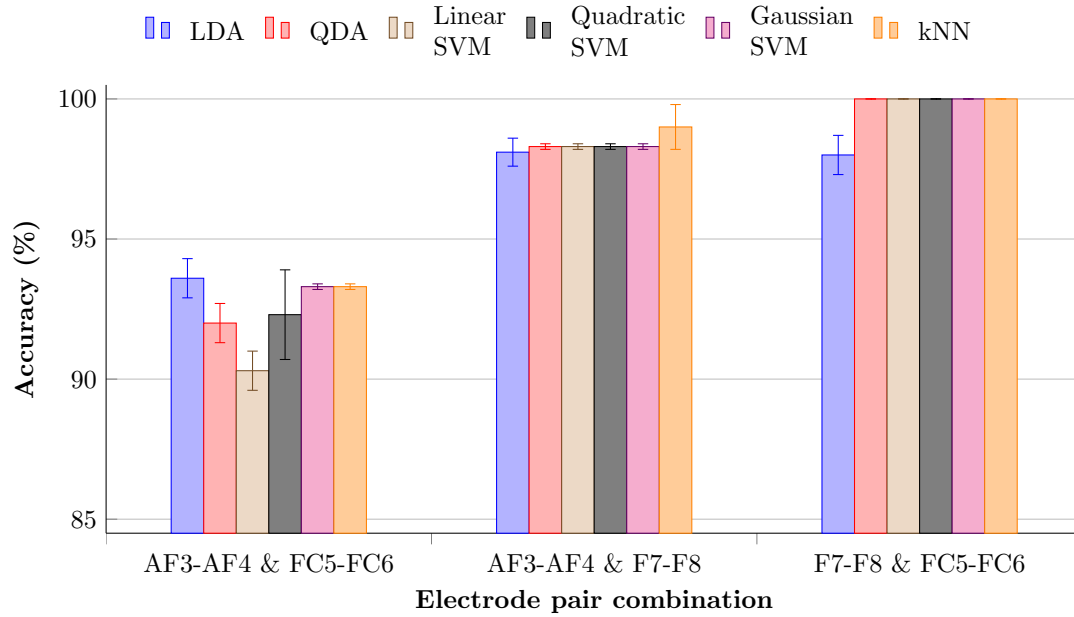
Table 4.2: Comparison of performances for different number of electrodes (ACC: Accuracy, FAR: False Acceptance Rate, and FRR: False Rejection Rate)

ML algorithm	FC5-FC6			AF3-AF4, FC5-FC6			AF3-AF4, F7-F8			F7-F8, FC5-FC6		
	ACC	SP	SE	ACC	SP	SE	ACC	SP	SE	ACC	SP	SE
LDA	87.4	100	78	93.3	100	98	98.1	100	98	98.1	100	98
QDA	94.7	100	98	92.0	100	96	98.3	100	100	100	100	100
Linear SVM	86.3	100	76	90.8	100	95	98.3	100	100	100	100	100
Quadratic SVM	83.1	100	96	91.5	100	98	98.3	100	99	100	100	100
Gaussian SVM	87.2	100	80	93.3	100	97	98.3	100	98	100	100	100
KNN	85.6	100	84	93.3	100	100	99.3	100	100	100	100	100

In order to increase accuracy further with minimum electrode setup, the model was trained again by considering sets of electrode pairs. 100% testing accuracy was shown by the four frontal electrodes (F7-F8 and FC5-FC6) for all classifiers except LDA. As seen in Fig 4.11, accuracy increases when combining other frontal electrode pairs. A Receiver Operating Characteristic (ROC) curve, created by plotting the true positive rate (TPR) against the false positive rate (FPR), was plotted for all subjects with F7-F8 and FC5-FC6 electrode combination. The AUC (area under the ROC curve) value of all classifiers was unity, which means the trained model was a perfect classifier. Considering user-friendliness of specific hardware design for EEG biometrics, the anterior frontal electrodes AF3-AF4 pair is better than FC5-FC6, which is nearer to the coronal center. Therefore, the AF3-AF4 and F7-F8 electrode setup also was tested, and $99.0 \pm 0.8\%$ (kNN), $98.3 \pm 0.1\%$ (QDA), $98.3 \pm 0.1\%$ (linear SVM), $98.3 \pm 0.1\%$ (quadratic SVM),



(a) Validation accuracies



(b) Testing accuracies

Figure 4.11: Accuracies of combination of 2 frontal electrode pairs which yielded higher accuracies

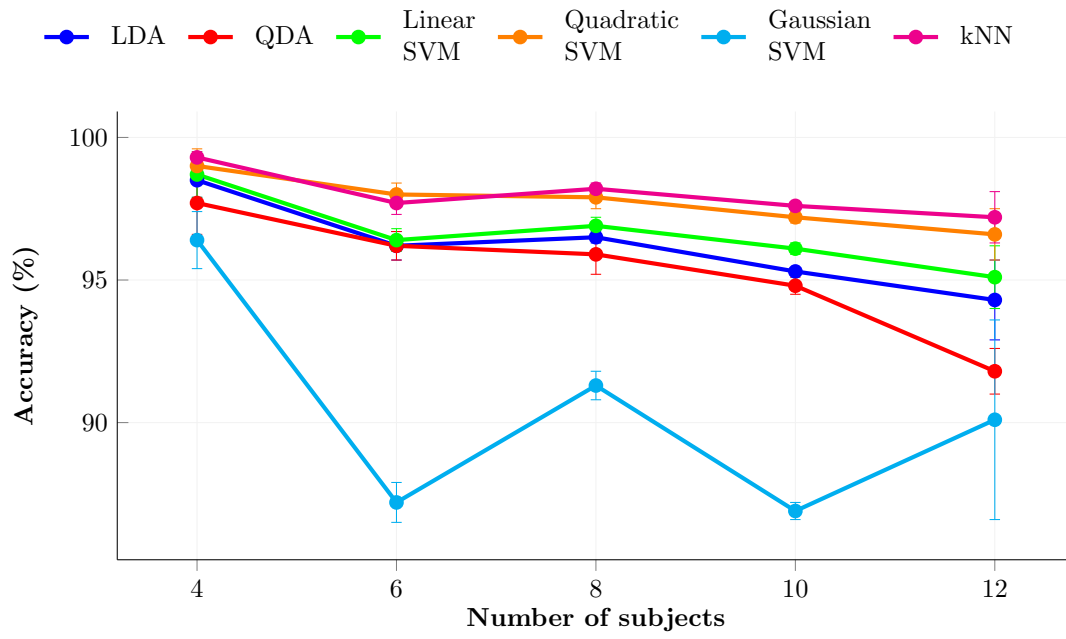
and $98.1 \pm 0.5\%$ (LDA) testing accuracies were achieved for relaxation phase. The average AUC value for these cases lies between 0.98 and 1. These results seem to accommodate lighter devices which require less calibration time, such as Muse [97]. Even though entire hemispheres

manifest asymmetry, the “frontal asymmetry” feature has been introduced in EEG analysis, calculated using frontal channels. Specifically, frontal asymmetry has been used in emotion and attention-related analysis [98, 99]. Since the frontal lobe is responsible for executive tasks [100], IHAR-based analysis for relaxation and mental recall phases shows high accuracy in frontal electrodes.

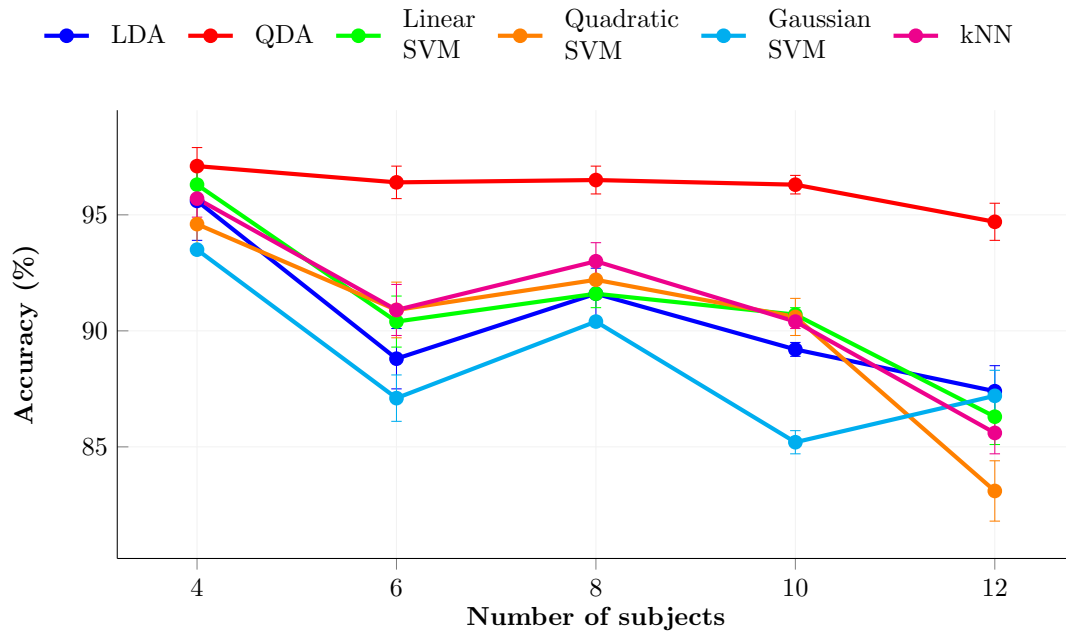
Specificity (true positive rate) and sensitivity (true negative rate) were calculated for electrode combinations which showed higher accuracies. Specificity is the ratio of number of trials that correctly classified as negatives to number of all negative testing trials, while sensitivity is the ratio of number of trials that correctly classified as positives to number of all positive testing trials. Models with high specificity values are better in the authentication domain because they decrease risk of granting access to imposters. As shown in Table 4.2, all electrode combinations achieved highest specificity value, which confirms suitability of IHAR method for this problem (better to tolerate occasional false rejection rather than allow false accepts).

More information can be captured using high-resolution EEG devices. Compared with consumer-grade devices, clinical grade devices have more electrodes. Even though high accuracy can be achieved with the help of many electrodes, lighter electrode setup provides more user-friendliness. As shown in Table 4.3, other approaches achieved high accuracy using more channels, for compound or complex tasks. Our approach achieved the same accuracy with only four frontal electrodes for a simple task. However, accuracy of the models cannot be guaranteed when increasing the number of subjects. Fig 4.12 shows the general degradation of accuracy while increasing the number of subjects. Average accuracy was calculated for 10 random combinations of subjects with FC5-FC6 electrode pair, which showed highest accuracy among other pairs. QDA classifier did not show rapid change of testing accuracy over increase of number of subjects. Therefore, it might be usable with more subjects without compromising accuracy significantly. In this study, 15 trials were conducted, but when increasing the number of subjects, number of trials also should be increased to maintain consistent accuracy.

Comparing the trial phases considered here, relaxation and mental recall showed higher accuracy. Selecting the simplest task among these three phases is complicated because there are



(a) Validation accuracies



(b) Testing accuracies

Figure 4.12: Variation of validation and testing accuracy for FC5-FC6 electrode pair of relaxation phase when increasing number of subjects using IHAR

merits and demerits for each. It is harder to concentrate or be relaxed in noisy environments, but visual stimulation would be easy. To stimulate the brain externally, some physical resource

Table 4.3: Comparison with other studies

Author	Electrodes	Task	Classified feature(s)	Classifier	Accuracy (%)
Ong et al. [52]	32	VEP	Power spectral density (PSD)	kNN	83.00
Alyasseri et al. [55]	6	Mental task (counting)	Multi-objective flower pollination algorithm with wavelet transform (MOFPA-WT)	ANN	85.12
Falzon et al. [53]	32	VEP	Frequency components up to 5th harmonic	kNN	91.70
Kouras et al. [101]	56	Sleep	Time domain descriptors (10), Frequency Domain Descriptors (17), Wavelet Domain Descriptors (4)	kNN	95.00
Fukami et al. [54]	4	VEP	5 frequency components	Mahalanobis distance	95.00
Yang et al. [56]	4	Motor movement, imagery	Wavelet log-DCT (WLD)	Fisher's Linear Discriminant	98.50
Kaewwit et al. [102]	4	Resting state	Combined ICA and AR	kNN	98.51
Arnau et al. [103]	32	Video stimulation	PSD	ANN	99.00
Thomas et al. [104]	19	Resting state	PSD	Mean correlation coefficients	99.00
Schetinin et al. [105]	64	Motor movement, imagery	Group Method of Data Handling (GMDH)	SVM	100.00
Proposed approach	4	Relaxation before stimulation	IHAR	QDA, SVM, kNN	100
	4	Visual stimulation	IHAR	kNN	98.8
	4	Mental recall	IHAR	QDA, SVM, kNN	100

is needed, but other tasks can be performed spontaneously. In our approach, the relaxation phase showed highest accuracy for the minimal (four) electrode setup.

Mental recall of a number can be realized in many ways, including visualization (imagining an image of the number), audiation or silent verbalization (thinking of a sound, such as a voice reciting the number), synesthetic association (such as association of digits or numbers with colors, flavors, musical notes, etc.) [106] or cross-modal correspondences, cardinal correspondences (such as thinking of sets enumerated by a number's digits), and spatial analogy (such as clock hour directions).

For an n -digit integer, $n \geq 2$, the likelihood of a repeated digit is

$$p(n) = 1 - \prod_{i=1}^{n-1} \frac{(10-i)}{10}. \quad (4.15)$$

For a random four-digit integer, the probability is almost half that at least one digit is repeated, and such a pattern could anchor its recall. All of these recall styles are possible practices, and the actual technique was left up to each subject. This vagueness could explain apparent uselessness of data from the mental recall phase.

A major problem in EEG-based biometric systems is instability of signal patterns over time. EEG patterns can change with environment, maturity, and psychological disorders [107]. This issue has not been addressed in the proposed approach. Therefore, accuracy can be degraded over considerable time period due to changing daily mental states. Even though relaxation phase has been used as refractory period in this study, merits and demerits of taking off headset cannot be addressed with this experimental setup. In addition, results can be changed with different headsets because of hardware characteristics (resolution, sampling rate, common-mode rejection ratio) and type of electrodes.

IHAR was tested with different MA windows sizes (L) No substantial differences were found for different parameter values, but comparatively better results were obtained for $L = 32$. As L decreases, the size of ripples in the frequency response increases. As shown in Fig 4.7, even when $L = 32$, a series of ripples is produced, although the height of the ripples is not

considerable.

4.7 Conclusion

In this research, we successfully deployed a novel feature, Inter-Hemispheric Amplitude Ratio (IHAR), to reveal personally unique information and distinguish people using EEG signals. With the proposed feature, highest accuracy could be achieved with a lower number of electrodes for a relatively simple task. Furthermore, this approach outperforms similar approaches with less computational power, suggesting deployment in portable devices with embedded low-power microprocessors. These promising results show that this approach has practical real-world applications. Also, this approach provides more convenience when training the system because there is no need of collecting large number of training trials. In the proposed approach, highest accuracy was achieved for the two frontal pairs of electrodes— FC5-FC6 and F7-F8. As a task phase to collect EEG data, relaxation is the best according to the results. Analysis showed the most suitable ML algorithms for classification are QDA, linear SVM, quadratic SVM, Gaussian SVM, and kNN. Moreover, AF3, AF4, F7, and F8 selective electrode arrangement can be used to develop tighter hardware design with high performance. However, accuracy would be affected if number of subjects increases. Also, brain signal patterns can significantly change over time, which would affect performance. For continued study, this approach can be further examined with a clinical-grade EEG system, and should be investigated to check whether the number of electrodes can be further reduced.

This page intentionally left blank.

5

Autoencoder-based one-class classification algorithm

5.1 Introduction

As discussed in Chapter 2, authentication can be simply expressed as 1:1 comparison, while subject identification can be interpreted as a 1-of- n comparison. Binary or multi-class classification tries to find a boundary (or boundaries) between classes which are usually used for subject identification (as explained in Chapter 4). Such classification techniques usually output the closest class label for any given input. However, most biometric authentication systems use pattern matching [108] or distance measurement [109] techniques, which don't necessarily use

multiple classes in training phase. In addition, one-class classification (OCC), a.k.a. unary classification, which name was coined by Moya and Hush in 1996 [110], can also be used to solve this problem. OCC is a method of identifying objects of a specific class amongst all objects, by learning from a training set that comprises objects of that class. Most popular OCC algorithms are Support Vector Data Description (SVDD) [111], which finds the smallest hypersphere that contains all objects of a specific class, and one-class SVM (OC-SVM) [112], which separates inliers from outliers by finding a hyperplane of maximal distance from the origin. We propose a novel OCC method based on autoencoders for EEG-based authentication.

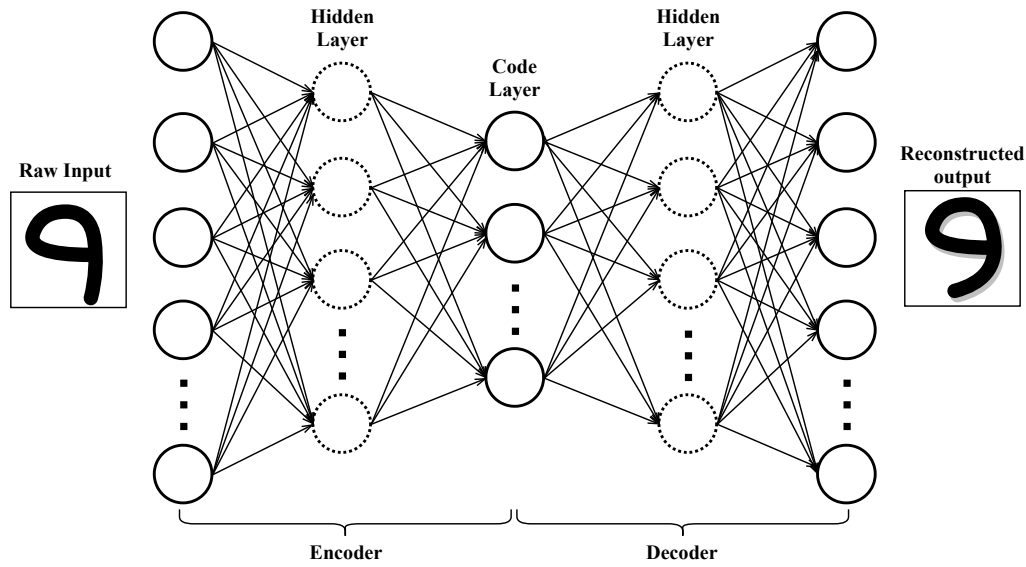


Figure 5.1: General structure of autoencoder

An autoencoder is a type of ANN which comes under the dimensionality reduction (or compression) category in ML. It basically, learns a representation (encoding) of a set of data in an unsupervised manner. This concept was first proposed by Geoffrey Hinton and the PDP group in the 1980s to address the problem of “back-propagation without a teacher” [113]. In a training phase, it extracts some important features in the encoding phase from raw data to make an abstract representation. Reconstructed output can be obtained as output of the decoder. This technique is effectively used for denoising, visualizing high-dimensional data, and anomaly detection. Basic structure of autoencoder comprises three layers, but additional hidden layers can also be added, as shown in Figure 5.1, and both encoder and decoder are fully-

connected feed-forward neural networks [114]. The middle layer, called the “bottleneck” or code layer, holds compressed data, and the network is usually symmetric across its code layer. However, several variants with different numbers of layers are being used depending on the application. The number of nodes in input and output layers must be same to reconstruct same-sized output. Besides using fully-connected layers, there are some autoencoder models with convolution layers, called deep autoencoders [115], that are used for image segmentation.

5.2 Methodology

As outlined in the previous section, the reconstructive nature of autoencoders is used to implement new OCC algorithms. Typical autoencoders follow the same phenomena as ANNs, so each node has connections with all nodes in the next layer (fully-connected layer) as seen in Figure 5.1. In our case, ReLU (rectified linear units) activation function is used in every layer. In training, once the decoder reconstructs encoded data, it determines the loss compared to actual data and adjust the weights to minimize the loss. The binary cross-entropy loss function is used because it is usually applied to problems involving binary decisions. To update weights of the network, AdaM (Adaptive Momentum) [116] optimizer is used.

As seen in Figure 5.2, first, autoencoder is trained with one specific class. Then, correlation coefficients are calculated with actual data and the reconstructed data.

$$Corr(x, y) = \frac{\sum_{i=1}^n (x_i - \bar{x})(y_i - \bar{y})}{\sqrt{\sum_{i=1}^n (x_i - \bar{x})^2 \sum_{i=1}^n (y_i - \bar{y})^2}}, \quad (5.1)$$

where x_i (input data), y_i (output data) are sample values and \bar{x}, \bar{y} are means of two populations (pixel grayscale values of images). A threshold is calculated using mean (μ) and standard deviation (σ) of array of correlation coefficients:

$$T = \mu_c - \frac{\sigma_c}{2}, \quad (5.2)$$

After saving the trained model and the threshold, trained model can be used as an OCC for

the trained class. In verification phase, correlation coefficient is calculated using given data and corresponding prediction. Calculated value is compared with the threshold, and if it is greater, given data is considered in same class.

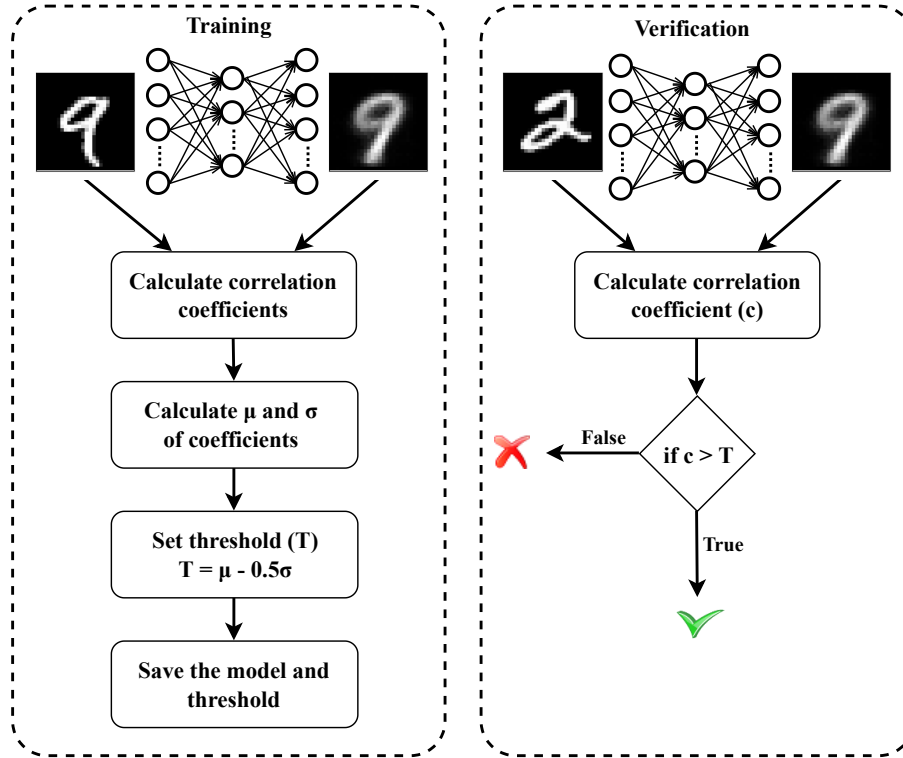


Figure 5.2: Structure of training and verification phases

5.2.1 Pilot experiment with MNIST dataset



(a) Images of 10 individual digits



(b) 10 sample images of digit 9

Figure 5.3: Sample images of MNIST dataset

Before testing with EEG data, a simple autoencoder model was designed for a publicly available dataset called MNIST which contains 70,000 images [117]. This dataset includes ten classes

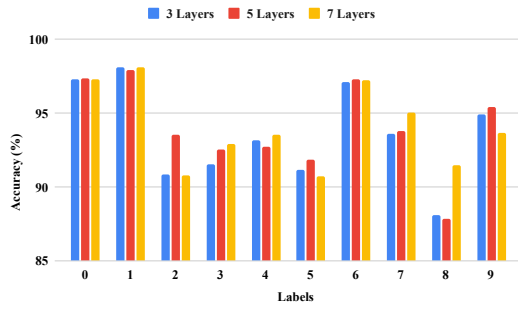
of images corresponding to handwritten digits 0 ~ 9 rendered as 28×28 pixels. It has been split into two sets—60,000 training and 10,000 testing images—to reduce the effort of pre-processing. Figure 5.3a shows sample images of 10 handwritten digits, and Figure 5.3b shows different sample images of digit 9. Normalized pixel values of these grayscale images are between 0 and 1.

Implementation was done in Python platform using Tensorflow [118] and Keras [119] libraries. Three variants of autoencoders with three, five, and seven fully-connected layers were used to test performance of the proposed method. The three-layer architecture was extended by adding a pair of layers with 256 nodes to create five layers. Another pair of layers with 512 nodes was added to five-layer architecture to make seven layers. Input and output layers always contain 784 (28×28) nodes, which is the total number of pixels in the image. Two code layers with 64 and 128 nodes each were also tested with all three autoencoder configurations. Each implemented autoencoder configuration was trained with 60,000 images and tested with 10,000 images.

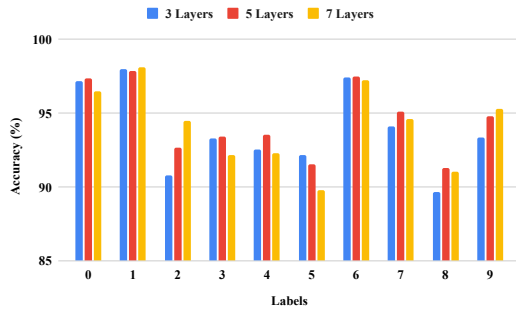
Results of pilot experiment

There is no substantial difference of accuracies in autoencoder configurations, as seen in Figure 5.4. Five-and seven-layer configurations showed slightly better accuracy compared to basic three-layer configuration, as seen in Figure 5.4c. Moreover, code layer with 128 nodes showed better accuracy in node configuration comparison, as seen in Figure 5.4b. According to the results, 94.51% average accuracy of all classes was achieved for the five layers and code layer with 128 nodes configuration.

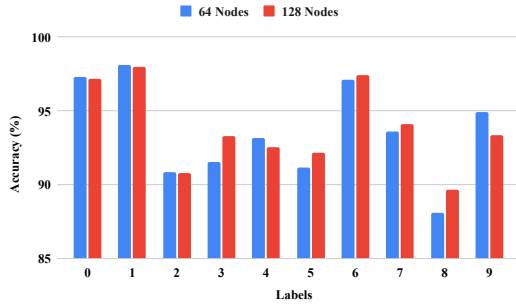
Receiver operating curve (ROC) and area under the ROC curve (AUC) values were generated with the calculated correlation coefficient values for each testing sample to further analyse performance. As seen in Figure 5.5, the threshold can be selected with a high true positive rate (TPR) and a low false-positive rate (FPR) for most of the classes. TPR, a.k.a. sensitivity or recall, measures the proportion of actual positives that are correctly classified and FPR, 1 – specificity, measures the proportion of actual negatives wrongly identified. If the TPR value is



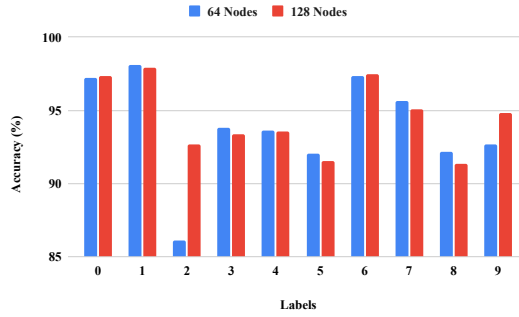
(a) Comparison of layer architecture with 64 nodes code layer



(b) Comparison of layer architecture with 128 nodes code layer



(c) Comparison of code layer nodes of 3 layers configuration



(d) Comparison of code layer nodes of 7 layers configuration

Figure 5.4: Comparison of accuracies

1 while FPR is 0 (AUC is 1), such a classifier can be considered perfect.

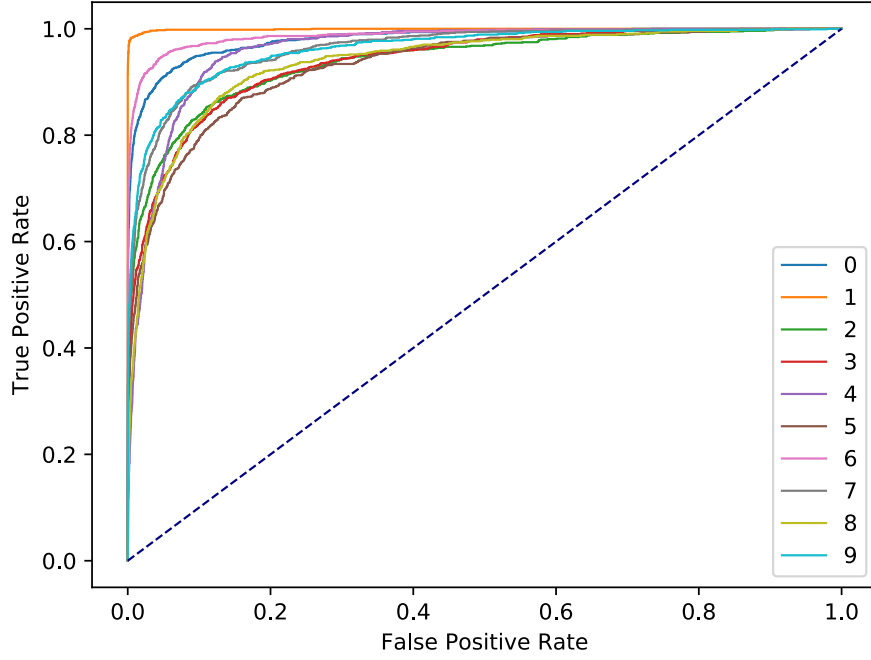


Figure 5.5: ROC curve of three layers and code layer with 64 nodes

Table 5.1: AUC values of all configurations

Configuration	0	1	2	3	4	5	6	7	8	9	AVG
3 layers, 64 nodes	0.981	0.999	0.939	0.937	0.96	0.93	0.987	0.962	0.937	0.962	0.959
5 layers, 64 nodes	0.989	0.999	0.941	0.954	0.967	0.927	0.984	0.932	0.92	0.968	0.958
7 layers, 64 nodes	0.988	0.999	0.944	0.909	0.944	0.936	0.981	0.966	0.94	0.968	0.957
3 layers, 128 nodes	0.992	0.999	0.949	0.955	0.966	0.937	0.985	0.964	0.911	0.964	0.962
5 layers, 128 nodes	0.983	0.999	0.928	0.952	0.954	0.932	0.984	0.968	0.926	0.96	0.958
7 layers, 128 nodes	0.989	0.999	0.949	0.962	0.952	0.933	0.981	0.965	0.925	0.962	0.961

Recognizability of digit 1 is maximum over other classes and digit 8 showed the lowest performance. This can happen because digit 8 has features similar to several other digits —such as 3, 9, and 6— whereas digit 1 is unique compared to other digits. Table 5.1 shows calculated AUC values for all configurations, and all values are over 0.9. Average AUC value of all classes and all the configuration is 0.96 ± 0.002 . Therefore, even minimum configuration can be used for such classification.

To further evaluate the trained model, distribution of calculated correlation coefficients in verification phase of the autoencoder that was trained for digit 0 was plotted. Figure 5.6 shows

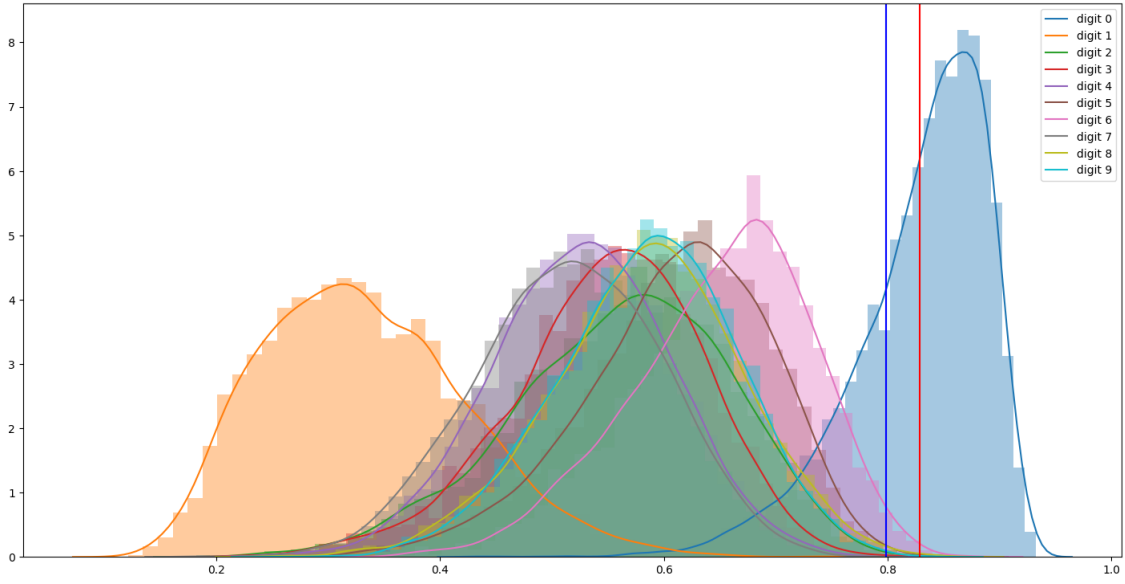


Figure 5.6: Distributions of correlation coefficients of each digit after training the model for digit 0. Red vertical line represents average of correlation coefficients of trained class, while blue vertical line represents defined threshold.

the distributions of correlation coefficients of each digit. As seen in the figure, digit 0 has higher correlation coefficients compared to other digits as expected. Area between two vertical lines, red and blue, represents how many observations (digits) count as positive class when changing the threshold. When the average (red vertical line) of correlation coefficients of trained class set as the threshold for verification, accuracy was significantly reduced, as seen in the plot. However, when defining the threshold as Equation 5.2 (blue vertical line), FPR is slightly increased. Therefore, overall accuracy was increased when the threshold selected as blue vertical line.

According all these evaluation results, proposed OCC approach has the potential to recognize positive class by training it with observations from a single class. Another advantage of this approach is flexibility of the threshold definition, which helps to adjust the specificity of the system. Such classifiers are better for authentication systems because it is difficult to collect data for the negative class (imposters).

5.2.2 Experiment with EEG data

To evaluate proposed one-class classification technique in EEG-based authentication domain, only the relaxation phase of same EEG dataset discussed in Chapter 4 was used. The

results obtained in pilot experiment were taken into consideration, and 3 layers with 64 nodes of code layer configuration was used for further test with EEG data. However, the number of nodes in the input and output layers of autoencoders were different depending on the number of samples in the feature set.

The proposed OCC approach was tested with raw EEG signals and two extracted feature sets, Inter-Hemispheric Amplitude Ratio (IHAR) and Power Spectral Density (PSD). The IHAR is a time-domain feature that is derived and tested for person identification using EEG data [13]. The PSD is a frequency-domain feature extraction method widely used in signal processing applications, including EEG-based authentication.

As the first step, each classifier was trained with 10 trials of raw signal data, IHAR, and PSD feature data from each subject. Thus, 12 autoencoders were trained for each case. The number of features for each case were 17920, 553, and 742 respectively. Remaining 60 trails for each case (5 trials from each subject) were used to evaluate the trained classifiers. Even if the accuracies were satisfactory, AUC values were near 0.5, meaning classifiers perform as random classifiers.

In order to improve performance of the classifiers, the dataset was expanded using signal augmentation techniques. Five techniques —jittering, magnitude warping, time warping, random downsampling (removal), permutation— were used to generate new EEG trials. Figure 5.7 shows visualization of raw and augmented signals using these techniques:

- *Jittering*: This is a process of adding random noise to the signal. Normally distributed random noise was generated with standard deviation of 0.05 to perturb original signal.
- *Magnitude warping*: This changes the magnitude of each sample by convolving each data window with a smooth curve varying around one.
- *Time warping*: This technique smoothly distorts the time intervals between samples.
- *Random downsampling*: In this process, some samples are randomly removed, interpolation remaining samples to recover the original length of the signal.

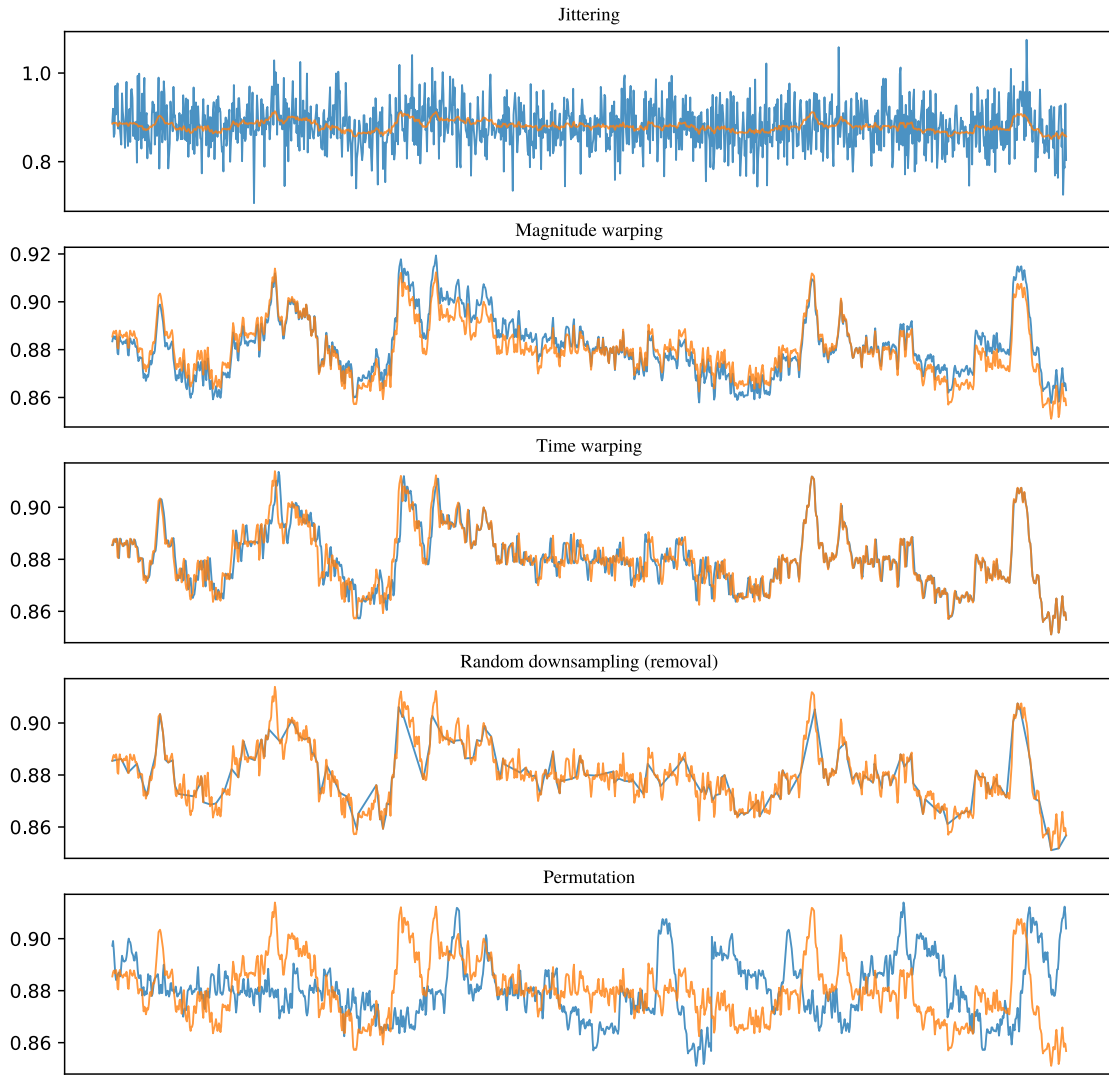


Figure 5.7: Visualization of raw and augmented signals subject to jittering, magnitude warping, time warping, random sampling, and permutation techniques. Orange trace represents the original raw signal, and blue trace represents the augmented signal in each plot.

- *Permutation:* In this process, the temporal location of within-window events are randomly shuffled. 4 randomly selected segments with random length (minimum 5 samples) were altered randomly.

A shuffled set of trials of each subject was partitioned into 10 training and 5 testing trials. Then 10 instances were generated from each augmentation technique, resulting in 510 total training trials for each subjects. The final training set contained $12 \times 510 = 6120$ trials in total. Remaining 60 trials (5 trials from each subject) were used to test performance of the classifier.

After augmentation, in addition to EEG raw signal, IHAR and PSD features were also extracted and tested with the implemented system.

Moreover, different channel configurations (8 and 4 frontal channels) were also tested to increase user-friendliness of the system. These channel combinations were selected by considering the results of previous work. AF3, AF4, F3, F4, F7, F8, FC5, and FC6 were selected as 8-channel configuration while F7, F8, FC5, and FC6 were selected as 4-channel configuration.

Results of experiment with EEG data

To evaluate performance of the OCC with both non-augmented and augmented datasets, accuracy, false positive rate (FPR), false negative rate (FNR), and area under the ROC curve (AUC) were used. Accuracy is not an adequate metric to evaluate performance because of fewer testing trials that makes the testing biased to each autoencoder. The AUC value can be used as a better metric to evaluate the system. In addition, since this authentication scenario identifies as high precision problem, the false positive rate should be minimum.

Table 5.2: Results of relaxation phase of all channels without data augmentation

Metric	Raw signal	IHAR	PSD
Accuracy	95%	88%	91%
FPR	0%	5.76%	1.21%
FNR	60%	85%	95%
AUC	0.7	0.55	0.52

The testing results of the dataset which does not include augmented trials is shown in Table 5.2. According to the results, raw signal dataset showed highest accuracy, while other two feature sets showed slightly lower accuracies. However, AUC values for both IHAR and PSD were close to 0.5 that performs as random classifier while raw signal dataset showed 0.7. Even if the model achieved high accuracy, reliability of the model output cannot be guaranteed because of low AUC value.

After using above-discussed augmentation techniques to expand the dataset, performance was increased for the raw signal dataset with no substantial difference for other feature sets. As shown in Table 5.3, AUC value for raw signal trial set increased to 0.96 with 93% accuracy. In

Table 5.3: Results of relaxation phase of all channels with data augmentation

Metric	Raw signal	IHAR	PSD
Accuracy	93%	85%	88%
FPR	7.27%	8.18%	5.91%
FNR	0%	85%	80%
AUC	0.96	0.53	0.57

contrast, FPR value (7.27%) was slightly higher compared to previous case (FPR = 0%). However, expanding the dataset using above augmentation techniques boosted the performance of autoencoders. Usually, encoder part of autoencoder acts as a feature extractor, and it has potential to find better features from raw data. This explains why the raw signal dataset achieved better results than extracted feature sets.

Table 5.4: Subject-wise performance evaluation. ACC: Accuracy; AUC: Area under the ROC; PRE: Precision; F1: F1 score

Channels, Metric		1	2	3	4	5	6	7	8	9	10	11	12	AVG
All	FPR	9.1	18.2	12.7	0.0	0.0	27.3	0.0	0.0	0.0	0.0	9.1	10.9	7.3
	FNR	0.0	0.0	0.0	0.0	0.0	0.0	0.0	0.0	0.0	0.0	0.0	0.0	0.0
	Precision	0.50	0.33	0.42	1.00	1.00	0.25	1.00	1.00	1.00	1.00	0.50	0.45	0.70
	F1 Score	0.67	0.50	0.59	1.00	1.00	0.40	1.00	1.00	1.00	1.00	0.67	0.63	0.79
	AUC	0.95	0.91	0.94	1.00	1.00	0.86	1.00	1.00	1.00	1.00	0.95	0.95	0.96
	Accuracy	91.7	83.3	88.3	100.0	100.0	75.0	100.0	100.0	100.0	100.0	91.7	90.0	93.3
8	FPR	0.0	0.0	0.0	0.0	0.0	20.0	0.0	0.0	0.0	0.0	0.0	0.0	1.7
	FNR	40.0	0.0	0.0	20.0	40.0	20.0	40.0	40.0	0.0	0.0	0.0	0.0	16.7
	Precision	1.00	1.00	1.00	1.00	1.00	0.27	1.00	1.00	1.00	1.00	1.00	1.00	0.94
	F1 Score	0.75	1.00	1.00	0.89	0.75	0.40	0.75	0.75	1.00	1.00	1.00	1.00	0.86
	AUC	0.80	1.00	1.00	0.90	0.80	0.80	0.80	0.80	1.00	1.00	1.00	1.00	0.91
	Accuracy	96.7	100.0	100.0	98.3	96.7	80.0	96.7	96.7	100.0	100.0	100.0	100.0	97.1
4	FPR	0.0	3.6	9.1	0.0	49.1	40.0	10.9	34.5	0.0	0.0	9.1	0.0	13.0
	FNR	0.0	60.0	0.0	0.0	80.0	20.0	40.0	60.0	0.0	0.0	20.0	0.0	23.3
	Precision	1.00	0.50	0.50	1.00	0.04	0.15	0.33	0.10	1.00	1.00	0.44	1.00	0.59
	F1 Score	0.00	0.99	0.00	0.00	0.07	0.31	0.66	0.19	0.00	0.00	0.87	0.00	0.26
	AUC	1.00	0.68	0.95	1.00	0.35	0.70	0.75	0.53	1.00	1.00	0.85	1.00	0.82
	Accuracy	100.0	91.7	91.7	100.0	48.3	61.7	86.7	63.3	100.0	100.0	90.0	100.0	86.1

Results of each subject for different channel configurations can be seen in Table 5.4. Precision and F1 score were also calculated because accuracy is not a reliable measurement in this case. Since authentication is a high precision problem, best channel configuration can be found by comparing precision values. According to the results, the highest precision (0.94) and F1 score (0.86) were shown for 8 channel configuration. Even though 4-channel configuration is better in terms of user friendliness, precision was considerably low; thus, this configuration is not acceptable for an authentication system. Moreover, subject 6 showed worst performance, es-

pecially precision in all channel configurations. The autoencoder trained for subject 6 failed to find a unique pattern from the given EEG data causing high FPR.

In this approach, precision for all channel configuration was low even if it achieved highest AUC value because the threshold definition is fixed. Nevertheless, having achieved high AUC value, threshold would be adjustable to increase precision. It is also possible to change this approach to find the optimal threshold value for the given FPR.

5.3 Conclusion

According to results of pilot experiment, the proposed approach can successfully be used as a one-class classifier. When using this method, each class can be trained independently, so it's an advantage for dynamic class problems such as user authentication. Traditional classification algorithms need to be retrained when adding a new class, and accuracy of the model can be highly affected. Moreover, this OCC approach can be used to authenticate people using their EEG signals collected using 8 frontal electrodes (AF3, AF4, F3, F4, F7, F8, FC5, and FC6) with relaxation task. Therefore, the proposed authentication system provides user-friendliness not only in training the model but also in data collection.

This page intentionally left blank.

6

Affect-guided soundscape exploration

6.1 Introduction

The discipline of music therapy recognizes the power of sound to induce relaxation, a power that has been well-understood by cultures around the world for millennia [120]. Selecting suitable sounds for a particular subject is challenging due to idiosyncratic tastes and circumstances [7]. Wolfe et al. performed a comparison in selection of relaxation music by musicians and non-musicians [8]. In the experiment described here, a reinforcement learning algorithm was used to analyze EEG signals of a listener to optimize a spatial soundscape for relaxation.

Reinforcement learning (RL) is a way of programming agents by rewards and penalties to achieve a goal [121]. Sub-elements of an RL system include a policy that defines a learn-

ing agent's way of behaving dynamically, a reward signal which defines a goal, a value function which specifies what is good in long run, and environment state [122]. Unlike other machine learning methods (supervised and unsupervised), RL uses state space as a parameter of its reward function, and is usually "online." RL is used in the video game development industry to automate the testing phase. There are several RL algorithms, including Q-Learning, SARSA (state-action-reward-state-action), and Deep Q Network (DQN). DQN was proposed in the DeepMind project developed by Google [123], and has been refined and deployed to play thousands of video games millions of times each.

In order to find the relaxation state of a listener, EEG signals were used. Lee et al. used monochord sounds and EEG signals to observe progressive muscle relaxation [124]. In this study, rewards and penalties are calculated by analysing the fluctuation of relative α (alpha) and β (beta) band power of collected EEG data. Among various human emotions classification methods, Russel's circumplex model of affect was utilized to derive reward calculation. Even though this scenario is different from a typical video game, an analogous environment was developed to feed parameters to an RL agent.

6.2 Methodology

The overall system can be divided into three parts: 1) Music generator: developed on Max/MSP development platform, which provides sound according to virtual position of an avatar, 2) Affect analysis environment: capture EEG signals from subject and calculate reward to feed to the RL agent, and 3) RL agent: controls the position of the avatar to change the sound according to the received reward. The complete system architecture can be seen in Figure 6.1. A stand-alone computer running both the Max patch and the agent software can perform exploration, the goal being to find a sweet spot in a 6-channel polyphonic (2D) space where the subject feels most relaxed.

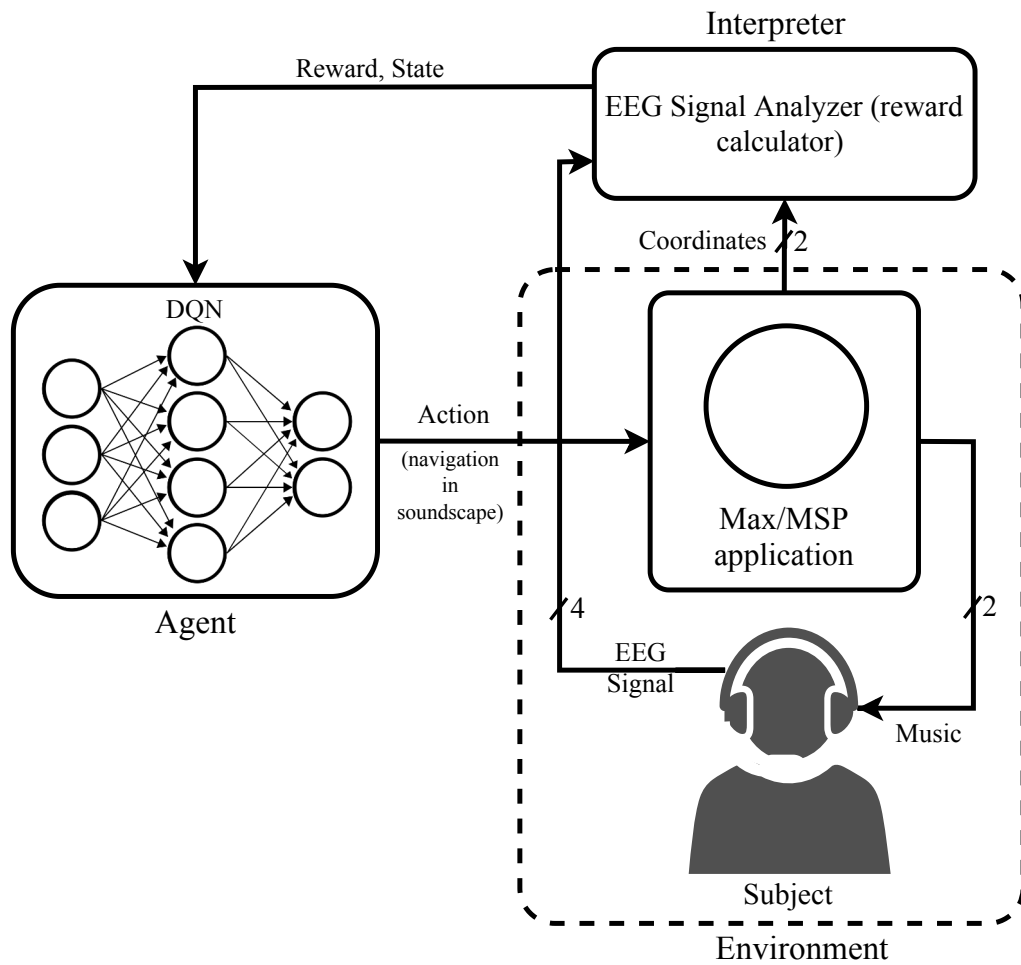


Figure 6.1: System architecture

6.2.1 Music generator

As shown in Figure 6.2, a Max/MSP patch was developed as a soundscape interface. Stereo headphones display a soundscape featuring six pantophonic sources arranged in a ring around the perimeter of the virtual space, which is parameterized not only by Cartesian position but also by processing attributes such as volume, pitch, reverb, and various parameters (center and cutoff frequencies, and resonance) for low-pass, high-pass, band-pass, and notch filtering. For runtime trials, these parameters are left at default settings. The six audio samples (which are selected from a larger gallery) are musical excerpts prepared by a composer specifically for this experiment. They originated from field recordings, digital synthesis, or a combination. The intention is to grow this gallery significantly into a much larger library of varying sounds, since

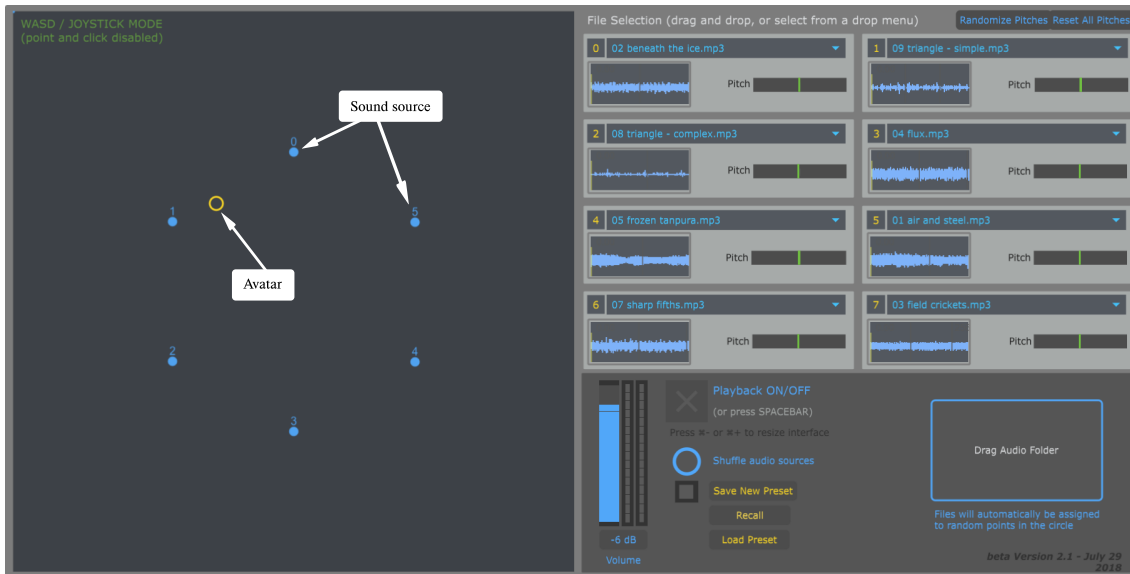


Figure 6.2: Max/MSP interface

individual sonic tastes can differ so much. Audio samples were selected eclectically without normalization. As seen in Figure 6.2, a yellow circle indicates the position of the avatar and the initial position is the center amidst all the sound sources. This interface generates sound based on distance from the avatar to each sound source. Avatar position can be programatically moved through 2D space by sending virtual keystrokes.

6.2.2 Affect analysis environment

The Muse EEG headband, shown in the Figure 6.3, was used in this experiment [97]. This headband is a BLE (Bluetooth low energy)-enabled portable device designed for meditation purposes. It has pairs of anterior frontal and temporo-parietal dry electrodes, labeled AF7 & AF8, and TP9 & TP10. As a reference it uses FpZ, which is placed on the center of forehead. Lightweight design and the shape of this device allows individuals to use it comfortably. Krigolson et al. [125] reported that the Muse headband can be used to conduct event-related brain potential (ERP) research from a single computer without the use of event-markers.

To capture signals from the head band, the “Muse Direct” Windows application was used and sampling rate was set to default value, which is 256 Hz. Captured signals were transferred to analysis environment using Open Sound Control (OSC) protocol. Data stream was col-

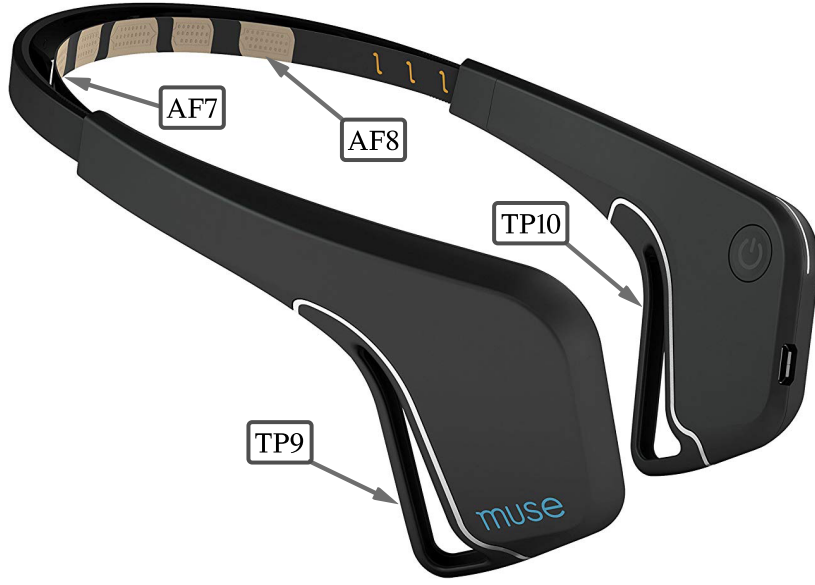


Figure 6.3: Muse wireless EEG headband

lected as 1 s chunks each comprising 256 data samples for further calculations. Welch’s method, a.k.a periodogram method, estimates power spectra by dividing the time signal into successive blocks then take the average by forming the periodogram for each block. This method is widely used in the signal processing domain to calculate power spectral density (PSD). Using this method, PSD for each frequency component can be computed. PSDs for four frequency bands— δ (0.5–4 Hz), θ (4–8 Hz), α (8–13 Hz), β (13–13 Hz)—and all bands (0.5–30 Hz) were calculated. Thereafter, relative PSDs were calculated by using following equation (for relative δ),

$$P_r = \frac{\Sigma P_{\delta}[n]}{\Sigma P_{all}[n]}, \quad (6.1)$$

where P_r is relative power of given frequency band, P_{δ} is element of given frequency component, and P_{all} is element of all considering frequency components (0.5–30 Hz).

For the reward calculation, Russell’s circumplex model of affect was used [126]. This model represents basic emotions of humans in a two-dimensional circular space. As seen in Figure 6.4, bottom right quadrant represents relaxed state. Therefore, the relaxed state can be found when valence is positive while arousal is negative. Al-Nafjan et al. reported several ways that can be

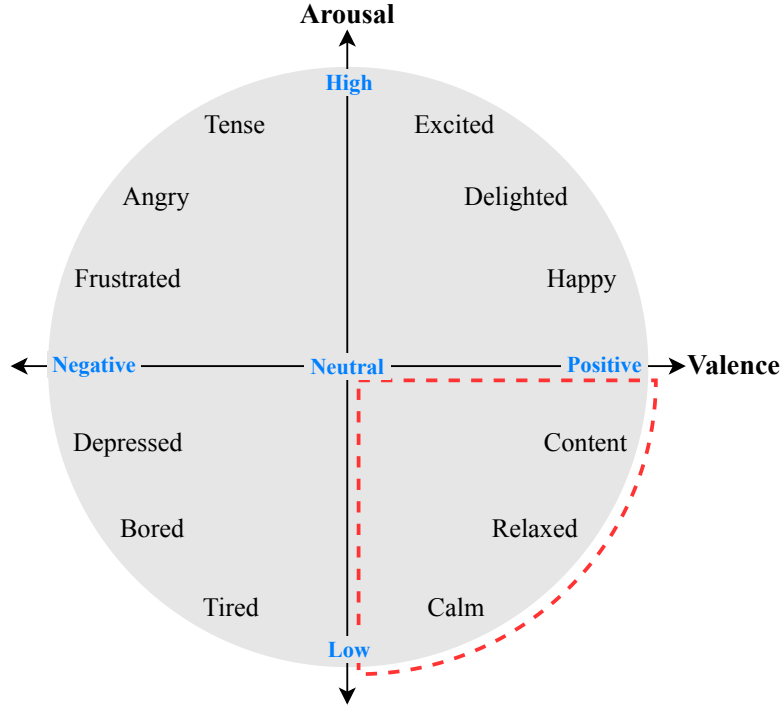


Figure 6.4: Russell's circumplex model of affect. Relaxed state quadrant has been highlighted in red, dashed line

used to calculate valence and arousal using EEG signals [127]. Valence is usually calculated by taking the power difference between right and left hemispheres ($R - L$), and valence is higher when power is high in right hemisphere. Arousal can be calculated by taking the ratio of beta and alpha power bands (β/α). However, in this case reward should be positive when the subject is in relaxed state, so the ratio α/β was taken. The reward calculation was derived using these aspects and equation is

$$r = \ln \left(\frac{\alpha_{AF8}}{\beta_{AF8}} \right) - \ln \left(\frac{\alpha_{AF7}}{\beta_{AF7}} \right), \quad (6.2)$$

where, R is the reward, α_{AF8} is alpha power of channel AF8, β_{AF8} is beta power of channel AF8, α_{AF7} is alpha power of channel AF7, and β_{AF7} is beta power of channel AF7. According to this equation, reward can be either negative (not relaxed) or positive (relaxed).

Analysis environment was implemented analogous to the OpenAI Gym [128] video game environment, designed for testing RL-algorithms. OpenAI Gym outputs four parameters:

- *Observation*: An environment-specific object representing observation of the environment. In our case, state includes avatar position (x and y coordinates) and relative powers of δ , ϑ , α , and β frequency bands.
- *Reward*: The amount of incremental reward achieved by the previous action. The goal is always to increase the total accumulated reward. In this case, Equation 6.2 was used to calculate the reward.
- *Done (boolean)*: Whether it's time to reset the environment. If there are five consecutive penalties (negative rewards) and avatar goes beyond soundscape, the environment is reset.
- *Info*: Diagnostic information useful for debugging, which can sometimes be useful for learning. Such information was not necessarily used in this experiment.

The core environment class of OpenAI Gym was extended with methods that output above parameters. When an action from the RL-agent is received as a discrete value, it is converted into a virtual keystroke to move the avatar in the 2D space of the Max/MSP application. Maximum number of steps that avatar can take is limited to 15 from the origin in any direction. Each keystroke was constrained by a time delay by making sure the avatar can reach the perimeter. The avatar only steps in right, left, up, or down direction (and cannot move diagonally). When the environment indicates reset state, the avatar directly moves to the origin (by sending reset key) without any time delay.

6.2.3 RL agent

As stated in Chapter 2, the DQN algorithm was used in this study. DQN is an extension of the Q learning technique by combination with deep learning. Q learning has a special table, called Q table, to store so-called Q values corresponding to actions and states [129]. The Bellman equation is used as an update rule to update Q values for newly taken actions:

$$Q(s, a) = r(s, a) + \gamma \max_a Q(s', a), \quad (6.3)$$

where $Q(s, a)$ is Q values from being at state s and selecting action a , including the immediate reward received, $r(s, a)$, plus the Q value possible from new state s' . γ is called discount factor, which controls the importance of long-term reward versus immediate gratification. DQN replaced the Q table with a neural network that tries to approximate Q values, and cost function of ANN is a derivation of the generalized Bellman equation:

$$Cost = [(r(s, a) + \gamma \max_a Q(s', a; \vartheta)) - Q(s, a; \vartheta)]^2, \quad (6.4)$$

where ϑ represents the trainable weights of the network.

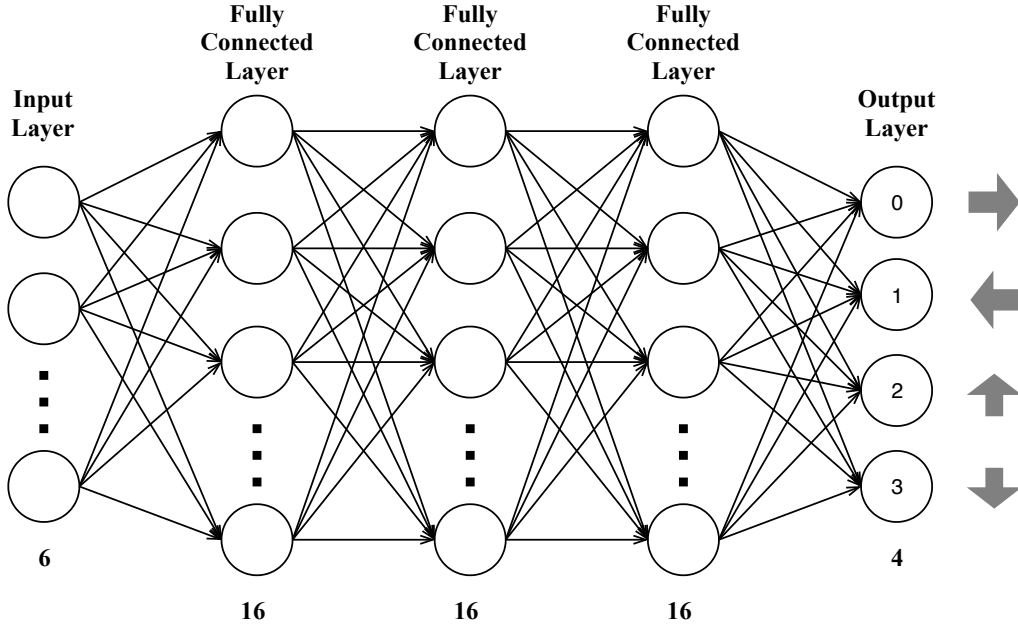


Figure 6.5: Structure of the neural network used in the RL agent

In our implementation, we used the keras-rl [130] Python-based library to create a RL-agent. This library comes with various RL algorithms and is compatible with OpenAI Gym. Figure 6.5 shows the structure of neural network used for the RL-agent, which including 5 fully-connected layers. The output layer with linear activation comprises 4 nodes, yielding discrete values that can be mapped as virtual keystrokes. Input layer takes 6 feature values, including Cartesian coordinates of avatar, relative powers of EEG signals corresponds to δ , ϑ , α , and β . To reduce the cost of the defined cost function, the AdaM (Adaptive Momentum) optimizer was used. Further, Boltzmann Q policy [131] was used as an exploration method which focuses

on action-selection. Boltzmann Q policy can be expressed as,

$$Pr(a|s) = \frac{\exp(Q(s, a)/T)}{\sum_{a' \in \mathcal{A}} \exp(Q(s, a')/T)}, \quad (6.5)$$

where $Pr(a|s)$ is the probability of action a for given state s , $a, a' \in \mathcal{A}$ is action space, and the “temperature” T controls the amount of exploration. Boltzmann Q policy is a method that uses action distribution to take either random or optimal action.

An instance of the implemented affect analysis class was passed to the RL-agent to obtain discrete numerical outputs. These discrete values were finally converted into virtual keystrokes (0: right, 1: left, 2: up, and 3: down), as seen in Figure 6.5. The Max/MSP interface must be focused while the program is running to change position of the avatar. A new soundscape is generated depending on the new avatar position and displayed to the subject. Then, the changed EEG signals evolve according to given music are analysed again to feed RL-agent and the same cycle repeats until it find the best position or “sweet spot.”

6.2.4 Simulator for Performance Test

Before testing the system with human subjects, a simulator was developed to test performance with an RL agent. A Cartesian space was created which contains 30×30 cells. Each cell represents a single step that the avatar can take and holds a reward value. Pseudo sweet spots were defined manually as 3rd axis on Cartesian coordinate system and interpolated through the other two axes. Random noise was added to make the distribution more inconsistent and shifted along 3rd axis in negative direction by half of the maximum value to obtain some negative values as penalties. Figure 6.6 shows heat maps of rewards and penalties for the given sweet spot values. The avatar roam without any time delay between each step in the simulator.

Furthermore, the calculated reward and penalties are converted into four alpha and beta components according to the reward calculation equation to obtain observations for the RL agent. Three values α_{AF8} , β_{AF8} , α_{AF7} were selected as random values and β_{AF7} was calculated using Equation 6.2 for the given reward value. When the RL agent takes a step, the simulator

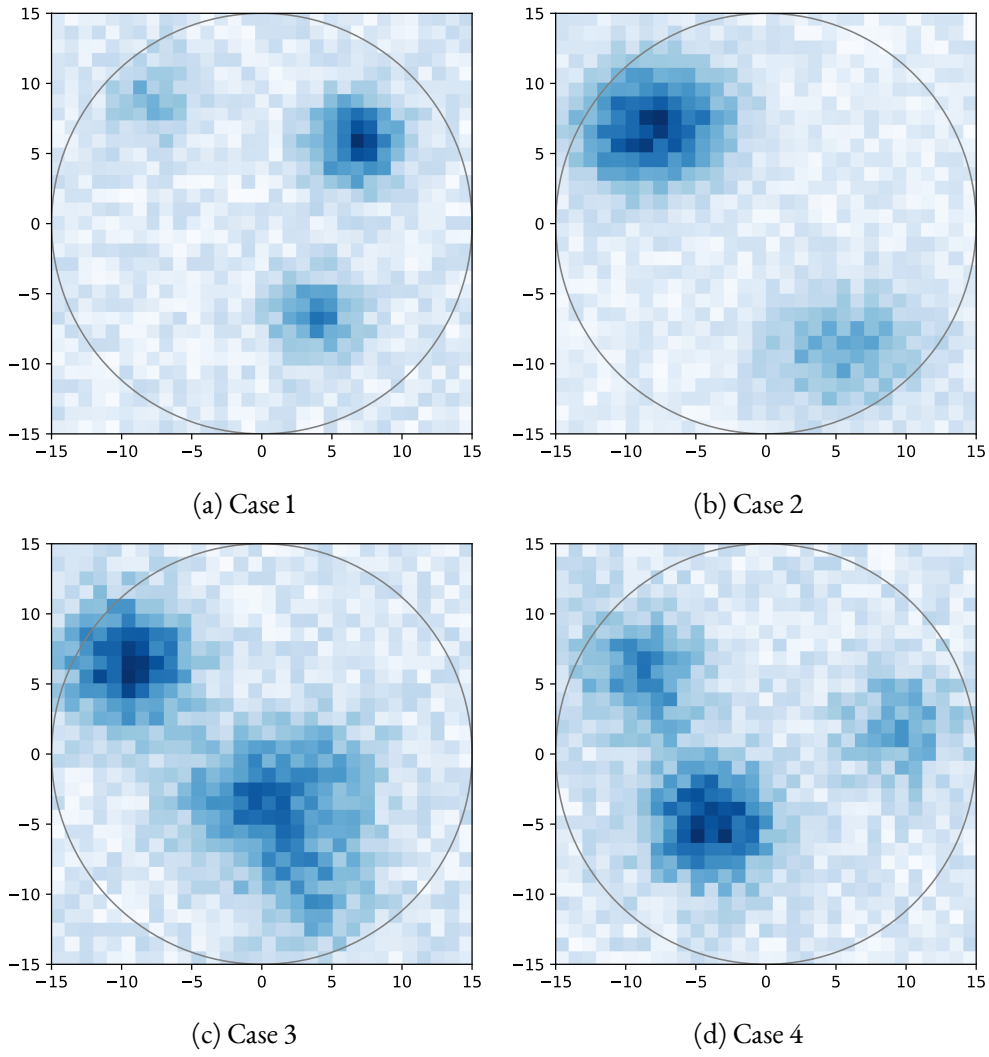


Figure 6.6: Heat maps of generated reward values. Darker spots represent higher rewards while lighter spots represent penalties.

provides pseudo reward and set of observations. Several cases with different sweet spots were used, as seen in the Figure 6.6. Darkest spot defined as the sweet spot for the each case. Moreover, two different heat maps were alternated while running the simulator to make it more realistic.

6.2.5 Experiment with human subjects

To test performances in real scenarios the implemented system was tested with 10 human subjects. A quiet room was used to conduct the experiment to avoid disturbances. Subjects

were instructed to be seated on a comfortable chair with closed eyes during the experiment. Typical stereo earphone was used to let the subjects to listen to the sound produced from the Max/MSP application. The exploration process was commenced after confirming the signal strength of the Muse headband using the Muse Direct application. The experiment was performed around 30 minutes for each subject to complete around 1000 steps.

6.3 Results and discussion

First, RL-agent was tested by feeding zeros as reward and observations. Results can be seen in Figure 6.7. Typical trace of the avatar movements of training phase in the Cartesian space are shown in Figure 6.7a. The avatar takes equal-sized steps for each keystroke generated by the RL-agent. The long lines directly radiating back to the origin are the environment resets. Each circle represents avatar's visit and bigger circles indicate higher the frequency of visits at that point. In training phase, the avatar roamed almost every direction in the Cartesian space, and in testing phase, avatar took short movements around the origin because there is no sweet spot in the space, as seen in Figure 6.7b.

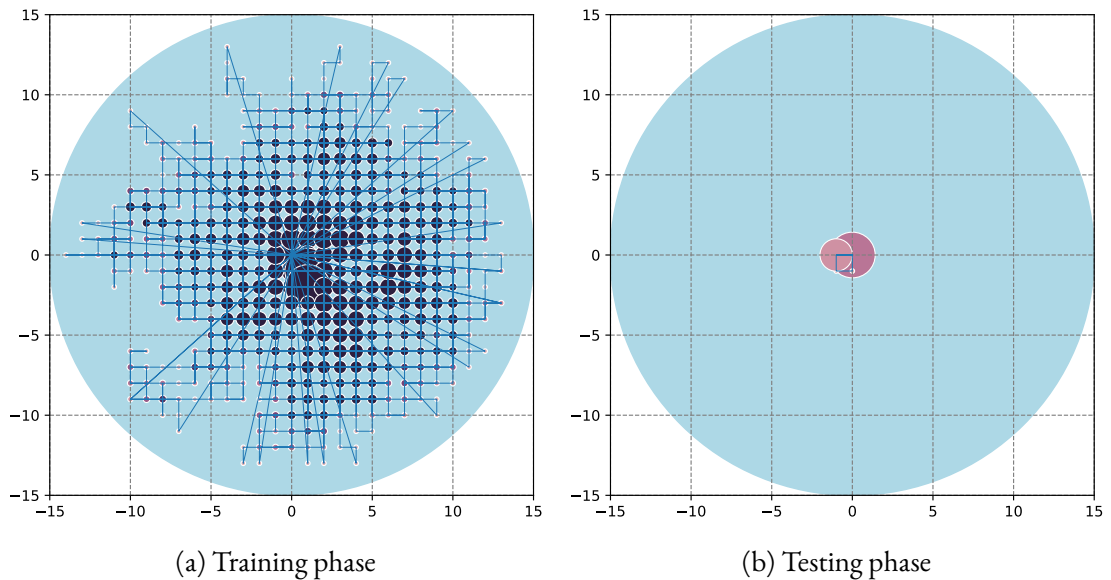


Figure 6.7: Visualization of avatar movements for equal rewards. Size of each circle represents frequency of the avatar's visits to that specific point.

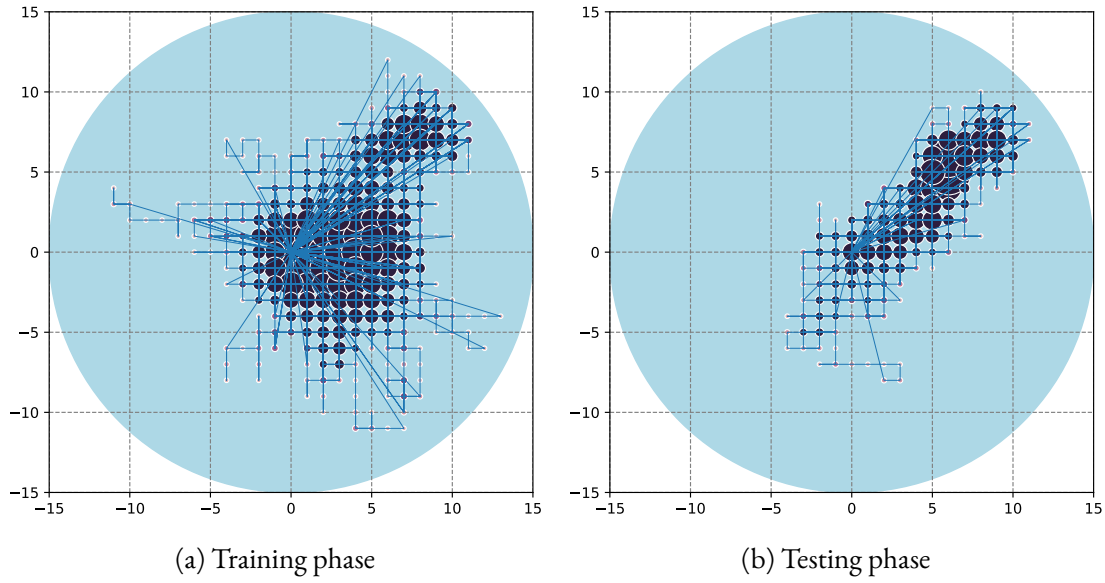


Figure 6.8: Visualization of avatar movements of case 1

When running the simulator for other cases, RL-agent could find the sweet spot for all cases within around 1000 steps. Because the RL-agent does not have an action to stop avatar movement, it took small back and forth movement at areas which contain highest rewards. According to the results shown in Figure 6.8a, RL-agent mostly have visited the right side of the Cartesian space because there are two sweet spots in the right side, as seen in Figure 6.6a. Also, it has taken similar path to the upper-right area multiple times because of high reward discounted that there was achieved in previous attempt. Frequency of steps near the upper-right area is comparatively high for this case. In the testing phase, avatar directly roam to the upper-right area, as seen in the Figure 6.8b. These results show that RL-agent has a potential to find an optimal sweet spot in this Cartesian space according to the reward values.

Figure 6.9 shows the graphs generated by the TensorBoard (a tool included in the TensorFlow library) while training the RL-agent for case 1. As seen in Figure 6.9a, cumulative reward value start to increase after around episode 40. According to the graph the RL-agent has found the sweet spot at around episode 55 and reward high because the avatar stayed at the point which has highest reward. Figure 6.9b shows the number of steps against episodes and number of steps are increasing with episodes which means RL-agent is getting close to the sweet spot.

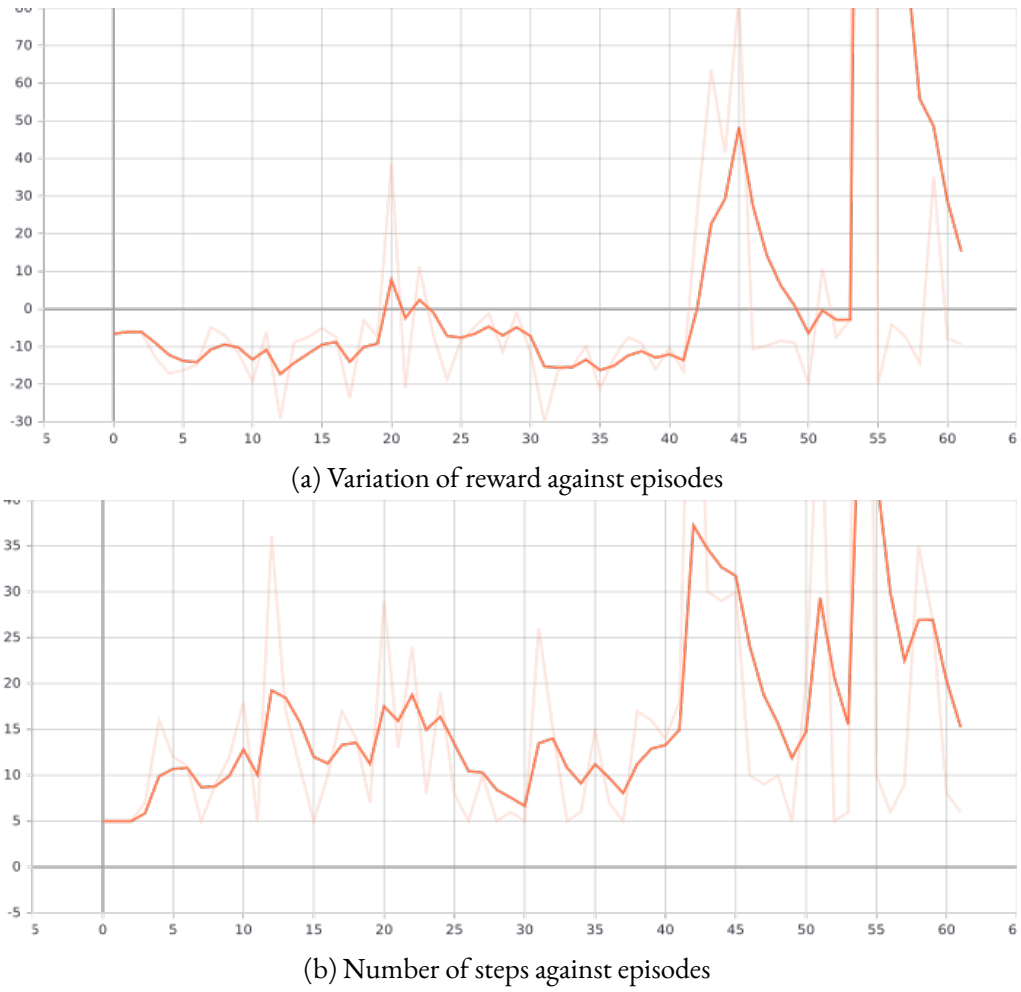


Figure 6.9: Training results of the simulator for case 1 generated using TensorBoard

These results confirmed that RL-agent has a capability to find the sweet spot with the given rewards and observations.

After confirming that the RL-agent is able to find a sweet spot in the virtual reward space, the system was tested with human subjects. Visualization of avatar's movements of training and testing phases can be seen in Figure 6.10. According to the testing results seen in Figure 6.10b, the avatar has found a sweet spot in the right-side of the Cartesian space. Even if the avatar has not visited that specific place in the training phase, as seen in Figure 6.10a, the avatar could find a new sweet spot in the testing phase. The TensorBoard results for the human subjects are not steady as the simulator because of the rapid changes of the mental state. However, according to the results as shown in Figure 6.11, after many episodes, a high cumulative reward value indicates

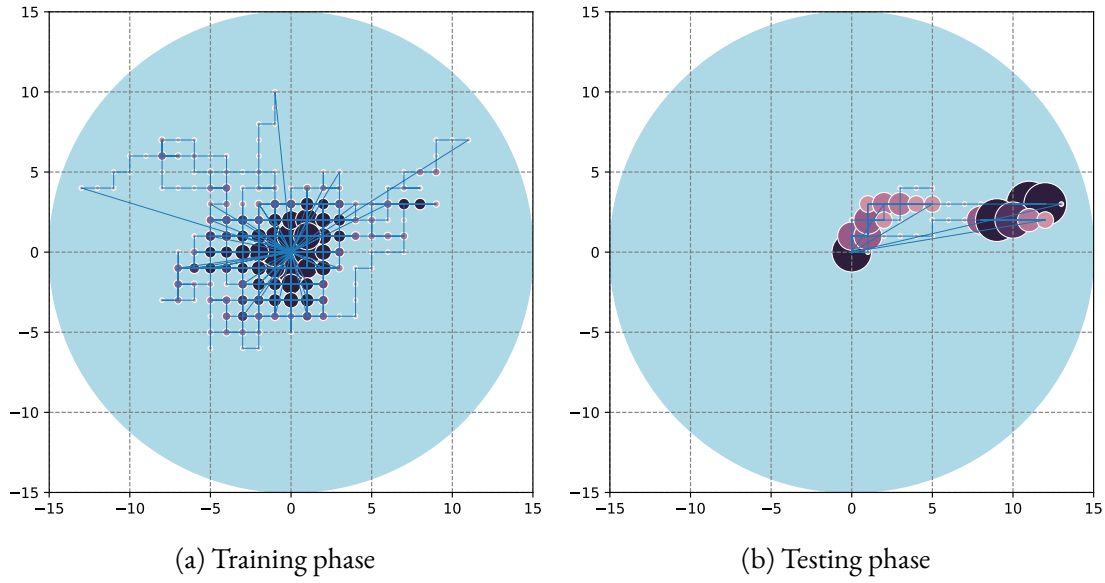


Figure 6.10: Visualization of avatar movements of subject 1

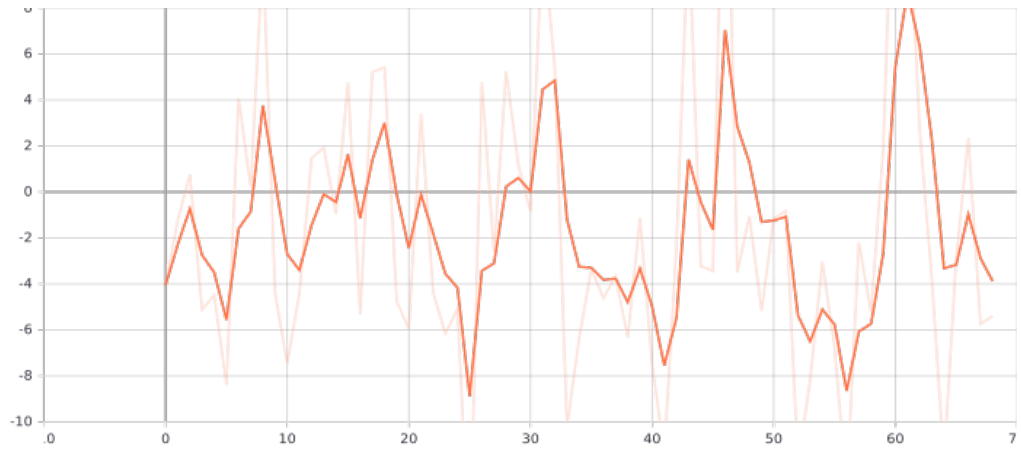
RL-agent has found a sweet spot.

As shown in the Figure 6.11a, several peaks can be seen and that could be happen because RL-agent found temporary sweet spots (local maxima). Similar pattern can be seen in Figure 6.11b as well. Around episode 60, maximum reward is achieved and that can be the global maximum in that epoch. However, it is difficult to conclude that the RL-agent found the global maximum since there could be other sweet spots as well.

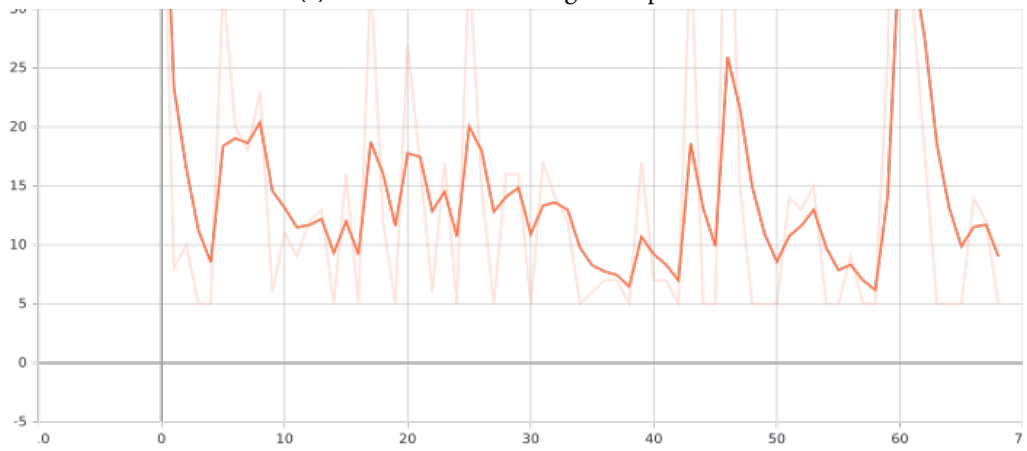
6.3.1 Conclusion

According to the results, DQN algorithm has a capability to find the sweet spot in the pantophonic soundscape using the reward calculated from EEG data. Our experiment assumes that relaxation can be described by a stable field across the pantophonic soundscape bounded by the annulus (ring) of a half-dozen musical sources. The sweet spot is probably not a point, but a locus, an area or collection of locations (perhaps noncontiguous, unconnected).

In this experiment, the RL-agent was trained in around 30 minutes, but increasing the time for training could affect the accuracy of the sweet spot exploration. Also, training the RL-agent in several sessions also would change the results. Performance could be increased using differ-



(a) Variation of reward against episodes



(b) Number of steps against episodes

Figure 6.11: Training results of subject 1 generated using TensorBoard

ent RL algorithms and a more precise way to find the relaxation state of a human. Moreover, combining another type of bio-signal such as ECG would increase the recognizability of the relaxation state.

This page intentionally left blank.

7

Conclusions

In this dissertation, idiosyncrasy or subjective difference were used to implement a brain-computer interface in two applications. Several scientific contributions reflect applications in both signal processing and machine learning domains. EEG as a brain-activity monitoring method making considerable impact in the emerging brain-computer interface field because of its affordability and convenience. EEG was used to utilize subjective difference to develop a better authentication system and generate sounds according to personal taste. EEG signals were collected using low-cost mobile headsets to accomplish the expected goal. Even though these headsets have low spatial resolution, both projects showed adequate performances on data collection.

EEG sensors usually capture electrical activities of neurons near the skull, and such data can

be noisy due to other electrical interferences such as ECG and GSR (Galvanic Skin Response). Despite that, these results showed it is feasible to extract meaningful information to recognize idiosyncrasy from EEG sensor data alone. Therefore, these findings encourage utilization of EEG data from consumer-grade devices for such applications. Affordability and convenience of these devices make this technology increasingly usable for general public.

EEG signal patterns are usually ambiguous, but a very few special patterns have been identified such as P300 (positive peak at 300 ms for visual stimulation), seizures, etc. Identifying these kind of patterns are important in medical diagnosis. However, when identifying subjective differences, it is not necessary to know specific patterns common to people. This explains why authentication or identification systems achieve high accuracies.

7.1 EEG-based authentication system

Authentication and identification systems are the best examples that utilize the unique features of people. As discussed in Chapters 4 and 5, it is possible to use bio-signals to uniquely identify or verify the identity. When identifying individuals from a group of people, classification algorithms can be used, because data for the entire population is available. Also, according to the results, engineered novel feature (IHAR) can be used with traditional machine learning techniques. Moreover, with these findings it can be anticipated that this type of algorithm can be embedded in a microchip to design a stand-alone authentication or identification device.

However, stability of the EEG signals can be changed over time and trained system might not respond anymore. In psychology as well as in philosophy, this is called persistence of identity problem. That means, identity of an individual might not steady, and can be changed due to various environment factors. Therefore, this problem is considerably relevant to such authentication systems due to mental changes and evolution.

7.2 Affect-guided soundscape analysis

Improvising sounds according to the personal taste is challenging. The proposed approach utilizes EEG to find the relaxation state with the best sound combinations. According to the

results of the simulator, it is confirmed that DQN model has a potential to find the sweetspot in the soundscape with the given reward and observations. Even when using human subjects, the implemented system performed fairly well. However, this task is very challenging because subjective mental state changes rapidly and does not have fixed status as in the simulator used in the experiment.

General abstraction of this approach is connecting human brain with artificial brain (AI algorithm). This will lead to unlock some mysteries of human brain function with the help of AIs. Also, the proposed RL approach using EEG signals can be used in other areas such as video gaming, health care, and education. Performance of this approach can be increased with advancements of AI and BCI fields.

This page intentionally left blank.

Acknowledgments

I would like to express my utmost gratitude to my supervisors, Prof. Michael Cohen and Dr. Senaka Amarakeerthi for guiding me throughout the doctoral program, and my dissertation committee members, Professors Qiangfu Zhao, Wenxi Chen, and Yuichi Yaguchi for providing their insight into my thesis.

I extend my sincere thanks to Prof. Michael Frishkopf at University of Alberta giving us the idea of affect-guided soundscape exploration project.

Other than the academic support, special thanks to Heiwa Nakajima foundation and Rotary Yoneyama foundation for their generous financial support for my research studies.

I would also like to thank my friends and colleagues, including Isuru Niroshana for encouragement and help throughout the past three years. Furthermore, I would like to thank staff at University of Aizu and friends outside the university for making a comfortable life throughout my study period.

Finally, this thesis would not have been possible without the unconditional support and encouragement from my parents, to whom I dedicate this work.

This page intentionally left blank.

References

- [1] A. Biondi, H. Nogueira, D. Dormont, M. Duyme, D. Hasboun, A. Zouaoui, M. Chantome, and C. Marsault, “Are the brains of monozygotic twins similar? A three-dimensional MR study.” *American journal of neuroradiology*, vol. 19, no. 7, pp. 1361–1367, 1998.
- [2] A. Jain, L. Hong, and S. Pankanti, “Biometric identification,” *Communications of the ACM*, vol. 43, no. 2, pp. 90–98, 2000.
- [3] A. K. Jain, P. Flynn, and A. A. Ross, *Handbook of biometrics*. Springer Science & Business Media, 2007.
- [4] A. A. Ross, K. Nandakumar, and A. K. Jain, *Handbook of multibiometrics: human recognition systems*. Springer, 2006.
- [5] M. V. Ruiz-Blondet, Z. Jin, and S. Laszlo, “CEREBRE: A novel method for very high accuracy event-related potential biometric identification,” *IEEE Transactions on Information Forensics and Security*, vol. 11, no. 7, pp. 1618–1629, 2016.
- [6] Y. Chen, A. D. Atnafu, I. Schlattner, W. T. Weldtsadik, M.-C. Roh, H. J. Kim, S.-W. Lee, B. Blankertz, and S. Fazli, “A high-security EEG-based login system with RSVP stimuli and dry electrodes,” *IEEE Transactions on Information Forensics and Security*, vol. 11, no. 12, pp. 2635–2647, 2016.
- [7] A. Hennion, “Music lovers: Taste as performance,” *Theory, Culture & Society*, vol. 18, no. 5, pp. 1–22, 2001.
- [8] D. E. Wolfe, A. S. O’Connell, and E. G. Waldon, “Music for relaxation: a comparison of musicians and nonmusicians on ratings of selected musical recordings,” *J. of Music Therapy*, vol. 39, no. 1, pp. 40–55, 2002.
- [9] M. L. Ibáñez, N. Álvarez, and F. Peinado, “Towards an emotion-driven adaptive system for video game music,” in *International Conference on Advances in Computer Entertainment*. Springer, 2017, pp. 360–367.
- [10] P. Hutchings and J. McCormack, “Using autonomous agents to improvise music compositions in real-time,” in *International Conference on Evolutionary and Biologically Inspired Music and Art*. Springer, 2017, pp. 114–127.
- [11] I. Jayarathne, M. Cohen, and S. Amarakeerthi, “Survey of EEG-based biometric authentication,” in *2017 IEEE 8th International Conference on Awareness Science and*

- Technology (iCAST)*. IEEE, 2017, pp. 324–329. [Online]. Available: <https://doi.org/10.1109/ICAwST.2017.8256471>
- [12] I. Jayarathne, M. Cohen, M. Frishkopf, and G. Mulyk, “Relaxation sweet spot exploration in pantophonic musical soundscape using reinforcement learning,” in *Proceedings of the 24th International Conference on Intelligent User Interfaces: Companion*. ACM, 2019, pp. 55–56. [Online]. Available: <https://doi.org/10.1145/3308557.3308686>
 - [13] I. Jayarathne, M. Cohen, and S. Amarakeerthi, “Person identification from EEG using various machine learning techniques with inter-hemispheric amplitude ratio,” *PloS one*, vol. 15, no. 9, p. e0238872, 2020.
 - [14] A. Naït-Ali, *Advanced biosignal processing*. Springer Science & Business Media, 2009.
 - [15] A. Schmidt, “Biosignals in human-computer interaction.” *interactions*, vol. 23, no. 1, pp. 76–79, 2016.
 - [16] M. Del Pozo-Banos, J. B. Alonso, J. R. Ticay-Rivas, and C. M. Travieso, “Electroencephalogram subject identification: A review,” *Expert Systems with Applications*, vol. 41, no. 15, pp. 6537–6554, 2014.
 - [17] C. C. Chernecky and B. J. Berger, *Laboratory Tests and Diagnostic Procedures-E-Book*. Elsevier Health Sciences, 2012.
 - [18] B. Farnsworth, “Top 14 EEG Hardware Companies [Ranked],” <https://imotions.com/blog/top-14-eeeg-hardware-companies-ranked/>, [Online; accessed 28-July-2019].
 - [19] H. H. Jasper, “The ten twenty electrode system of the international federation,” *Electroencephalography and Clinical Neurophysiology*, vol. 10, pp. 371–375, 1958.
 - [20] G.-E. Chatrian, E. Lettich, and P. L. Nelson, “Modified Nomenclature for the” 10%” Electrode System1.” *J. of Clinical Neurophysiology*, vol. 5, no. 2, pp. 183–186, 1988.
 - [21] R. Oostenveld and P. Praamstra, “The five percent electrode system for high-resolution EEG and ERP measurements,” *Clinical Neurophysiology*, vol. 112, no. 4, pp. 713–719, 2001.
 - [22] F. Chella, V. Pizzella, F. Zappasodi, and L. Marzetti, “Impact of the reference choice on scalp EEG connectivity estimation,” *Journal of neural engineering*, vol. 13, no. 3, p. 036016, 2016.
 - [23] S. Sanei and J. A. Chambers, *EEG Signal Processing*. John Wiley & Sons, 2013.
 - [24] U. R. Acharya, S. V. Sree, G. Swapna, R. J. Martis, and J. S. Suri, “Automated EEG analysis of epilepsy: a review,” *Knowledge-Based Systems*, vol. 45, pp. 147–165, 2013.
 - [25] IMOTIONS, *EEG Pocket Guide*. IMOTIONS, 2016.

- [26] N. J. Hill, T. N. Lal, M. Schroder, T. Hinterberger, B. Wilhelm, F. Nijboer, U. Mochty, G. Widman, C. Elger, B. Scholkopf *et al.*, “Classifying EEG and ECoG signals without subject training for fast BCI implementation: comparison of nonparalyzed and completely paralyzed subjects,” *IEEE transactions on neural systems and rehabilitation engineering*, vol. 14, no. 2, pp. 183–186, 2006.
- [27] R. Maskeliunas, R. Damasevicius, I. Martisius, and M. Vasiljevas, “Consumer-grade EEG devices: are they usable for control tasks?” *PeerJ*, vol. 4, p. e1746, 2016.
- [28] Y. Wang, Z. Wang, W. Clifford, C. Markham, T. E. Ward, and C. Deegan, “Validation of low-cost wireless EEG system for measuring event-related potentials,” in *2018 29th Irish Signals and Systems Conference (ISSC)*. IEEE, 2018, pp. 1–6.
- [29] C. M. Bishop, *Pattern recognition and machine learning*. springer, 2006.
- [30] Y. LeCun, Y. Bengio, and G. Hinton, “Deep learning,” *nature*, vol. 521, no. 7553, p. 436, 2015.
- [31] M. E. Whitman and H. J. Mattord, *Principles of Information Security*. Cengage Learning, 2011.
- [32] G. Doe, “Difference Between Identification & Authentication,” <http://itstillworks.com/difference-between-identification-authentication-3471.html>, [Online; accessed 26-June-2017].
- [33] L. Bunt, *Music therapy: An art beyond words*. Routledge, 2003.
- [34] E. L. Barratt and N. J. Davis, “Autonomous Sensory Meridian Response (ASMR): a flow-like mental state,” *PeerJ*, vol. 3, p. e851, 2015.
- [35] O. Eriksson and P. Lindau, “Evaluating an adaptive music system in an adventure game environment,” 2013.
- [36] S. Aav, “Adaptive Music System for DirectSound,” 2005.
- [37] M. Z. Land and P. N. McConnell, “Method and apparatus for dynamically composing music and sound effects using a computer entertainment system,” May 24 1994, uS Patent 5,315,057.
- [38] J. R. Evans and A. Abarbanel, *Introduction to quantitative EEG and neurofeedback*. Elsevier, 1999.
- [39] J. N. Demos, *Getting started with neurofeedback*. WW Norton & Company, 2005.
- [40] “Meet Your Personal Meditation Assistant,” <https://choosemuse.com/muse-app/>, [Accessed: 2018-08-20].
- [41] R. S. Sutton, “Reinforcement learning architectures for animats,” in *From Animals to Animats: Proceedings of the First International Conference on Simulation of Adaptive Behavior*, 1991, pp. 288–296.

- [42] H. S. Chang, M. C. Fu, J. Hu, and S. I. Marcus, "Google Deep Mind's AlphaGo," *OR/MS Today*, vol. 43, no. 5, pp. 24–29, 2016.
- [43] V. Mnih, K. Kavukcuoglu, D. Silver, A. Graves, I. Antonoglou, D. Wierstra, and M. Riedmiller, "Playing atari with deep reinforcement learning," *arXiv preprint arXiv:1312.5602*, 2013.
- [44] A. C. Weaver, "Biometric authentication," *Computer*, vol. 39, no. 2, pp. 96–97, 2006.
- [45] V. Zorkadis and P. Donos, "On biometrics-based authentication and identification from a privacy-protection perspective: Deriving privacy-enhancing requirements," *Information Management & Computer Security*, vol. 12, no. 1, pp. 125–137, 2004.
- [46] A. Almeahmadi and K. El-Khatib, "The state of the art in electroencephalogram and access control," in *2013 Third International Conference on Communications and Information Technology (ICCIT)*. IEEE, 2013, pp. 49–54.
- [47] E. Maiorana, D. La Rocca, and P. Campisi, "On the permanence of EEG signals for biometric recognition," *IEEE Transactions on Information Forensics and Security*, vol. 11, no. 1, pp. 163–175, 2015.
- [48] T. Pham, W. Ma, D. Tran, D. S. Tran, and D. Phung, "A study on the stability of EEG signals for user authentication," in *2015 7th International IEEE/EMBS Conference on Neural Engineering (NER)*. IEEE, 2015, pp. 122–125.
- [49] F. Vogel, *Genetics and the Electroencephalogram*. Springer, 2000, vol. 16.
- [50] M. Poulos, M. Rangoussi, and E. Kafetzopoulos, "Person identification via the EEG using computational geometry algorithms," in *9th European Signal Processing Conference (EUSIPCO 1998)*. IEEE, 1998, pp. 1–4.
- [51] M. Abo-Zahhad, S. M. Ahmed, and S. N. Abbas, "A new multi-level approach to EEG based human authentication using eye blinking," *Pattern Recognition Letters*, vol. 82, pp. 216–225, 2016.
- [52] Z. Y. Ong, A. Saidatul, and Z. Ibrahim, "Power Spectral Density Analysis for Human EEG-based Biometric Identification," in *Proc. Int. Conf. on Computational Approach in Smart Systems Design and Applications (ICASSDA)*. IEEE, 2018, pp. 1–6.
- [53] O. Falzon, R. Zerafa, T. Camilleri, and K. P. Camilleri, "EEG-based biometry using steady state visual evoked potentials," in *Proc. 39th Annual Int. Conf. of the Engineering in Medicine and Biology Society (EMBC)*. IEEE, 2017, pp. 4159–4162.
- [54] T. Fukami, Y. Abe, T. Shimada, and B. Ishikawa, "Authentication System Preventing Unauthorized Access of a Third Person Based on Steady State Visual Evoked Potentials," *Int. J. of Innovative Computing Information And Control*, vol. 14, no. 6, pp. 2091–2100, 2018.

- [55] Z. A. A. Alyasseri, A. T. Khader, M. A. Al-Betar, J. P. Papa, O. A. Alomari, and S. N. Makhadmeh, "Classification of eeg mental tasks using multi-objective flower pollination algorithm for person identification," *Int. J. of Integrated Engineering*, vol. 10, no. 7, 2018.
- [56] S. Yang, S. Hoque, and F. Deravi, "Improved time-frequency features and electrode placement for EEG-based biometric person recognition," *IEEE Access*, vol. 7, pp. 49 604–49 613, 2019.
- [57] B. Johnson, T. Maillart, and J. Chuang, "My thoughts are not your thoughts," in *Proceedings of the 2014 ACM International Joint Conference on Pervasive and Ubiquitous Computing: Adjunct Publication*. ACM, 2014, pp. 1329–1338.
- [58] J. Thorpe, P. C. Van Oorschot, and A. Somayaji, "Pass-thoughts: authenticating with our minds," in *Proceedings of the 2005 workshop on New security paradigms*. ACM, 2005, pp. 45–56.
- [59] X. Zhang, L. Yao, C. Huang, T. Gu, Z. Yang, and Y. Liu, "DeepKey: An EEG and gait based dual-authentication system," *arXiv preprint arXiv:1706.01606*, 2017.
- [60] B. Sabarigiri and D. Suganyadevi, "An Efficient Multimodal Biometric Authentication based on IRIS and Electroencephalogram (EEG)," in *5th International Conference on Control, Communication and Power Engineering (CCPE); Chennai, India*, 2014.
- [61] A. Riera, A. Soria-Frisch, M. Caparrini, I. Cester, and G. Ruffini, "Multimodal physiological biometrics authentication," *Biometrics: Theory, Methods, and Applications*, pp. 461–482, 2009.
- [62] C.-H. Im, *Computational EEG Analysis: Methods and Applications*. Springer, 2018.
- [63] J. Klonovs, C. K. Petersen, H. Olesen, and A. Hammershoj, "ID proof on the go: Development of a mobile EEG-based biometric authentication system," *IEEE Vehicular Technology Magazine*, vol. 8, no. 1, pp. 81–89, 2013.
- [64] N. E. Huang, *Hilbert-Huang transform and its applications*. World Scientific, 2014, vol. 16.
- [65] M. Poulos, M. Rangoussi, N. Alexandris, and A. Evangelou, "Person identification from the EEG using nonlinear signal classification," *Methods of information in Medicine*, vol. 41, no. 01, pp. 64–75, 2002.
- [66] A. Riera, A. Soria-Frisch, M. Caparrini, C. Grau, and G. Ruffini, "Unobtrusive biometric system based on electroencephalogram analysis," *EURASIP J. on Advances in Signal Processing*, vol. 2008, p. 18, 2008.
- [67] Z. Mu, J. Hu, and J. Min, "EEG-based person authentication using a fuzzy entropy-related approach with two electrodes," *Entropy*, vol. 18, no. 12, p. 432, 2016.
- [68] R. Palaniappan, "Two-stage biometric authentication method using thought activity brain waves," *International journal of neural systems*, vol. 18, no. 01, pp. 59–66, 2008.

- [69] L. Ma, J. W. Minett, T. Blu, and W. S. Wang, "Resting state EEG-based biometrics for individual identification using convolutional neural networks," in *2015 37th Annual International Conference of the IEEE Engineering in Medicine and Biology Society (EMBC)*. IEEE, 2015, pp. 2848–2851.
- [70] C. Ashby, A. Bhatia, F. Tenore, and J. Vogelstein, "Low-Cost Electroencephalogram (EEG)-Based Authentication," in *NER: Proc. 5th Int. IEEE/EMBS Conf. on Neural Engineering*, 2011, pp. 442–445.
- [71] J. Chuang, H. Nguyen, C. Wang, and B. Johnson, "I think, therefore I am: Usability and security of authentication using brainwaves," in *Proc. Int. Conf. on Financial Cryptography and Data Security*. Springer, 2013, pp. 1–16.
- [72] D. La Rocca, P. Campisi, B. Vegso, P. Cserti, G. Kozmann, F. Babiloni, and F. D. V. Fallani, "Human brain distinctiveness based on EEG spectral coherence connectivity," *IEEE Trans. on Biomedical Engineering*, vol. 61, no. 9, pp. 2406–2412, 2014.
- [73] S.-K. Yeom, H.-I. Suk, and S.-W. Lee, "Person authentication from neural activity of face-specific visual self-representation," *Pattern Recognition*, vol. 46, no. 4, pp. 1159–1169, 2013.
- [74] A. P. Anokhin, N. Birbaumer, W. Lutzenberger, A. Nikolaev, and F. Vogel, "Age increases brain complexity," *Electroencephalography and clinical Neurophysiology*, vol. 99, no. 1, pp. 63–68, 1996.
- [75] H. Ledoux and C. Gold, "An efficient natural neighbour interpolation algorithm for geoscientific modelling," in *Proc. Developments in Spatial Data Handling*. Springer, 2005, pp. 97–108.
- [76] T. T. Um, F. M. Pfister, D. Pichler, S. Endo, M. Lang, S. Hirche, U. Fietzek, and D. Kulić, "Data augmentation of wearable sensor data for parkinson's disease monitoring using convolutional neural networks," in *Proceedings of the 19th ACM International Conference on Multimodal Interaction*, 2017, pp. 216–220.
- [77] R. J. Davidson and K. Hugdahl, *Brain Asymmetry*. MIT Press, 1996.
- [78] A. W. Toga and P. M. Thompson, "Mapping brain asymmetry," *Nature Reviews Neuroscience*, vol. 4, no. 1, p. 37, 2003.
- [79] G. Mohammadi, P. Shoushtari, B. Molae Ardekani, and M. B. Shamsollahi, "Person identification by using AR model for EEG signals," in *Proc. World Academy of Science, Engineering and Technology*, vol. 11, 2006, pp. 281–285.
- [80] G. K. Singhal and P. RamKumar, "Person identification using evoked potentials and peak matching," in *Proc. Biometrics Symp.* IEEE, 2007, pp. 1–6.
- [81] X. Huang, S. Altaht, D. Tran, and D. Sharma, "Human identification with electroencephalogram (EEG) signal processing," in *Proc. Int. Symp. on Communications and Information Technologies (ISCIT)*. IEEE, 2012, pp. 1021–1026.

- [82] S. W. Smith, *The Scientist and Engineer's Guide to Digital Signal Processing*. California Technical Pub. San Diego, 1997.
- [83] J. M. Łęleski and N. Henzel, "ECG baseline wander and powerline interference reduction using nonlinear filter bank," *Signal Processing*, vol. 85, no. 4, pp. 781–793, 2005.
- [84] V. Kaiser, I. Daly, F. Pichiorri, D. Mattia, G. R. Müller-Putz, and C. Neuper, "Relationship between electrical brain responses to motor imagery and motor impairment in stroke," *Stroke*, vol. 43, no. 10, pp. 2735–2740, 2012.
- [85] N. Birbaumer, T. Elbert, A. G. Canavan, and B. Rockstroh, "Slow potentials of the cerebral cortex and behavior," *Physiological Reviews*, vol. 70, no. 1, pp. 1–41, 1990.
- [86] P. Geethanjali, Y. K. Mohan, and J. Sen, "Time domain feature extraction and classification of EEG data for brain computer interface," in *9th Int. Conf. on Fuzzy Systems and Knowledge Discovery*. IEEE, 2012, pp. 1136–1139.
- [87] A. D. Chan and G. C. Green, "Myoelectric control development toolbox," *Canadian Medical and Biological Engineering Society (CMBES) Proc.*, vol. 30, no. 1, 2007.
- [88] G. James, D. Witten, T. Hastie, and R. Tibshirani, *An introduction to statistical learning*. Springer, 2013, vol. 112.
- [89] R. H. Riffenburgh, "Linear Discriminant Analysis," Ph.D. dissertation, Virginia Polytechnic Institute, 1957.
- [90] S. Mika, G. Ratsch, J. Weston, B. Scholkopf, and K.-R. Mullers, "Fisher discriminant analysis with kernels," in *Neural Networks for Signal Processing IX, Proc. Signal Processing Society Workshop*. IEEE, 1999, pp. 41–48.
- [91] M. A. Hearst, S. T. Dumais, E. Osuna, J. Platt, and B. Scholkopf, "Support vector machines," *IEEE Intelligent Systems and Their Applications*, vol. 13, no. 4, pp. 18–28, 1998.
- [92] S. Amari and S. Wu, "Improving support vector machine classifiers by modifying kernel functions," *Neural Networks*, vol. 12, no. 6, pp. 783–789, 1999.
- [93] E. Strickland, "Neuroscience Experts Weigh in on Elon Musk's Mysterious 'Neural Lace' Company," *IEEE Spectrum*.
- [94] J. E. Bennett and J. Trinder, "Hemispheric laterality and cognitive style associated with transcendental meditation," *Psychophysiology*, vol. 14, no. 3, pp. 293–296, 1977.
- [95] R. J. Davidson, "What does the prefrontal cortex "do" in affect: perspectives on frontal EEG asymmetry research," *Biological Psychology*, vol. 67, no. 1-2, pp. 219–234, 2004.
- [96] J. A. Coan and J. J. Allen, "Frontal EEG asymmetry as a moderator and mediator of emotion," *Biological Psychology*, vol. 67, no. 1-2, pp. 7–50, 2004.
- [97] "Muse— Meditation Made Easy," <https://choosemuse.com/>, [Accessed: 2018-12-20].

- [98] R. E. Wheeler, R. J. Davidson, and A. J. Tomarken, "Frontal brain asymmetry and emotional reactivity: A biological substrate of affective style," *Psychophysiology*, vol. 30, no. 1, pp. 82–89, 1993.
- [99] E. Harmon-Jones and J. J. Allen, "Behavioral activation sensitivity and resting frontal EEG asymmetry: Covariation of putative indicators related to risk for mood disorders." *J. Abnormal Psychology*, vol. 106, no. 1, p. 159, 1997.
- [100] A. Miyake, N. P. Friedman, M. J. Emerson, A. H. Witzki, A. Howerter, and T. D. Wager, "The unity and diversity of executive functions and their contributions to complex "frontal lobe" tasks: A latent variable analysis," *Cognitive Psychology*, vol. 41, no. 1, pp. 49–100, 2000.
- [101] A. Koutras and G. K. Kostopoulos, "EEG-Based Person Identification Using Rhythmic Brain Activity During Sleep," in *Int. Conf. on Artificial Neural Networks*. Springer, 2018, pp. 682–692.
- [102] C. Kaewwit, C. Lursinsap, P. Sophatsathit *et al.*, "High accuracy EEG biometrics identification using ICA And AR Model," *J. of Information and Communication Technology (JICT)*, vol. 16, no. 2, pp. 354–373, 2017.
- [103] P. Arnau-González, M. Arevalillo-Herráez, S. Katsigiannis, and N. Ramzan, "On the influence of affect in EEG-based subject identification," *IEEE Trans. on Affective Computing*, 2018.
- [104] K. P. Thomas and A. P. Vinod, "EEG-based biometric authentication using gamma band power during rest state," *Circuits, Systems, and Signal Processing*, vol. 37, no. 1, pp. 277–289, 2018.
- [105] V. Schetinin, L. Jakaite, N. Nyah, D. Novakovic, and W. Krzanowski, "Feature extraction with GMDH-type neural networks for EEG-based person identification," *Int. J. of Neural Systems*, vol. 28, no. 06, p. 1750064, 2018.
- [106] C. A. Chun and J.-M. Hupé, "Are synesthetes exceptional beyond their synesthetic associations? A systematic comparison of creativity, personality, cognition, and mental imagery in synesthetes and controls," *British J. of Psychology*, vol. 107, no. 3, pp. 397–418, 2016.
- [107] M. Roohi-Azizi, L. Azimi, S. Heysieattalab, and M. Aamidfar, "Changes of the brain's bioelectrical activity in cognition, consciousness, and some mental disorders," *Medical J. of the Islamic Republic of Iran*, vol. 31, p. 53, 2017.
- [108] M. Aljamea, T. Athar, C. S. Iliopoulos, S. P. Pissis, and M. S. Rahman, "A novel pattern matching approach for fingerprint-based authentication," in *PATTERNS 2015: The Seventh International Conferences on Pervasive Patterns and Applications*, 2015, pp. 45–49.
- [109] F. Sufi, I. Khalil, and I. Habib, "Polynomial distance measurement for ECG based biometric authentication," *Security and Communication Networks*, vol. 3, no. 4, pp. 303–319, 2010.

- [110] M. M. Moya and D. R. Hush, "Network constraints and multi-objective optimization for one-class classification," *Neural Networks*, vol. 9, no. 3, pp. 463–474, 1996.
- [111] D. M. Tax and R. P. Duin, "Support vector data description," *Machine learning*, vol. 54, no. 1, pp. 45–66, 2004.
- [112] L. M. Manevitz and M. Yousef, "One-class SVMs for document classification," *Journal of machine Learning research*, vol. 2, no. Dec, pp. 139–154, 2001.
- [113] D. E. Rumelhart, G. E. Hinton, and R. J. Williams, "Learning internal representations by error propagation," California Univ San Diego La Jolla Inst for Cognitive Science, Tech. Rep., 1985.
- [114] P. Baldi, "Autoencoders, unsupervised learning, and deep architectures," in *Proceedings of ICML workshop on unsupervised and transfer learning*, 2012, pp. 37–49.
- [115] K. G. Lore, A. Akintayo, and S. Sarkar, "LLNet: A deep autoencoder approach to natural low-light image enhancement," *Pattern Recognition*, vol. 61, pp. 650–662, 2017.
- [116] D. P. Kingma and J. Ba, "Adam: A method for stochastic optimization," *arXiv preprint arXiv:1412.6980*, 2014.
- [117] Y. LeCun, L. Bottou, Y. Bengio, P. Haffner *et al.*, "Gradient-based learning applied to document recognition," *Proceedings of the IEEE*, vol. 86, no. 11, pp. 2278–2324, 1998.
- [118] M. Abadi, P. Barham, J. Chen, Z. Chen, A. Davis, J. Dean, M. Devin, S. Ghemawat, G. Irving, M. Isard *et al.*, "Tensorflow: A system for large-scale machine learning," in *12th {USENIX} Symposium on Operating Systems Design and Implementation ({OSDI} 16)*, 2016, pp. 265–283.
- [119] F. Chollet *et al.*, "Keras," <https://keras.io>, 2015.
- [120] N. M. Weinberger, "Music and the brain," *Scientific American*, vol. 291, no. 5, pp. 88–95, 2004, ISBN 978-1-848933-01-8.
- [121] L. P. Kaelbling, M. L. Littman, and A. W. Moore, "Reinforcement Learning: A survey," *J. of Artificial Intelligence Research*, vol. 4, pp. 237–285, 1996.
- [122] R. S. Sutton and A. G. Barto, *Reinforcement Learning: An Introduction*. MIT press, 2018, ISBN 0-262-19398-1.
- [123] H. Van Hasselt, A. Guez, and D. Silver, "Deep Reinforcement Learning with Double Q-Learning." in *AAAI*, vol. 2. Phoenix, AZ, 2016, p. 5.
- [124] E.-J. Lee, J. Bhattacharya, C. Sohn, and R. Verres, "Monochord sounds and progressive muscle relaxation reduce anxiety and improve relaxation during chemotherapy: a pilot EEG study," *Complementary Therapies in Medicine*, vol. 20, no. 6, pp. 409–416, 2012.
- [125] O. E. Krigolson, C. C. Williams, A. Norton, C. D. Hassall, and F. L. Colino, "Choosing MUSE: Validation of a low-cost, portable EEG system for ERP research," *Frontiers in neuroscience*, vol. 11, p. 109, 2017.

- [126] J. A. Russell, "A circumplex model of affect." *Journal of personality and social psychology*, vol. 39, no. 6, p. 1161, 1980.
- [127] A. Al-Nafjan, M. Hosny, A. Al-Wabil, and Y. Al-Ohali, "Classification of human emotions from electroencephalogram (EEG) signal using deep neural network," *Int. J. Adv. Comput. Sci. Appl*, vol. 8, no. 9, pp. 419–425, 2017.
- [128] G. Brockman, V. Cheung, L. Pettersson, J. Schneider, J. Schulman, J. Tang, and W. Zaremba, "OpenAI Gym," 2016.
- [129] C. J. Watkins and P. Dayan, "Q-learning," *Machine learning*, vol. 8, no. 3-4, pp. 279–292, 1992.
- [130] M. Plappert, "keras-rl," <https://github.com/keras-rl/keras-rl>, 2016.
- [131] C. J. C. H. Watkins, "Learning from delayed rewards," 1989.